CHAPTER 5

CHAPTER 5

RECIPROCATING WEAR BEHAVIOUR OF Ti-TiB COMPOSITES SYNTHESIZED VIA VACUUM ARC MELTING

This chapter presents results about the characterization of raw powders and preparation of composites, along with the reciprocating friction and wear behavior analysis of these composites with different normal load and sliding frequencies. The stroke length of 5 mm was kept constant throughout the experiment at all load and frequencies. The detailed study on reciprocating wear (i.e., results and discussion) with change in sliding frequency under normal loads of 10, 15, 20, and 25 N, which are presented in four parts; Reciprocating wear behavior of the composites at (a) 4 Hz, (b) 7Hz, (c) 10 Hz, and (d) 15 Hz.

5.1 RESULTS

5.1.1 CHARACTERIZATION OF POWDERS

Figure 5.1 shows the SEM morphologies of Ti and TiB_2 powders used in the present study. Both Ti and TiB_2 (99 % pure) powder particles are observed to be plate-like in shape with a particle size of 100 μm and 325 μm, respectively.

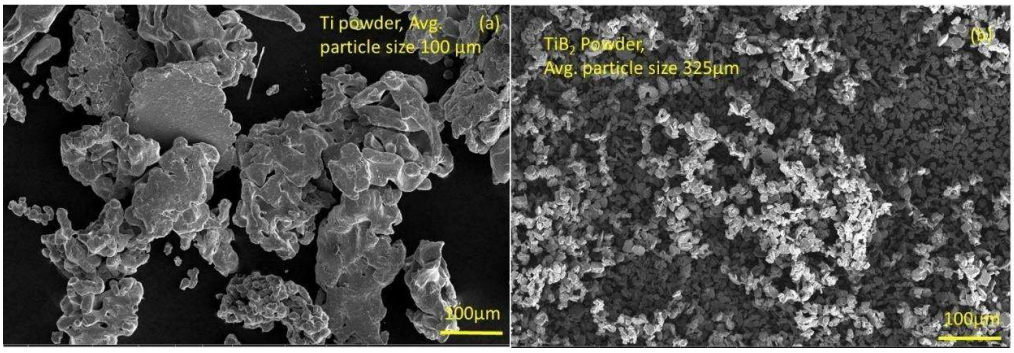

Figure 5. 1 SEM micrographs of feedstock powder (a) Ti and (b) TiB_2

5.1.2 CHARACTERIZATION OF COMPOSITES

Figure 5.2 presents the X-ray diffraction patterns of pure Ti and Ti-TiB composites synthesized in the present study. All the diffraction patterns corresponding to composites show the peak corresponding to TiB and β-Ti phases and confirm the occurrence of a complete reaction between raw Ti and TiB_2 to produce *in-situ* TiB. Furthermore, no peaks corresponding to TiB_2 could be seen in the X-ray diffraction pattern, indicating that the whole TiB_2 was consumed during the reaction leading to TiB formation. The designation, hardness, surface roughness, and density of the samples are given in Table 5.1.

The SEM micrographs of the microstructure for pure Ti, TiB50, TiB60, TiB70, TiB80, and TiB85 are presented in Figs. 2 (a through q), respectively. No cracks or pores are observed in the microstructures, indicating the synthesis of fully dense structures. The presence of TiB in two different shapes (i) whiskers and (ii) blocky could be seen in the insets shown in Figs. 2 (b and c) corresponding to composites TiB50, TiB60 and high magnification micrograph of TiB85 presented in Figs. 2 (k and q). The Blocky shape appears to be increasing with increasing concentration of TiB from 50 to 85 vol. % (as shown in BSE micrographs (l through q). These observations are consistent with samples

processed by VAM [89-91]. The elemental distribution of the elements in the TiB70 composite is shown in Fig. 2 (g through j). The density increases with an increase in TiB vol.%. The presence of blocky TiB as a result of the agglomeration of TiB whiskers can also be seen in Fig. 2 (k). Similar observations have been reported earlier [92].

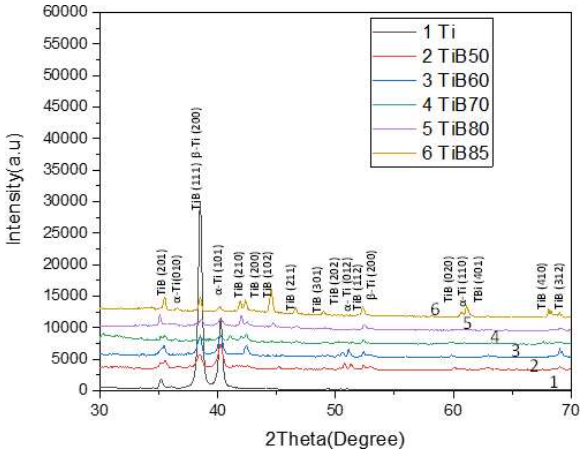

Figure 5. 2 XRD pattern of composites (a)Ti, (b)TiB50, (c) TiB60, (d) TiB70, (e) TiB80, and (f) TiB85

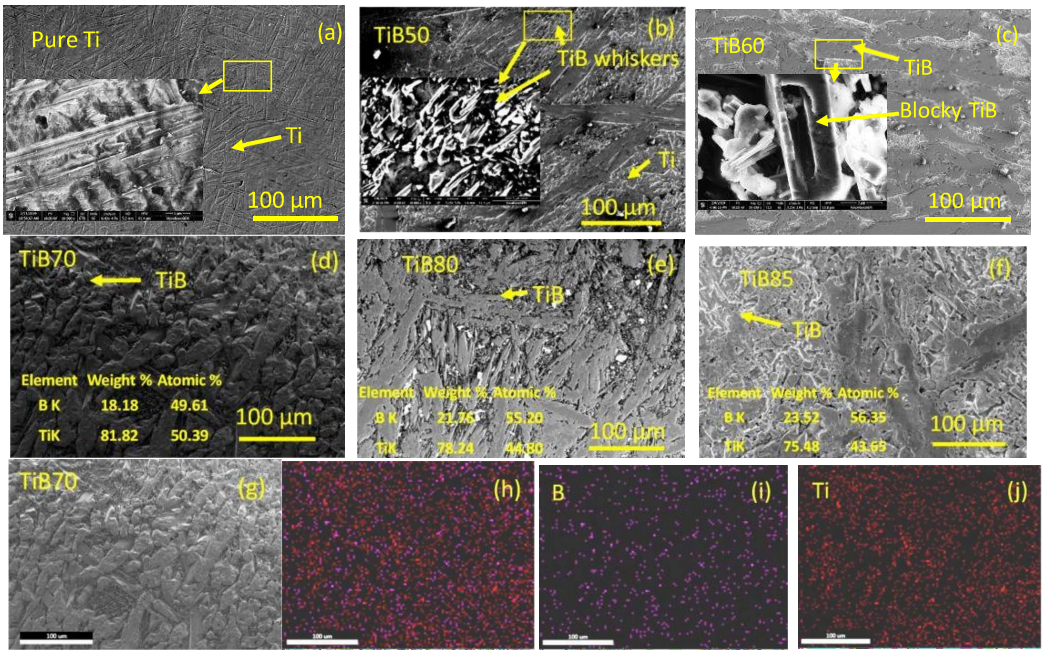

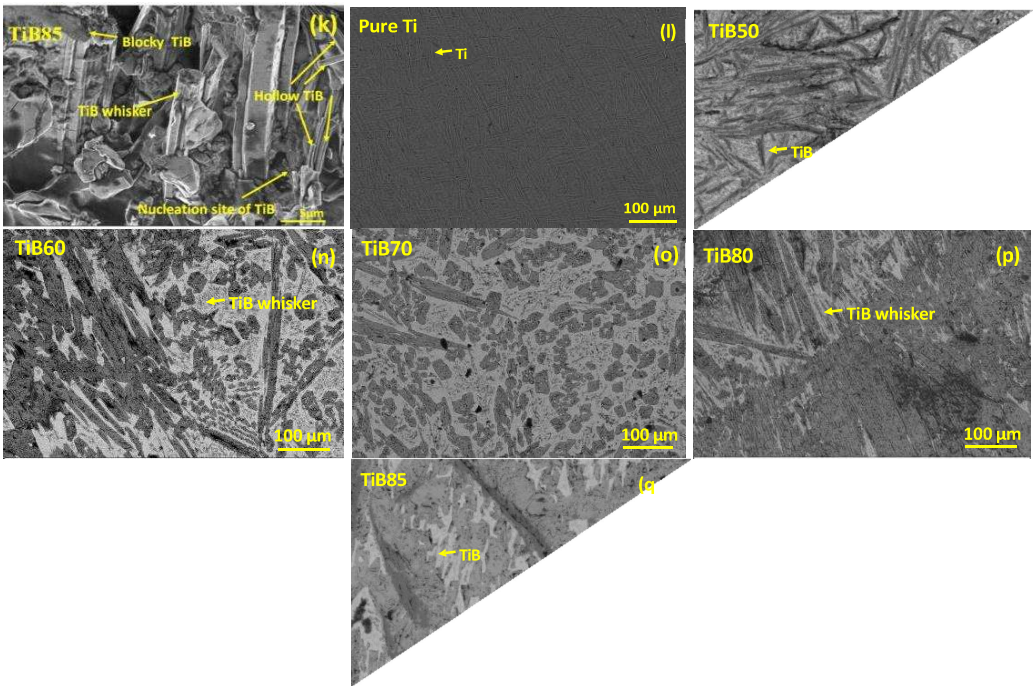

Figure 5. 3 Scanning electron micrographs (a-k) and BSE images (l-q) showing microstructure of composites (a) pure Ti, (b) TiB50, (c) TiB60, (d) TiB70,(e) TiB80, (f) TiB85,and elemental distribution of TiB70 (g-j), (k) Magnified region showing blocky and whiskers nature of TiB in composite TiB85, (l) pure Ti, (m) TiB50, (n)TiB60, (o) TiB70, (p)TiB80, (q) TiB85.

The hardness of composites increases with increasing TiB amount from 50 to 85 vol.% as evident from Table 1. One may observe that the hardness of pure Ti increased by more than three times just by reinforcement of 50 vol. % TiB. Among the composites, TiB50 has shown the minimum hardness of 799 HV, whereas the maximum hardness of 895 HV is observed for TiB85. The measured hardness values are 807, 854, and 878 HV, respectively, for TiB60, TiB70 and TiB80. The surface roughness values of the composites measured using a surface profilometer (AMETEK Taylor Hobson, USA) before the test are given in Table5.1.

Table 5.1 Designation, hardness, density, and surface roughness of composites

Designation	Composition	Hardness (HV_1)	Relative Density (%)	R_a (μm)
Ti	0 vol.% TiB	236.03 ± 5	98.96	0.122 ± 0.012
TiB50	50 vol.% TiB	799.02 ± 5	98.25	0.140 ± 0.019
TiB60	60 vol.% TiB	807.2 ± 3	98.29	0.140 ± 0.016
TiB70	70 vol.% TiB	854.48 ± 2	98.52	0.141 ± 0.019
TiB80	80 vol.% TiB	878.37 ± 1	98.89	0.144 ± 0.012
TiB85	85 vol.% TiB	895.48 ± 3	99.26	0.144 ± 0.020

5.1.3 FRICTION AND WEAR BEHAVIOR OF COMPOSITES

(i) Variation of coefficient of friction with time

Figure 5.4 (a through f) demonstrate the variation of coefficient of friction (COF) with time at different loads for pure Ti, TiB50, TiB60, TiB70, TiB80, and TiB85 respectively. The variation of coefficient of friction is observed to be steady for Ti at all loads with almost no running-in stage due to a relatively small surface roughness (Table 5.1) and plastic deformation of soft asperities which results in an early attainment of better conformity between the tribo-pair. Similar observation has been reported by earlier [103]. However, the amplitude of fluctuations for Ti is quite less, and the fluctuations appear to increase slightly with increasing load from 10 to 25 N as seen from Fig. 5.4 (a). A relatively larger fluctuation in amplitude could be observed in Figs. 5.4 (d, e and f) in comparison to Figs. (b and c) depending on the applied load. However, after the run-in stage the fluctuations appear to die down and a steady state is attained depending on the initial surface roughness of the composite (Table 5.1) and the applied load. The COF

appears to get stabilized relatively earlier (600 s) for TiB50 at loads of 15 and 20 N in comparison to 10 and 25 N loads (800 s), as evident from Fig. 5.4 (b). For TiB60, COF at all the loads is observed to stabilize soon after the run-in period is over ~ 200 s as shown in Fig. 5.4 (c), whereas for TiB70 it shows little fluctuation around a mean level at 10 and 15 N throughout the test duration, however, COF gets stabilized after 200 s 20 and 25 N before dropping further a little after 1000 s beyond which it appears to stabilize again as seen from Fig. 5.4 (d). In the case of TiB80, the COF is initially stable at 10 N load, but the amplitude of fluctuation starts increasing after 600 s. In contrast, at loads of 15 and 20 N, the amplitude of fluctuations is more at the beginning, and COF stabilizes after 600 s as seen from Fig. 5.4 (f). However, at a load of 25 N the COF appears to be stable till 500 s and after that the amplitude of fluctuations rises till 900 s before stabilizing again, as evident from Fig. 5.4 (f). The COF for composite TiB85 is observed to get stabilized after 400 s at all the loads but the amplitude of fluctuations is relatively large at higher loads of 20 and 25 N than for 10 and 15 N.

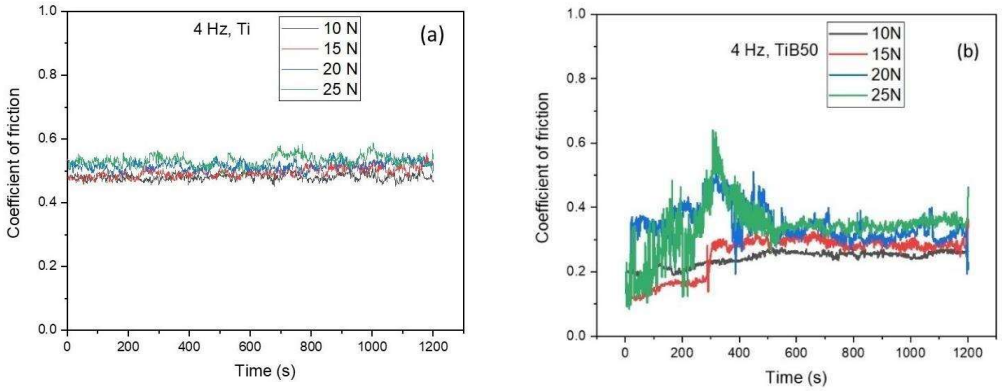

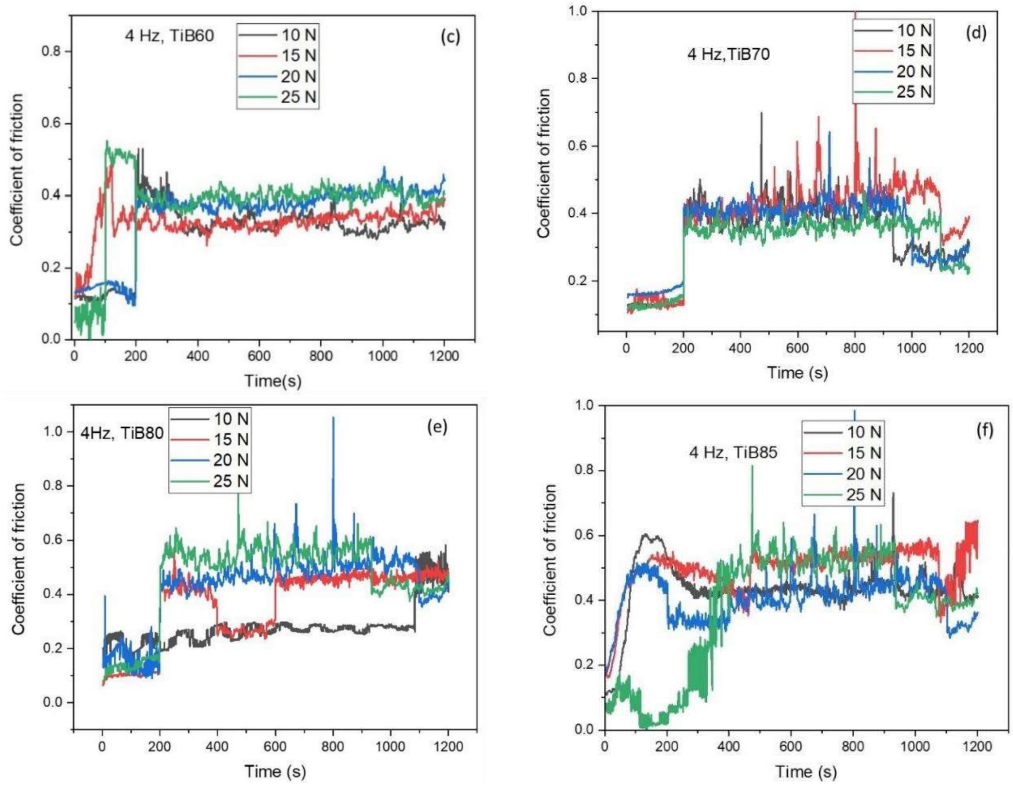

Figure 5. 4 Variation of coefficient of friction with time for 10,15,20, and 25 N (a) Ti, (b)TiB50, (c)TiB60, (d)TiB70, (e)TiB80, and (f) TiB85 composites at different loads.

(ii) Variation of average coefficient of friction with normal load and composition

Figure 5.5 (a) presents the variation of average steady state coefficient of friction with the normal load whereas the variation with respect to composition is illustrated in Fig. 5.5 (b). The steady state average COF is found to increase with increasing load for pure Ti as well as the composites and the steady state average COF for Ti is the highest for all loads as evident from Fig.5.5 (a). The increase in COF is relatively sharp for TiB50 as one moves from 10 to 15 N load. TiB80 has shown a consistently lower COF among all the composites at all the loads, as evident from Fig. 5.5 (a). At a load of 10 N, the steady state average COF is observed to increase with increasing TiB content from 50 to 70 vol. % before decreasing again till 80 vol. % followed by a slight increase beyond that,

as seen from Fig. 5.5 (b). However, at other loads i.e., 15, 20, and 25 N the steady state average COF decreases as the amount of TiB increases from 50 to 60 vol. %, followed by an increase till 70 vol. % TiB and a reduction thereafter for 80 vol.% TiB which is again followed by a marginal increase as the TiB amount is raised to 85 vol. % as evident from Fig. 5.5 (b).

(iii) Variation of wear rate with normal load and composition

The variation of wear rate (mm^3/m) with load for all the composites shown in Fig. 5.6 (a) reveals that the wear rate increases with increasing load for all the composites. Pure Ti has the highest wear rate among all the materials at all the loads. As far as composites are concerned, the wear rate shown by TiB50 is the highest among all the composites, whereas that shown by TiB80 is the lowest. At relatively lower loads, i.e., 10, 15, 20 N, the wear rate is shown by TiB60 is lower than that shown by TiB70. However, at the highest load of 25 N, the wear rate for TiB50, TiB60, and TiB70 appears to be the same, with TiB70 showing a marginally low rate of wear, as seen from Fig. 5.6 (a). One may also observe that the wear rate shown by TiB80 and TiB85 are the same at loads of 10, 15, and 20 N, whereas at 25 N, the wear rate of TiB80 is slightly less than TiB85.

The variation of wear rate with TiB vol.% depicted in Fig.5.6 (b) indicates a sharp decrease in wear rate from pure Ti to TiB50 at all the loads. The wear rate is observed to decrease with increasing TiB content from 50 to 60 vol.% at the loads of 10, 15, and 20 N before increasing slightly to 70 vol.%, but for 25 N it increases slightly from TiB50 to TiB60 then decreases till TiB80 before further increasing marginally at TiB85. However, for 10, 15, and 20 N the wear rate decreases from TiB70 to 80 vol.% and thereafter increases marginally at TiB85. At a load of 25 N, no change is wear rate is observed with

increasing TiB content from 60 to 70 vol.%, beyond which it decreases till 80 vol.% and then remains the same till TiB85 as seen from Fig. 5.6 (b).

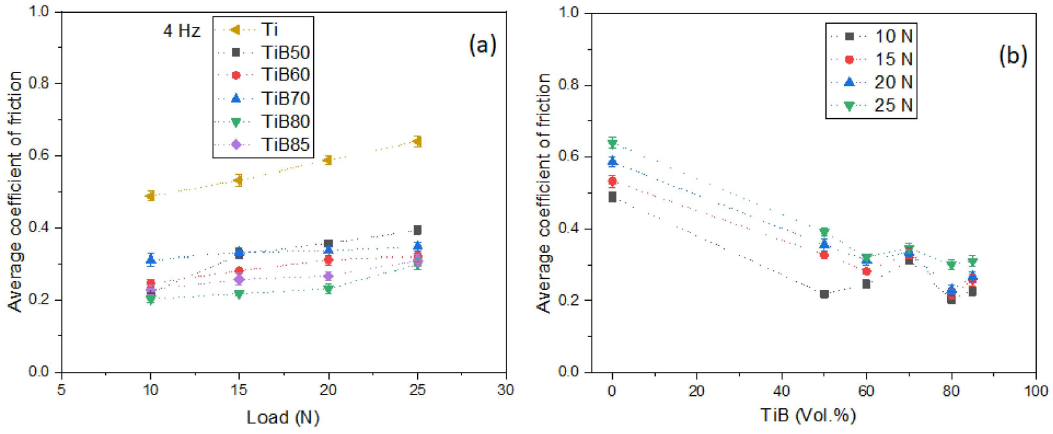

Figure 5. 5 Variation of average coefficient of friction (a) load and (b) composites TiB (Vol.%).

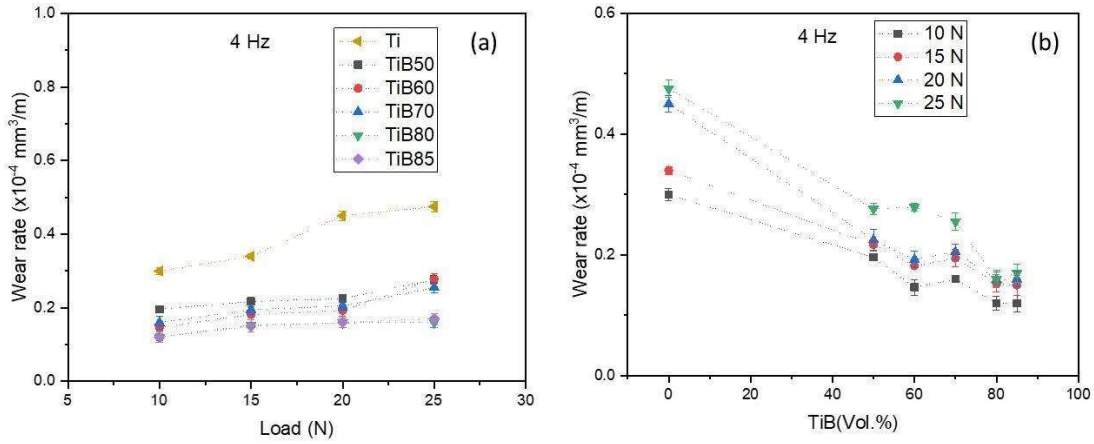

Figure 5. 6 Variation of wear rate of the composites with (a) load and (b) composites TiB (vol.%)

5.1.4 WORN SURFACE MORPHOLOGY OF COMPOSITES

Figures 5.7, 5.8, 5.9, and 5.10 present SEM micrographs of worn surfaces of TiB50, TiB60, TiB70, TiB80, and TiB85 composites after sliding at the loads of 10, 15, 20, and 25 N, respectively. Figure 5.7 (a-g) presents the SEM images of the surface of

composites worn under a load of 10 N. Fig. 5.7 (a) shows the ploughing and sliding marks along with some transfer layer on the worn surface of pure Ti. The worn surface of TiB50 shown in Fig. 5.7 (b) reveals the presence of sliding marks with the occurrence of delamination at a few places. In contrast, the worn surface of TiB60 shows the presence of a compacted transfer layer along with prominent sliding marks as evident from Fig. 5.7 (c). Some loose debris in the form of particles and plates could be seen on the worn surface of TiB70 (Fig.5.7 (d)). However, the worn surface of TiB80 (Fig. 5.7 (e)) displays the presence of a compacted transfer layer of wear debris along with some loose debris particles. The worn surface of TiB85 shows a few ploughing marks along with a compacted layer of wear debris as seen from Fig. 5.7 (f). EDS analysis of different spots at the worn surface of TiB50 reveals the presence of oxygen and Fe, which might have been transferred from the counterface ball, as evident from Fig. 5.7 (g). This indicates the possibility of the presence of oxides in the transfer layer along with loose metallic debris.

Figure 5.8 (a through f) depicts the micrographs of the worn surface of composites slid under a load of 15N as examined under SEM. The worn surface of pure Ti presents ploughing marks along with a transfer layer probably of oxides as seen from Fig.5.8 (a). The worn surface of TiB50 shown in Fig. 5.8 (b) reveals a smooth surface with the presence of a loosely bound transfer layer (shown in magnified view in the inset) along with some wear particles, whereas the layer appears to be a bit compacted with some signs of delamination at a few locations TiB60 as seen from Fig. 5.8(c). A loose and scattered transfer layer of wear debris, probably of oxides, could be observed on the worn surface of TiB70 as EDS analysis reveals the presence of high oxygen and iron content (transferred from the counterface) on the worn surface as seen from Fig. 5.8 (d). Figure 5.8 (e), corresponding to TiB80, shows sliding marks that appear to be covered by a compacted transfer layer (shown in magnified view) along with loose debris particles.

A discontinuous transfer layer could be seen on the worn surface of TiB85, along with a few locations from where it appears to have got detached (Fig. 5.8(f)).

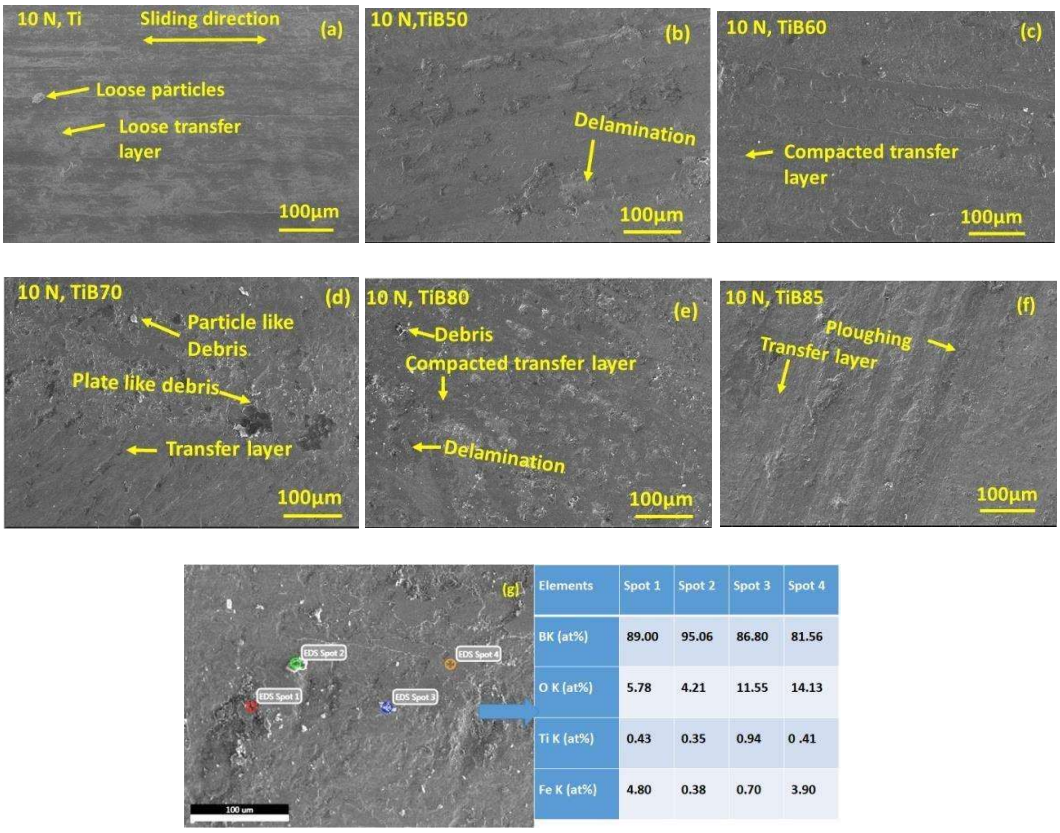

Elements	Spot 1	Spot 2	Spot 3	Spot 4
BK (at%)	89.00	95.06	86.80	81.56
O K (at%)	5.78	4.21	11.55	14.13
Ti K (at%)	0.43	0.35	0.94	0 .41
Fe K (at%)	4.80	0.38	0.70	3.90

Figure 5. 7 SEM images of worn surfaces of composite at a load of 10 N (a)Ti, (b) TiB50, (c) TiB60, (d) TiB70, (e) TiB80, (f) TiB85, and (g) EDS of worn surface for TiB50

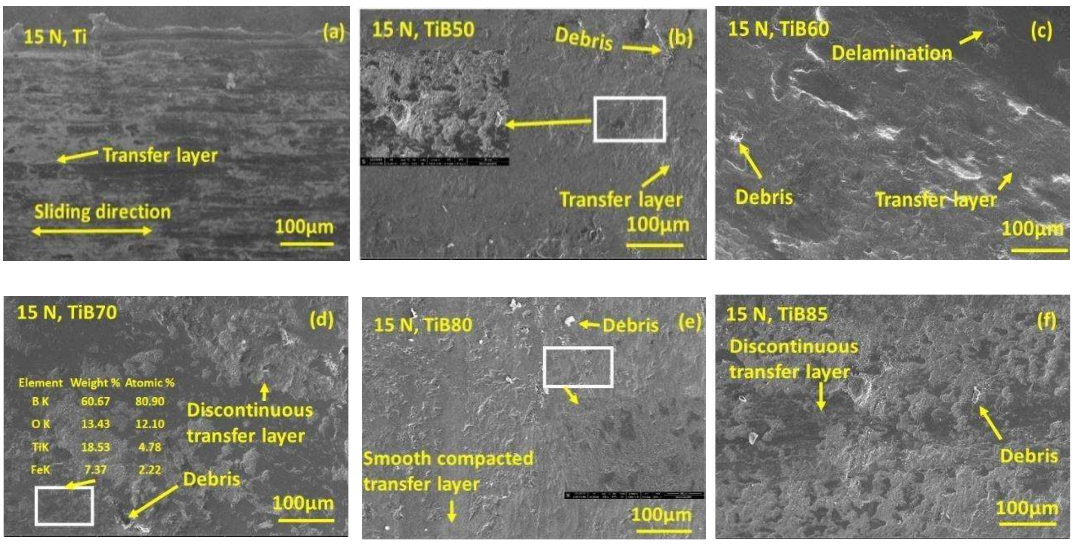

Figure 5. 8 SEM and EDS of worn surfaces of composite at a load of 15 N (a) Ti, (b) TiB50, (c) TiB60, (d) TiB70, (e) TiB80 and, (f) TiB85

Figure 5.9 (a through f) depicts the micrographs of the worn surface of composites slid under a load of 20 N as examined under SEM. The worn surface of pure Ti presents ploughing marks along with plastic deformation in a few regions as seen in Fig.5.9 (a). The worn surface of TiB50 shown in Fig. 5.9 (b) reveals a broken surface with a loosely bound transfer layer along with delamination and large wear particles, whereas some delamination, a few large debris marked by an arrow, and cracks at a few locations of TiB60 as seen from Fig. 5.9 (c). A highly delaminated and broken surface could be observed on the worn surface of TiB70 as seen in Fig. 5.9 (d). Figure 5.9 (e), corresponding to TiB80, shows sliding marks that appear to be covered by a smooth compacted continuous transfer layer and few signs of delamination. A discontinuous transfer layer could be seen on the worn surface of TiB85, which appears to have detached and delaminated at a few locations (Fig. 5.9 (f)).

The worn surface morphologies of pure Ti and composites slid under a load of 25 N are presented in Fig. 5.10 (a through f). The worn surface of pure Ti (Fig. 5.10 (a)) shows the presence of ploughing, plastic deformation on edges, along with a transfer layer of oxides. One may observe the presence of a transfer layer and signs of delamination over the worn surface of all the composites (Figs. 5.10 (b to f)) but with a different area of coverage and degree of compaction, except for TiB70 and TiB85, which also reveal some ploughing marks as indicated by arrows on respective micrograph. EDS of worn surfaces of all the composites has revealed the presence of oxygen over the surface as seen in Fig. 5.10 (a through f).

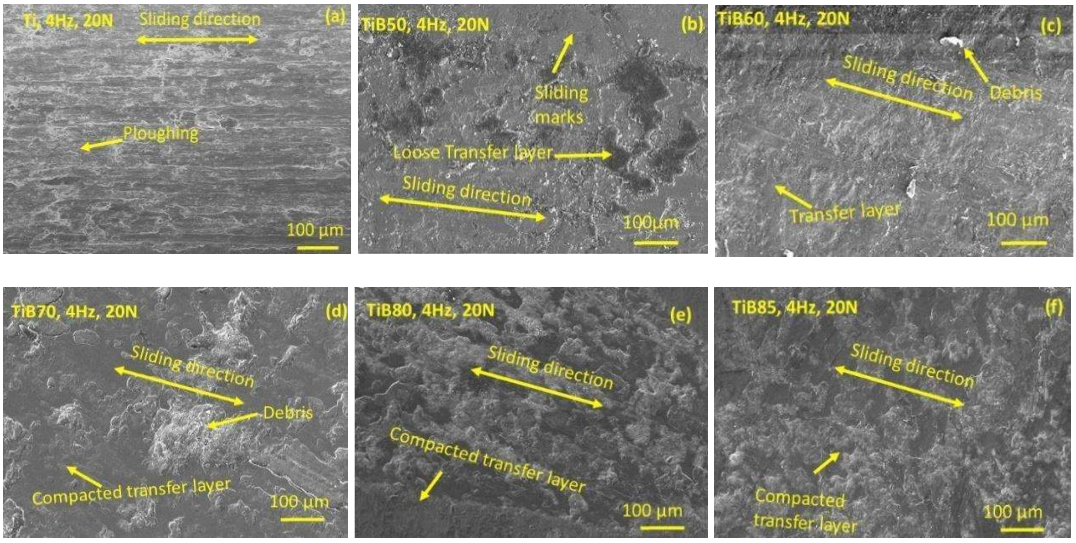

Figure 5. 9 SEM images of worn surfaces of composite at a load of 20 N (a)Ti, (b) TiB50, (c) TiB60, (d) TiB70, (e) TiB80 and, (f) TiB85

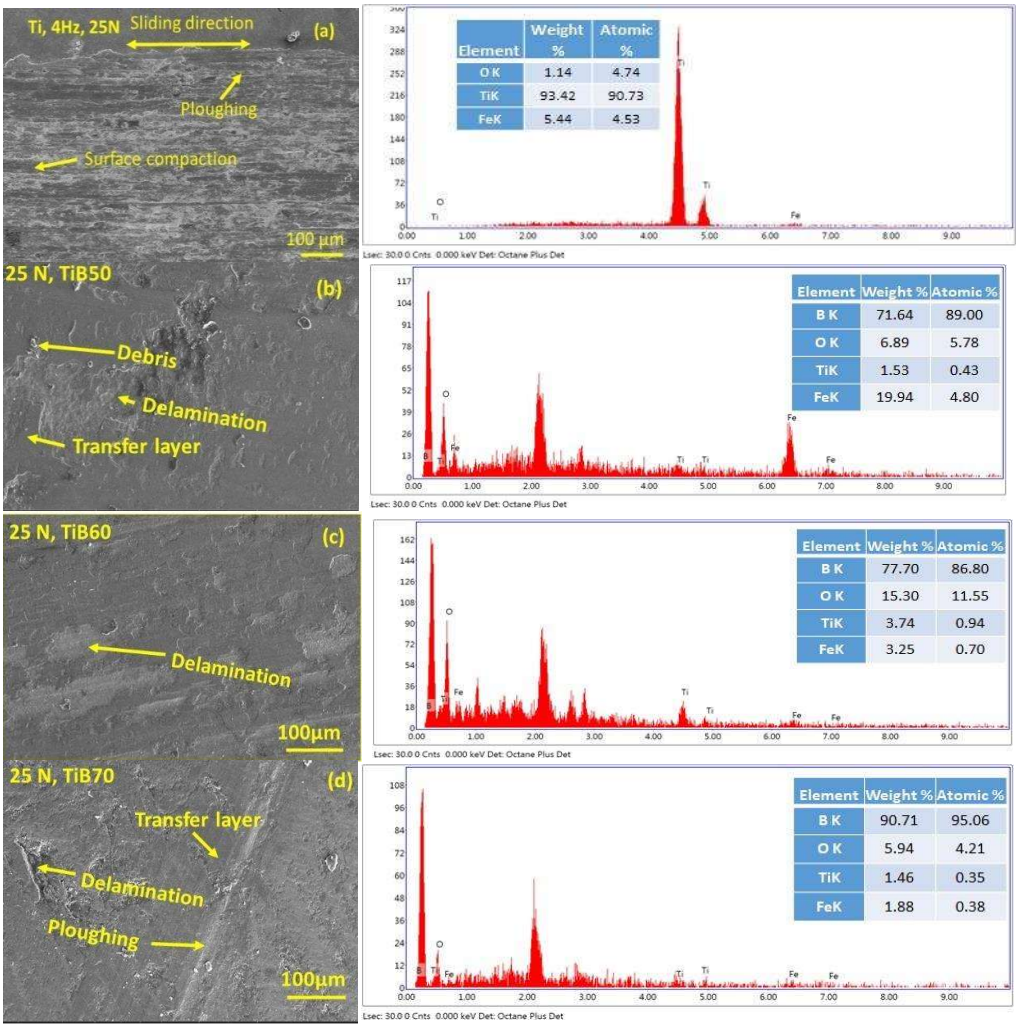

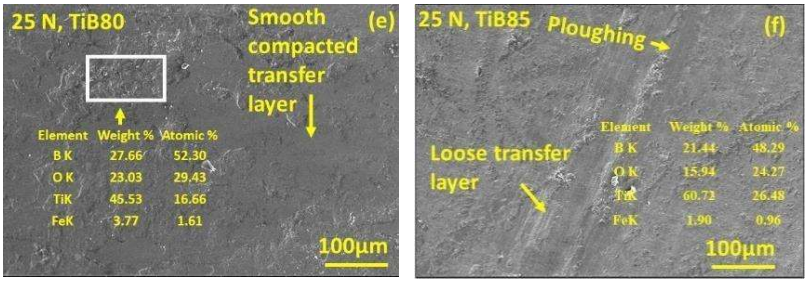

Figure 5. 10 SEM images and EDX of worn surfaces of composite at a load of 25 N (a)Ti, (b) TiB50, (c) TiB60, (d) TiB70, (e) TiB80 and, (f) TiB85

5.1.5 WORN SURFACE MORPHOLOGY OF COUNTERFACE

The morphologies of the worn surfaces of steel ball slid against Ti, TiB50, TiB60, TiB70 TiB80, and TiB85 composite at the loads of 10, 15, 20, and 25 N are illustrated in Fig. 5.11, 5.12, 5.13 and 5.14 (a through f). Figure 5.11 (a through f) depicts the micrographs of the counterface ball slid under a load of 10 N as examined under SEM. The worn surface of ball slid against pure Ti shows the presence of the transfer layer of material which might have been transferred from Ti along with a few regions from where this layer appears to have got detached, as seen in Fig.5.11 (a). The worn surface of counterface ball used against TiB50 shown in Fig. 5.11 (b) reveals the presence of sliding marks along with a transfer layer and loose wear particles. Similar features are observed on the worn surface of ball slid against TiB60, TiB70, TiB80 and TiB85 as seen from Figs. 5.11 (c), (d), (e) and (f), respectively, with varying extent of coverage of transfer layer over the surface and detachment of this layer. The worn surface of ball slid against TiB80 appears to have the largest coverage with almost no signs of detachment.

Figures 5.12 (a through f) show the SEM images of the worn surface of the counterface ball slid against Ti and TiB composites under normal load of 15 N. The worn surface of the ball slid against pure Ti presents sliding marks along with smooth transfer layer (Fig.5.12 (a)). The worn surface of counterface ball used against TiB50 shown in Fig. 5.12 (b) reveals a rough surface and smooth transfer layer with delaminated regions

along with some debris particles, whereas the worn surface slid against TiB60 shows wider sliding marks along with a transfer layer with little area coverage as seen from Fig. 5.12 (c). A loosely compacted and broken transfer layer surface could be observed on the worn surface counterface ball used against TiB70 as seen in Fig. 5.12 (d). Figure 5.12 (e), corresponding to the counterface ball used against TiB80, is observed to be covered with a well compacted and continuous transfer layer with a relatively larger area of coverage of worn surface in comparison to others. A loosely bound transfer layer could be seen on the worn surface of the counterface ball slid against TiB85, which appears to be detached at a few locations (Fig. 5.12 (f)).

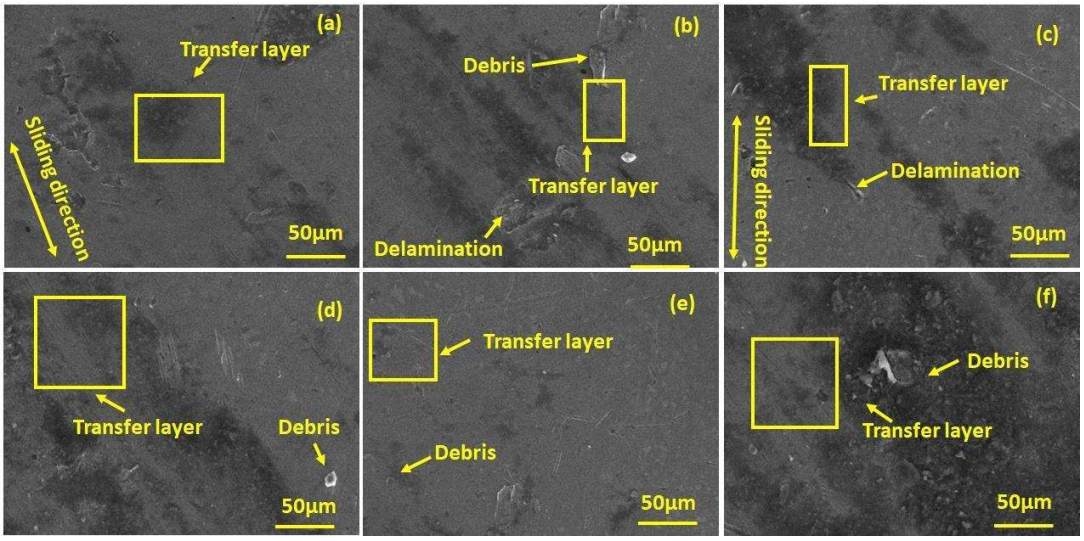

Figure 5. 11 SEM images of worn surfaces of bearing steel ball at a load of 10 N (a) Ti, (b) TiB50, (c) TiB60, (d) TiB70, (e) TiB80, and (f) TiB85

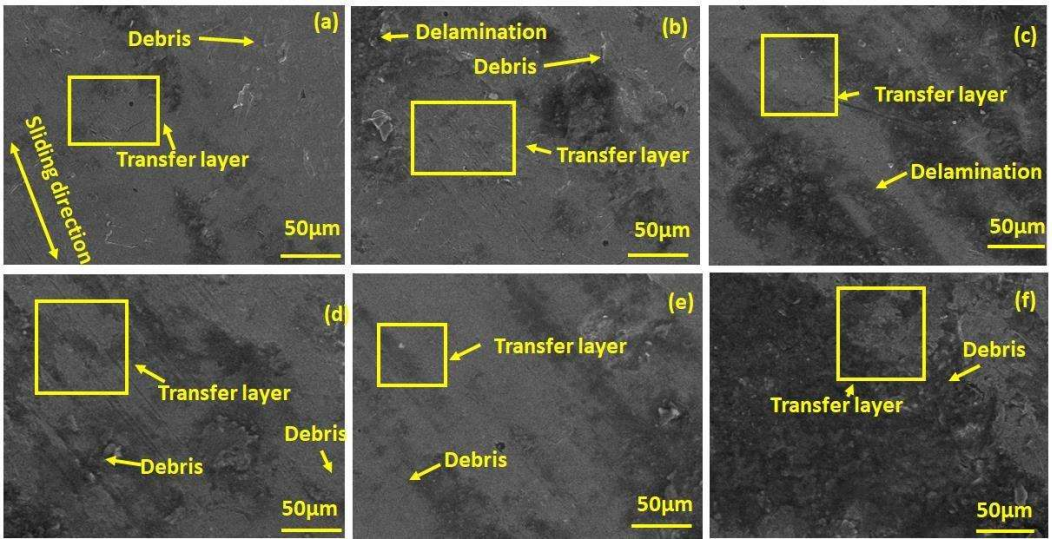

Figure 5. 12 SEM images of worn surfaces of bearing steel ball at a load of 15 N (a)Ti, (b) TiB50, (c) TiB60, (d) TiB70, (e) TiB80 and, (f) TiB85

Figures 5.13 (a through f) show the SEM images of worn surface of the counterface slid against Ti and TiB composites under a normal load of 20 N. The worn surface slid against pure Ti is observed to have a smooth transfer layer as seen in Fig.5.13 (a). The worn surfaces of balls used against TiB50 (Fig. 5.13 (b)) and TiB60 (Fig. 5.13 (c)) reveals present a deeply torn and rough surface probably due to abrasive action of TiB. A loosely compacted and broken transfer layer could be observed on the worn surface counterface ball used against TiB70 as seen in Fig. 5.13 (d) whereas the surface slid against TiB80 reveal the presence of transfer layer and worn patches indicating the removal of material (Figure 5.13 (e)). A relatively thin transfer layer along with fine sliding marks could be seen on the worn surface of the counterface ball used against TiB85 as evident from Fig. 5.13 (f).

The worn surface of ball slid against pure Ti presents sliding marks along with a smooth transfer layer in a few regions and EDS reveals the presence of O on the surface

as seen from Fig.5.14 (a). The worn surface of ball used against TiB50 shown in Fig. 5.14 (b) reveals a rough surface with a scattered presence of transfer layer, whereas the worn surface of ball slid against TiB60 presents a smooth and compacted transfer layer TiB60(Fig. 5.14 (c)). A loosely bound transfer layer could be observed on the worn surface counterface ball used against TiB70 (Fig. 5.14 (d)) while a smooth, well compacted and continuous transfer layer is the feature of the worn surface of ball slid against TiB80 as seen from Fig. 5.14 (e). The transfer layer present on the worn surface of ball slid against TiB85 is observed to have cracked. EDS spectra of the worn surface against all the composites has revealed the presence of Ti and B with varying contents which indicate the transfer of material from the composite to counterface and presence of O reflects the occurrence of oxidation.

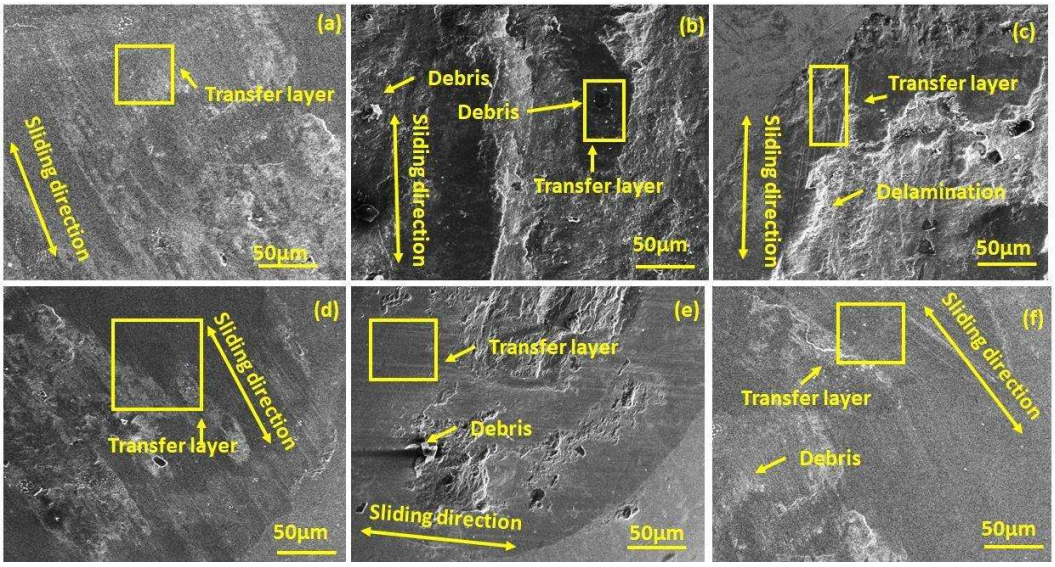

Figure 5. 13 SEM images of worn surfaces of bearing steel ball at a load of 20 N (a)Ti, (b) TiB50, (c) TiB60, (d) TiB70, (e) TiB80 and, (f) TiB85

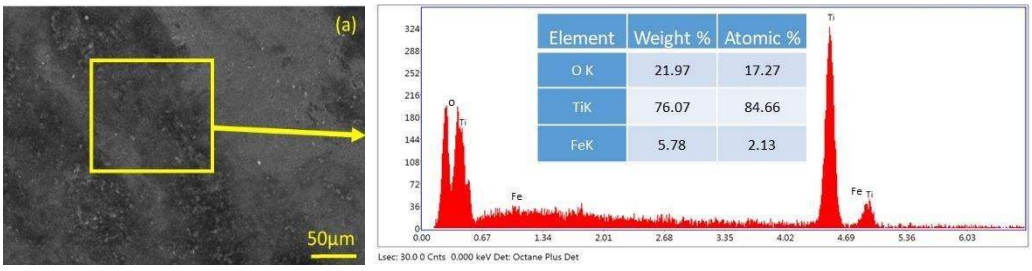

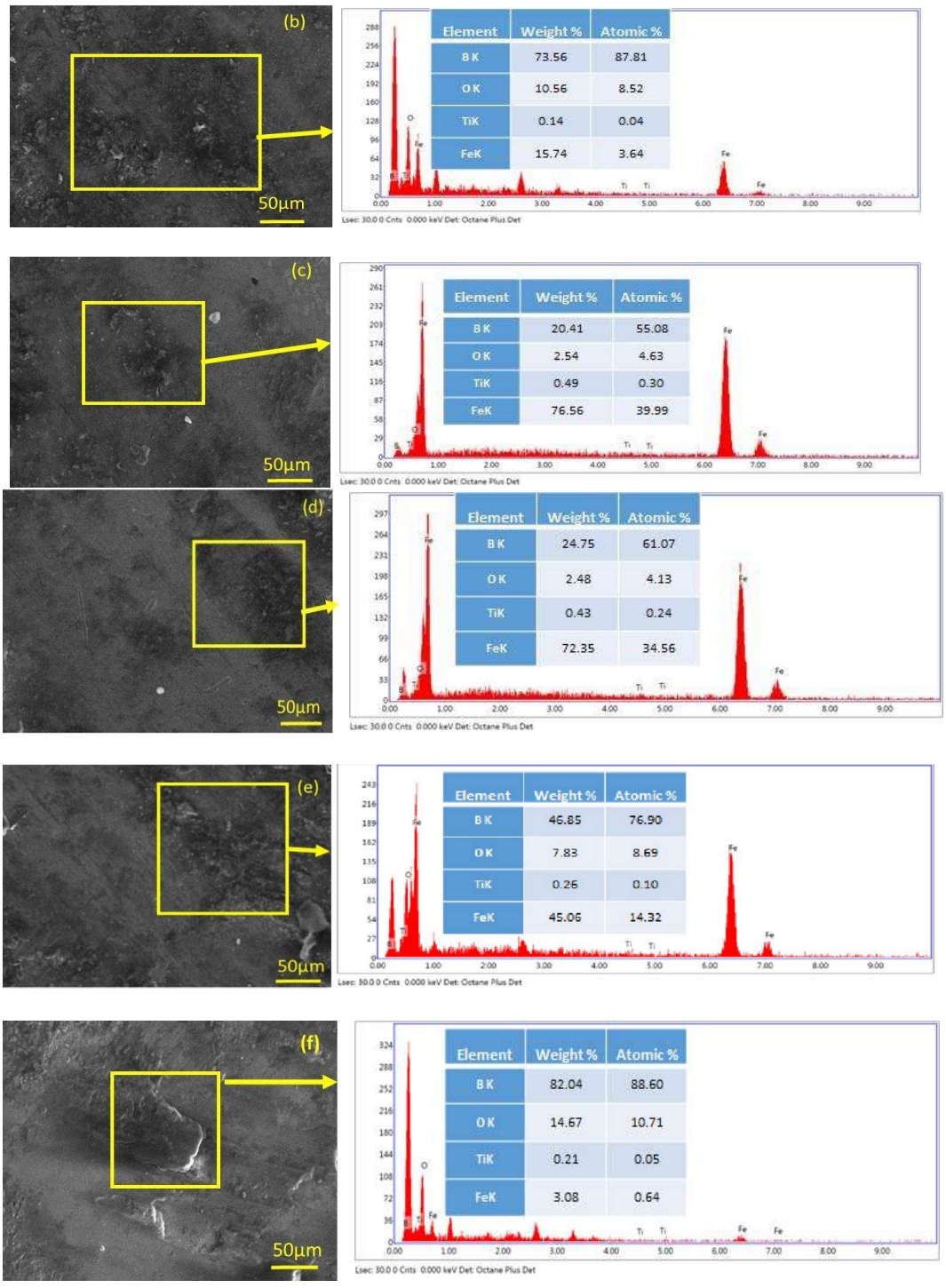

Figure 5. 14 SEM and EDS images of worn surfaces of bearing steel ball at a load of 25 N (a)Ti, (b) TiB50, (c) TiB60, (d) TiB70, (e) TiB80 and, (f) TiB85

5.1.6 MORPHOLOGY OF DEBRIS

Figure 5.15 (a through d) illustrates the SEM micrographs and EDS of wear debris collected after the wear tests for Ti and composites. Since the amount of wear debris was less, the debris for a particular composite at all the loads was pooled together before subjecting to examination under SEM. The debris collected after the wear test of pure Ti consists of fine particles, and EDS analysis reveals the presence of oxygen and iron in the worn debris, as seen from Fig. 5.15 (a). However, the debris corresponding to composites shows the presence of plate-like debris, fine irregular-shaped debris particles, along with some loose lumps of wear particles, as evident from Figs. 5.15 (b), (c), (d), (e) and (f). However, the amount of lumps and size of the plate-like debris appears to be for TiB70 and TiB80, whereas the size is relatively less for TiB50 and EDS of the marked area in debris indicates the presence of the oxygen and iron in high content with in TiB80 while it is low for other composites as seen from the EDS analysis shown on the micrographs.

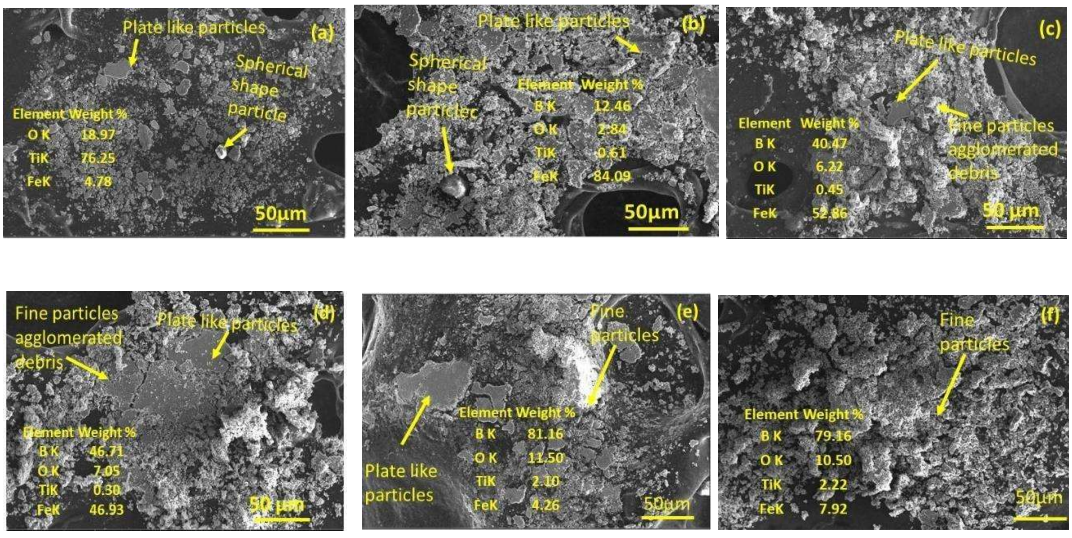

Figure 5. 15 SEM and EDS images of worn surfaces of pooled debris (a)Ti, (b) TiB50, (c) TiB60, (d) TiB70, (e) TiB80, and (f) TiB85

X-ray diffraction pattern of the wear debris of pure Ti given in Fig. 5.16(a) reveals the presence of peaks corresponding to Ti, TiO_2, TiO, and Fe_2O_3. Since, the amount of

wear debris for individual composites was too small to be subjected to X-ray diffraction, the wear debris of all the composites was pooled together for XRD analysis. Figure 5.16 (b) illustrates the X-ray diffraction pattern of the pooled debris which shows the peaks corresponding to Ti, TiB, TiO, FeTi, TiO_2 and B_2O_3 as mapped using high score plus software and its reference cards [Ti (ICSD 98-005-2522), TiB (ICSD 98-061-5596), B_2O_3 (ICSD 98-065-4204), FeTi (ICSD 98-063-3925), TiO (ICSD 98-004-0125), TiO_2 (ICSD 98-006-9331), Fe_2O_3 (ICSD 98-020-1099)]. However, the strong peaks correspond to Ti and its oxides.

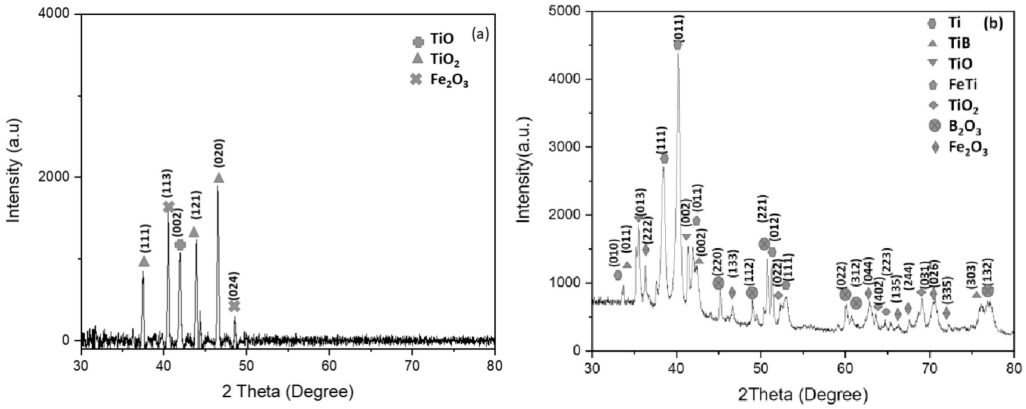

Figure 5. 16 XRD spectra of the debris

5.1.7 XPS ANALYSIS OF DEBRIS

X-ray photoelectron spectroscopy (XPS) has been performed to study the structural and chemical state of the elements present in wear debris. Figure 5.17 (a) shows the XPS spectra of the pooled debris of composites whereas the detailed spectra corresponding to B 1s, Fe 2p, and Ti 2p are shown in Figs. 5.17 (b), (c) and (d), respectively. The presence of some peak of carbon in Fig. 5.17 (a) may be due to carbon tape which might have stuck to some debris particles during processing to prepare the specimen for XPS. The spectra given in Figs. 5.17 (b, c and d) indicate that B_2O_3, H_3BO_3, TiO, TiO_2, and Fe_2O_3 are formed during the sliding process. Fig. 5.17 (b) shows the high-

resolution XPS spectrum of the B1s wherein two bands at 192.9 and 193.3 eV are detected which correspond to the presence B_2O_3 and H_3BO_3 and the results have been reported earlier [93-94]. The high-resolution XPS spectra of Ti 2p given in Fig.5.17 (c) shows peaks at 458.46, 458.59 and 464.1 eV which are assigned to Ti $2p_{3/2}$ and Ti $2p_{1/2}$ core levels. The presence of Fe doublets in Fig. 5.17 (d) indicates that the peak located at the binding energy of 710.55 eV corresponds to FeO while the peak at 724.14 eV pertains to Fe_2O_3 as reported by other researchers also [95,96]. The presence of iron oxides reflects the transfer of iron from ball during wear process and its oxidation due to frictional heating.

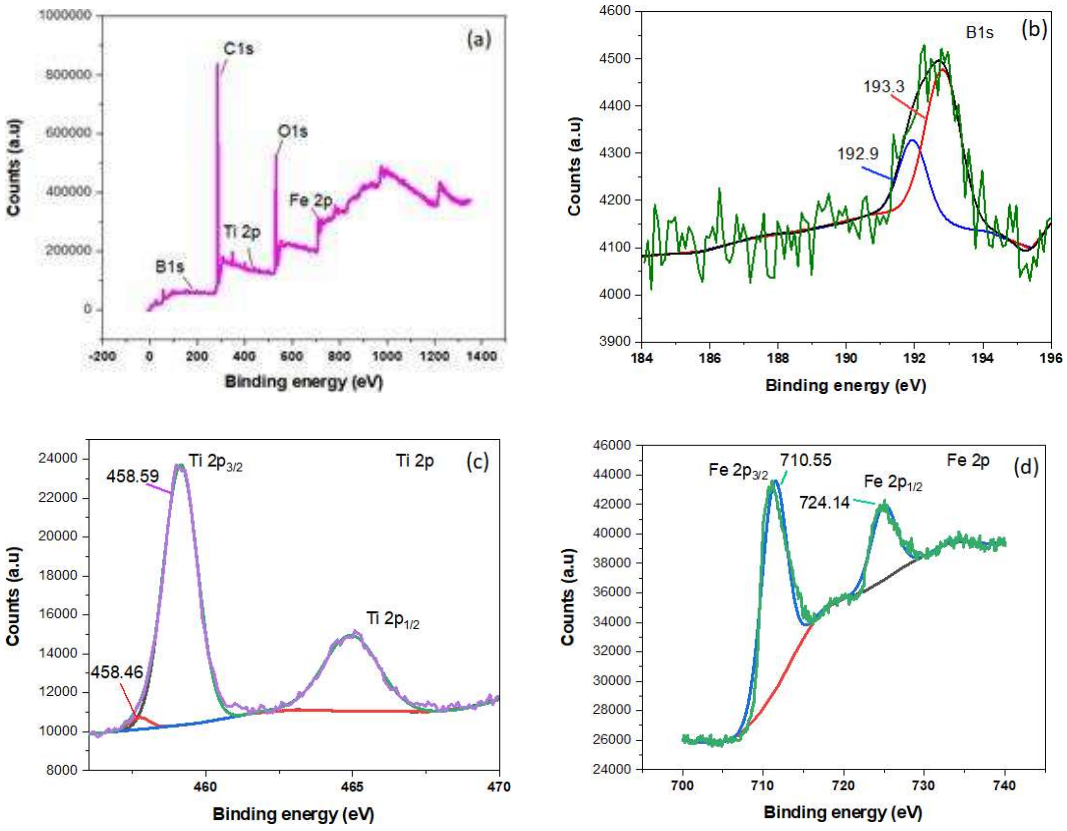

Figure 5. 17 High resolution XPS spectra of pooled debris of composites (a) full XPS spectra (b) B1s, (c) Ti 2p and (d) Fe 2p

5.2 DISCUSSION

The observed change in morphology of TiB from high aspect ratio whiskers to blocky TiB with increasing TiB vol. % is consistent with the earlier observations [97-99]. It may be explained on the basis of the mean-free path available for the growth of TiB whiskers from the TiB_2 particles and the nature of diffusion of B in TiB and backward diffusion of Ti in TiB_2 as suggested earlier [100]. The presence of hollow TiB whiskers (Fig. 5.3 (k)) may be due to shrinkage during transformation as reported by Tjong and Mai [101]. The hardness has been found to increase from 799 to 895 HV with an increase in TiB from 50 to 85 vol.%. The Vickers hardness value of TiB is 1800 HV as reported by Chandran et al [102]. Due to its higher hardness, the TiB phase imparts strength to the composites, and therefore, higher TiB content in the composites might have resulted in higher hardness with respect to pure Ti. Similar observations have been reported by other researchers [103,104] as well.

A fluctuating trend of variation of coefficient of friction with time observed in Figs.5.4 (a-f) may be attributed to the initial roughness of the contacting surfaces. It is well known that the surfaces of the engineering are rough and have asperities. As the relative sliding motion between the two bodies ensues, contact occurs at these asperities, which causes fluctuation in amplitude during sliding. However, the surfaces evolve to attain better conformity to each other after a certain period of sliding, leading to stabilization depending on the conditions of speed, load and microstructure as seen from Fig. 5.3 (a-f). Both the coefficient of friction and the wear rate have been observed to increase with increasing load for all the materials used in the present study i.e., Ti, TiB50, TiB60, TiB70, TiB80, TiB85 as seen from Figs. 5.4 (a) and 5.5 (a) indicating the followance of Archard's law [105]. An increase in load results in an increased generation

of wear debris which either gets trapped in-between the mating surfaces or comes out of the sliding interface as wear particles giving rise to mass loss and hence, increased wear rate. The entrapped wear debris may either (i) remain as loose particles, causing more loss of material to abrasive action, or (ii) get churned into finer particles and form a transfer layer of debris which may either be loosely bound or well-compacted depending on the working conditions. A loosely bound transfer layer results in abrasion and also can be detached easily from the surface. Both of these lead to an increase in the coefficient of friction as well as wear rate with an increase in load, as observed from Figs. 5.4 (b) and 5.5 (b).

In contrast, the formation of a smooth and compacted transfer layer of debris avoids the direct contact between the mating bodies and leads to a reduction in both friction and wear. A comparative analysis of the surfaces worn under loads of 10, 15, 20, & 25 N and presented as Figs. 5.6 to 5.10 (a through f) reflect the occurrence of ploughing and delamination, which appear to have increased with increasing load. Pure Ti shows abrasive wear, which increases with increasing load as evident from Figs. 5.6 (a) to 5.10 (a). Delamination occurs due to cyclic stress on the surface, leading to the pulling of TiB colonies from the matrix and formation of loose particles via brittle fracture leading to the accelerated material removal rate as evident from several areas with features of microfracture on the worn surfaces and counterface i.e., Figs. 5.6 to 5.10, and 5.11 to 5.14. However, microfracture events seem to be less probable on surfaces of composites either worn under lower load or containing a higher fraction of TiB. Hence, an increase in COF and wear rate for each composite with increasing load may be attributed to the formation of the loose particles at relatively low loads due to low stress scratching abrasion and three-body abrasion at relatively higher loads where the particles trapped

between the surface get crushed leading to high-localized stress and cause the loss of material by abrasive action.

The variation of COF as well as wear rate with respect to TiB vol.% may be explained on the basis of the interplay of the following factors, i.e., (i) the presence of loose wear particles over the worn surface, (ii) formation of a transfer layer of wear debris over the surface, (iii) the degree of compaction and the extent of cover provided by the transfer layer to the underlying material and (iv) presence of oxides in the wear debris/transfer layer. The increase in average COF from TiB50 to TiB70 at a 10 N load (Fig. 5.15 (a)) may be attributed to the formation of a larger amount of wear debris with increasing content of TiB, which remains loose and is not able to get compacted as seen from a comparison of Figs. 5.15 (b, c, & d). However, the debris appears to have formed a compacted transfer layer over the surface of TiB80 (Fig. 5.15(f)), which might have reduced the friction by avoiding the direct contact between the mating materials as seen from Fig. 5.15 (e). A decrease in wear rate from TiB50 to TiB80 may again be explained on the basis of the fact that the amount of debris increases with increasing load and TiB content which forms a protective transfer layer as stated earlier. The increased amount of wear debris offers more opportunity for agglomeration and the formation of a transfer layer covering the larger area fraction of the sliding interface. This transfer layer gets compacted due to the increased frictional heat at relatively higher loads and forms a smooth plateau over the surface. This reduces direct metal-metal contact between sliding bodies and, hence, both friction and wear with an increasing amount of TiB in the composites. The formation-compaction-detachment-reformation of the transfer layer leads to the generation of wear particles of different sizes varying from fine to plate-like, as seen from Fig. 5.15. The transfer layer has been observed to contain oxides, as evident from the EDS analyses given in Figs. (5.6 - 5.10 and 5.11-5.14), X-ray diffraction of the

wear debris (Fig. 5.16) and XPS of the wear debris (Fig. 5.17) along with the material transferred from composite to counterface steel (Fig. 5.11-5.14). Hence, the contact occurs between the transfer layer on the composite surface containing oxides and the material transferred to the counterface which helps in reducing both friction and wear [106]. Another factor contributing to the decrease in friction and wear rate may be the presence of the lubricious oxides of Ti namely, TiO, TiO_2, B_2O_3 and H_3BO_3 [107–110] in the wear debris as evident from X ray diffraction analysis and XPS given in Figs. 5.16 and 5.17. The presence of B_2O_3 and H_3BO_3 has been reported to be beneficial in improving the wear resistance with a simultaneous reduction in COF in Ti-based composites [111]. SEM examination of worn surfaces, XRD and XPS analyses of wear debris indicate that the wear mechanism of pure Ti is a mix of ploughing, adhesion and oxidation. However, the operative mechanisms for Ti-TiB composites are adhesion, oxidation, delamination and abrasion.

Based on the results, it can be concluded that 80 Vol.% TiB has the optimum performance in terms of coefficient of friction and wear rate under the sliding conditions used in the current study. The composite having 85 vol. % TiB has shown a slightly higher coefficient of friction as compared to TiB80 due to the presence of a loose transfer layer on the worn surface of TiB85, as evident from Figs. 5.6 (f) to 5.10 (f), which results in abrasion by hard debris particles and consequent increase in coefficient of friction.

Based on the results and discussion presented above it can be inferred that the present investigation on the synthesis and tribological characterization of in-situ Ti-TiB composites has led to following salient conclusions.

1. In-situ Ti-TiB composites containing different (50, 60, 70, 80, and 85) vol.% of TiB were successfully synthesized by a cost-effective vacuum arc melting

process. The morphology of TiB changed from needle-like whiskers to blocky structures with increasing content of TiB. The hardness of the composites increased with increasing content of TiB from 50 to 85 vol. % due to the higher intrinsic hardness of TiB.

2. Both the coefficient of friction and wear rate increased with increasing load for all the composites. At a given load, the coefficient of friction and the wear rate of the composites decreased from 50 to 60 Vo.% TiB followed by an increase for 70 Vol.% and a reduction thereafter till 80 vol.% and remained almost the same thereafter till 85 vol.% TiB.
3. The composite having 80 vol.% TiB showed the lowest coefficient of friction and wear rate among all the composites. The observed behavior has been explained on the basis of the formation of a transfer layer of wear debris over the surface, its degree of compaction and presence of lubricious oxides (TiO_2, B_2O_3 and H_3BO_3).
4. The operative mechanism of wear is a mixture of ploughing, adhesion and oxidation for pure Ti whereas the same for composites is adhesion, oxidation, delamination and abrasion. The results indicate that these composites offer an opportunity to be used in sliding wear applications.

PART B

5.3 FRICTION AND WEAR BEHAVIOR OF COMPOSITES

In the present section, the results on the effect of load on reciprocating wear behavior of vacuum arc melted composites examined by conducting friction and wear tests under different loads of 10, 15, 20, and 25 N at a fixed sliding frequency of 7 Hz.

5.3.1 (i) Variation of coefficient of friction with time

Figure 5.18 (a through f) demonstrates the variation of coefficient of friction (COF) with time at different loads for pure Ti, TiB50, TiB60, TiB70, TiB80, and TiB85 respectively. The variation of coefficient of friction with time for pure Ti shows a stable trend with a minute fluctuation in amplitude and effectively no running-in period as seen from Fig. 5.18 (a). A relatively larger fluctuation in amplitude could be observed in Figs. 5.18 (b, c and d) in comparison to Figs.5.18 (e and f) depending on the applied load even after the running-in period. The COF appears to get stabilized relatively earlier (200 s) for TiB50 at loads of 15, and 20 N in comparison to 10 and 25 N load (400 s), as evident from Fig. 5.18 (b). For TiB60, COF at all the loads is observed to stabilize soon after the run-in period of ~ 200 s as shown in Fig. 5.4 (c), whereas for TiB70 it shows relatively larger fluctuations around a mean level at 10 N, however, COF gets stabilized after 100 s for 20 N whereas for 15 and 25 N it stabilizes around 600 s as seen from Fig. 5.18 (d). In case of TiB80 and TiB85, the COF is found to stabilize after the running in-in period is over depending on the load as seen from Figs. 5.18 (e and f).

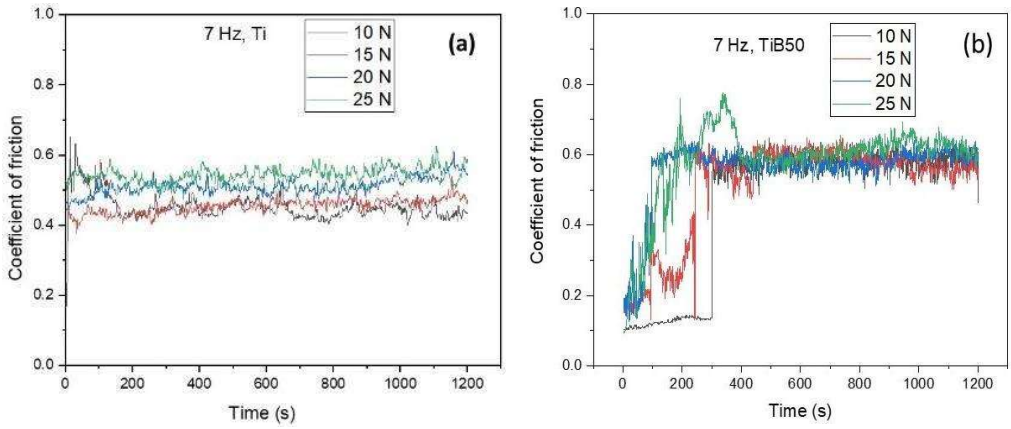

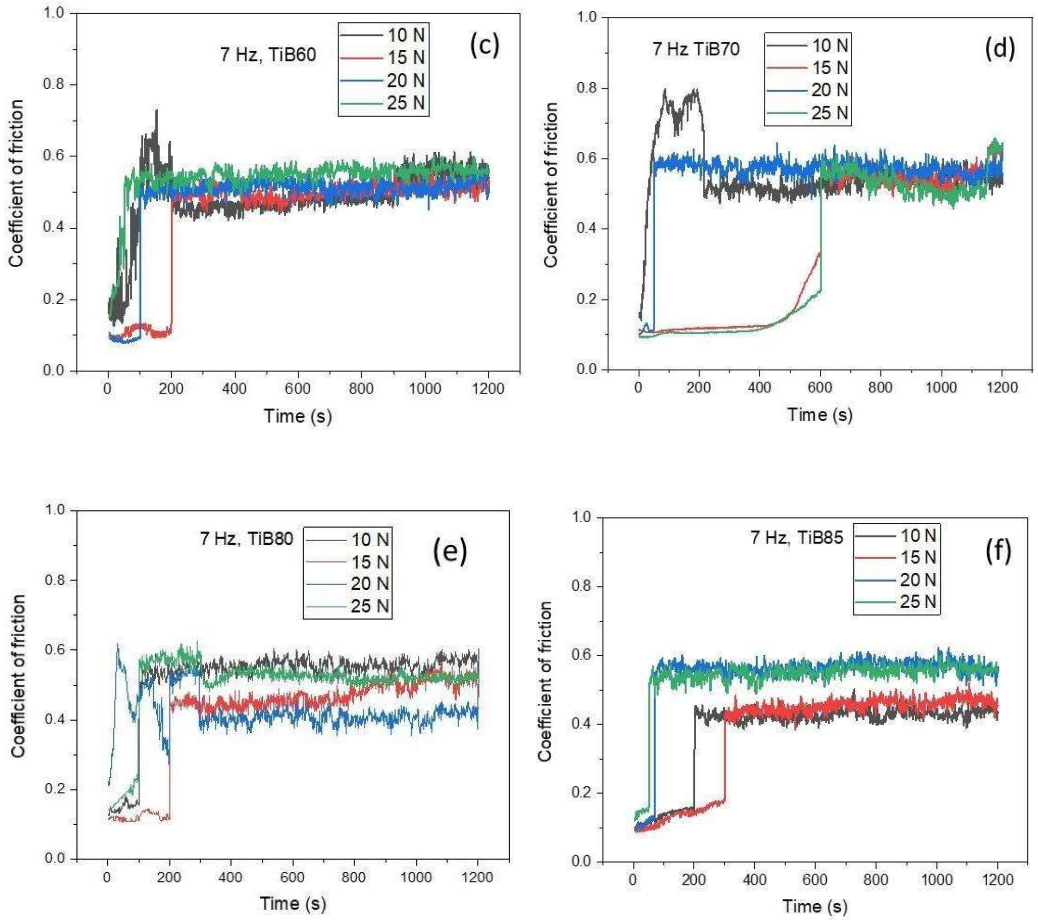

Figure 5. 18 Variation of coefficient of friction with time for 10 N, 15 N, 20 N, and 25N at 7 Hz of different composites (a) Ti, (b) TiB50, (c) TiB60, (d)TiB70, (e) TiB80, and (f) TiB85.

(i) Variation of average steady coefficient of friction with normal load and composition

Figure 5.19 (a) presents the variation of average steady state coefficient of friction with the normal load whereas the variation with respect to composition is illustrated in Fig. 5.19 (b). The value of the average steady state coefficient of friction has been estimated by discarding the initial running-in period. The average COF is found to increase with increasing load for pure Ti. The average COF is the highest for 25 N as

evident from Fig.5.19 (a), whereas under the loads of 10 and 15 N, it has shown a lower coefficient of friction than TiB50 and TiB60. The coefficient of friction is observed to decrease with increasing load for all the composites and TiB80 has revealed the lowest coefficient of friction at all the loads as seen from Fig. 5.19 (a). One may observe an increase in steady state COF at the loads of 10 and 15 N as one moves from Ti to TiB50 which is followed by a decrease till TiB80 before increasing again for TiB85, as seen from Fig. 5.19 (b). However, at the loads of 20 and 25 N the steady state average COF has been observed to decrease from Pure Ti to TiB80 followed by an increase at 85 vol. % TiB as evident from Fig. 5.19 (b).

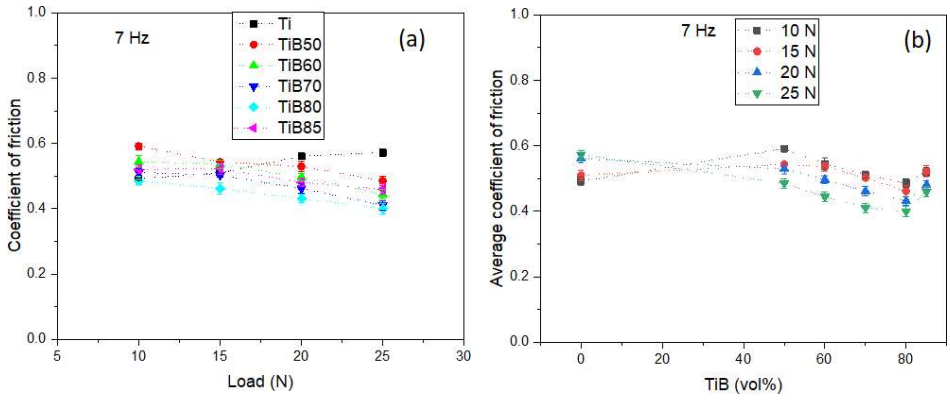

Figure 5. 19 Variation of average coefficient of friction with (a) load and (b) Composition

(ii) Variation of wear rate with normal load and composition

The variation of wear rate (mm^3/m) with load for all the composites shown in Fig. 5.20 (a) reveals that the wear rate increases with increasing load for Ti, however the increase is relatively sharp from 10 to 15 N, and it has the highest wear rate among all the materials at all loads. As far as composites are concerned, the wear rate has also been found to increase with load except for TiB50 which has shown an increase from 10 to 15 N followed by a decrease till 25 N. TiB80 has shown a consistently lower wear rate at all the loads as seen from Fig. 5.20 (a). The variation of wear rate with TiB vol.% depicted

in Fig.5.20 (b) indicates a sharp decrease in wear rate from pure Ti to composite TiB50 at all loads, indicating the effectiveness of TiB addition in reducing the wear rate. The wear rate is observed to decrease with increasing TiB content from 50 to 80 vol.% at loads of 10 and 20 N before increasing slightly to 85 vol.%, but for 10 and 25 N it is found to increase slightly from TiB50 to TiB60 before decreasing till TiB80 followed by a marginal increase for TiB85.as seen from Fig. 5.20 (b).

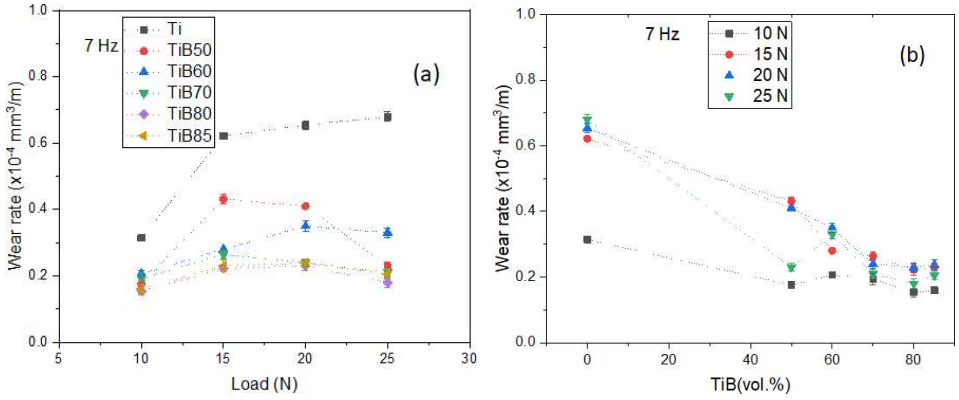

Figure 5. 20 Variation of wear rate with (a) load and (b) Composition

5.3.2 WORN SURFACE MORPHOLOGY OF COMPOSITE

Figures 5.21 (a through f) show the scanning electron micrographs of surfaces of Ti-TiB composites worn under the load of 10 N. Fig. 5.21 (a) corresponding to pure Ti shows the presence of ploughing marks along with a loosely bound transfer layer containing fine debris particles whereas one may observe the presence of a well compacted transfer layer on the worn surface of TiB50 (Fig. 5.21 (b)) with signs of delamination at a few places. The presence of transfer layer may explain the sharp decrease in wear rate from pure Ti to TiB50. The worn surfaces of TiB60, TiB70, TiB80 and TiB85 presented, respectively, in Figs. 5.21 (c), (d), (e) and (f) also reveal the

presence of a continuous and compacted transfer layer with varying extent of coverage and locations from where the layer appears to have got detached.

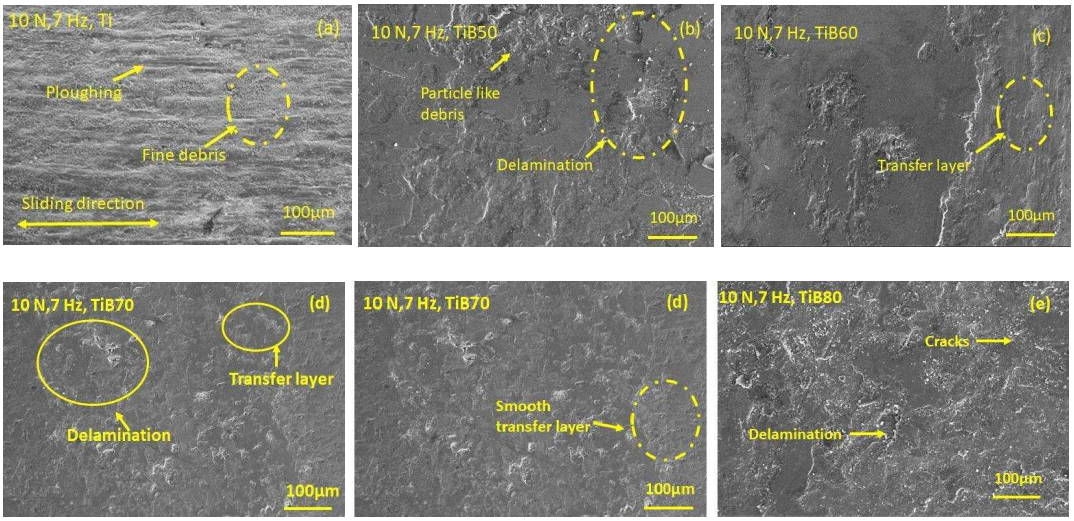

Figure 5. 21 SEM images of worn surface of TiB composite (a)Ti, (b) TiB50, (c) TiB60 (d)TiB70 (e) TiB80, and (f) TiB85 at 7 Hz and10 N

Figure 5.22 (a through f) depicts the micrographs of the worn surface of composites slid under a load of 15 N as examined under SEM. The worn surface of pure Ti reveals the presence of a loose transfer layer of wear debris as seen in Fig.5.22 (a). The worn surface of TiB50 shown in Fig. 5.22 (b) reveals a rough surface with the presence of a compacted transfer layer at a few locations and loosely bound layer along with some wear particles, whereas the layer appears to be relatively compact with some signs of delamination at a few locations TiB60 as seen from Fig. 5.22 (c). A loose and scattered transfer layer of wear debris, could be observed on the worn surface of TiB70 as seen in Fig. 5.22 (d). Figure 5.22 (e), corresponding to TiB80, shows sliding marks that appear to be covered by a compacted transfer layer along with loose debris particles. A discontinuous transfer layer and its delamination at a few locations could be seen for TiB85 (Fig. 5.22 (f)).

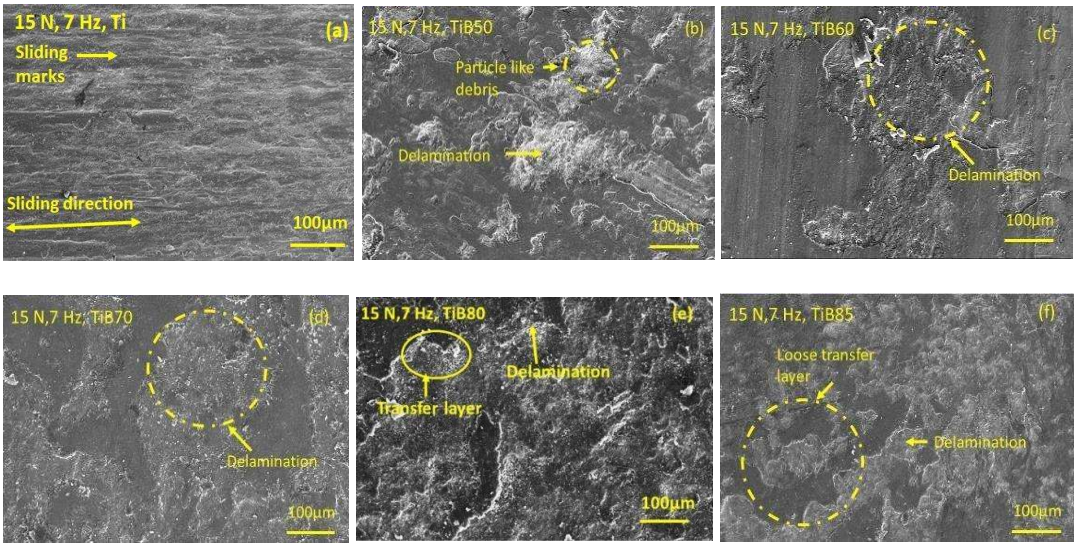

Figure 5. 22 SEM images of worn surface of TiB composite (a)Ti, (b) TiB50, (c) TiB60 (d)TiB70 (e) TiB80, and (f) TiB85 at 7 Hz and15 N

Figure 5.23 (a through f) depicts the micrographs of the worn surface of composites slid under a load of 20 N as examined under SEM. The worn surface of pure Ti presents deep ploughing marks and rough surface as seen in Fig.5.23 (a). The worn surface of TiB50 shown in Fig. 5.23 (b) reveals the presence of a transfer layer covering relatively less area of the surface, whereas the layer appears to be a bit compacted with some signs of delamination at a few locations TiB60 as seen from Fig. 5.23 (c). A transfer layer of loosely bound wear particles could be observed on the worn surface of TiB70 along with some delamination as seen in Fig. 5.23 (d). Figure 5.23 (e), corresponding to TiB80, shows a compacted transfer layer along with loose debris particles cover almost the entire surface whereas a discontinuous transfer layer with cracking at a few locations could be observed on the worn surface of TiB85(Fig. 5.23 (f)).

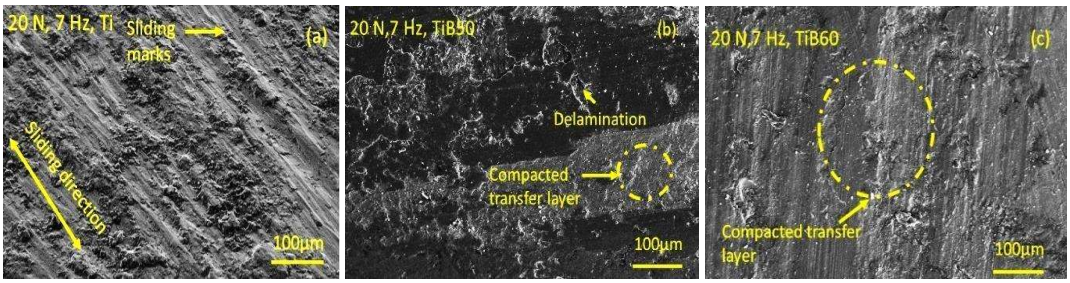

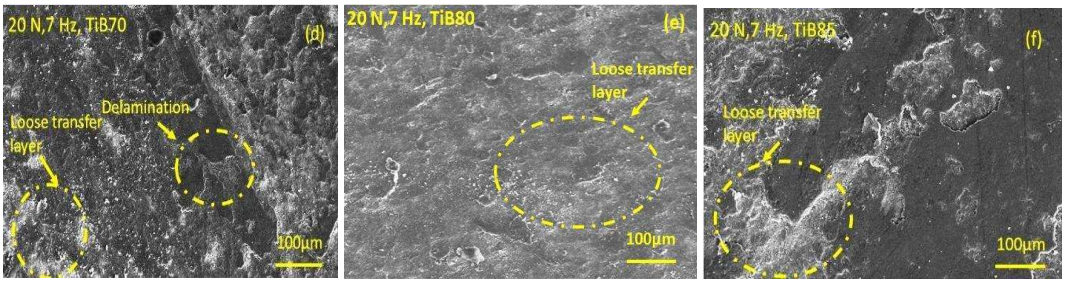

Figure 5. 23 SEM images of worn surface of TiB composite (a)Ti, (b) TiB50, (c) TiB60 (d)TiB70 (e) TiB80, and (f) TiB85 at 7 Hz and 20 N

Fine particle along with ploughing marks could be observed on the worn surface of Ti after sliding at a load of 25 N with very less oxidation on the surface as seen in EDS and micrograph presented as Fig. 5.24 (a). Worn surface of TiB50 shows surface compaction, delamination along with particle-like debris, EDS also reveals the presence of some O and Fe content (which might have been transferred from counterface ball) as seen in Fig. 5.24 (b). The worn surface of TiB60 shows presence of transfer layer, sliding marks & ploughing and EDS shows the O and Fe content is more compared to TiB50 as seen in Fig. 5.24 (c). Loose transfer layer at few points delamination and debris all over the surface could be seen for TiB70 (Fig. 5.24(d)) whereas a well-compacted transfer layer and a few delaminated regions are the features seen from worn surface TiB80 given in Fig. 5.24 (e). The worn surface of TiB85 (Fig. 5.24 (e)) reveals the presence of delamination and fine debris particles. All the EDS spectra show the presence of oxygen indicating the transfer layer may be containing the oxidised debri particles and oxides of Ti and Fe.

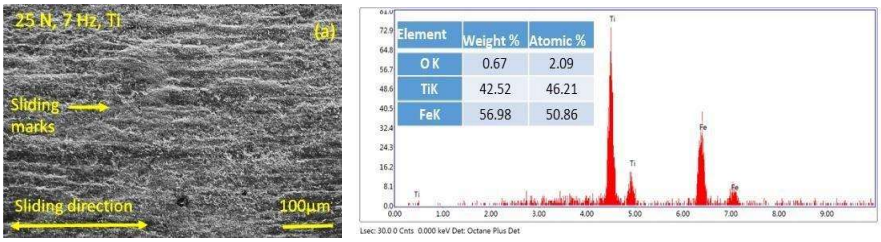

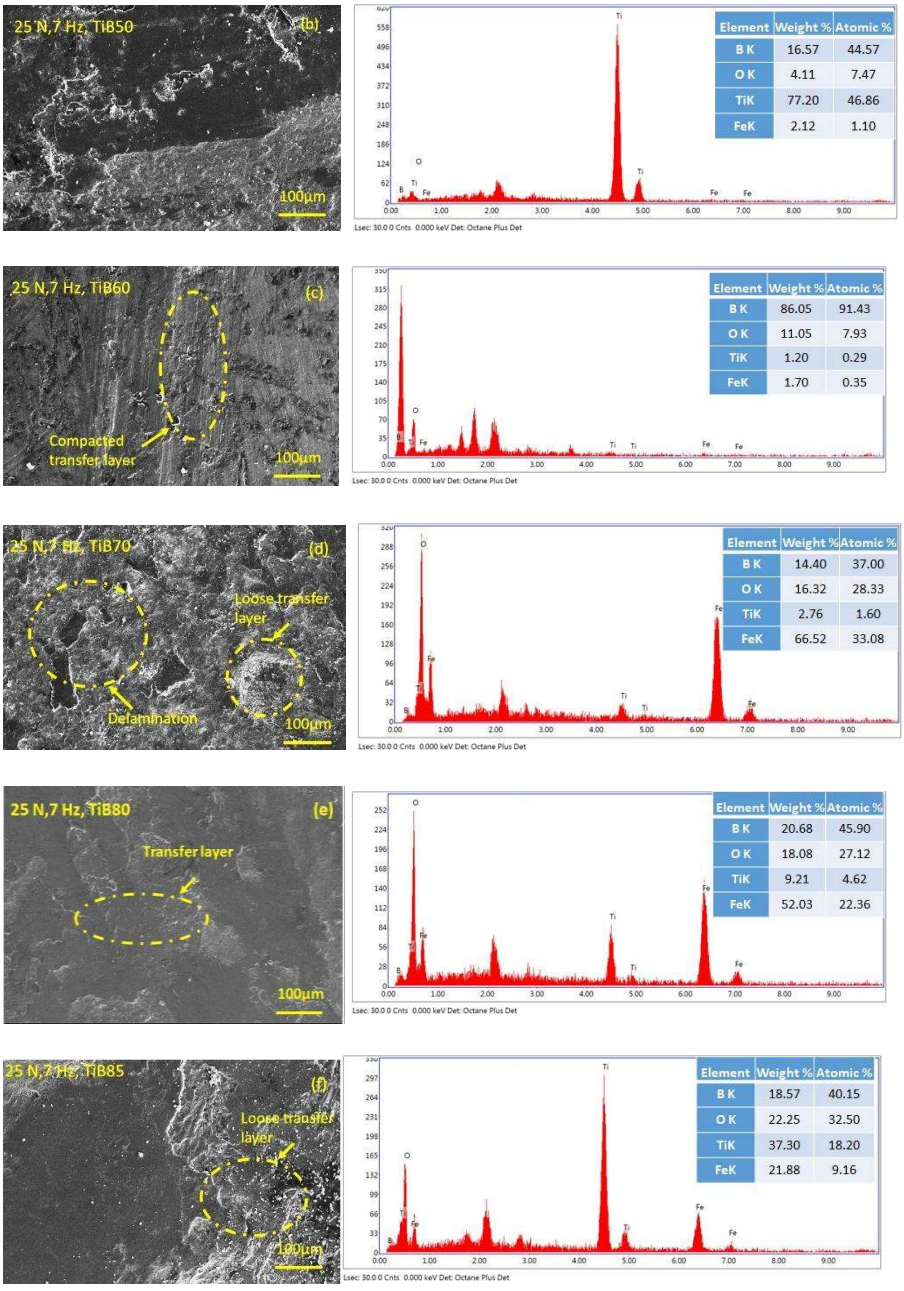

Figure 5.24 SEM and EDS images of worn surface of TiB composite (a)Ti, (b) TiB50, (c) TiB60 (d)TiB70 (e) TiB80, and (f) TiB85 at 7 Hz and 25 N

5.3.3 Worn Surface Morphology of counterface

The morphologies of the surface of counterface balls worn under the loads of 10, 15, 20, and 25 N have been examined under HR-SEM to elucidate the type of wear occurring during sliding of the balls against Ti as well as composites which are useful in

determining the type of wear mechanisms and material transfer, if any. Figure 5.25 (a through f) depicts the micrographs of the counterface ball slid under a load of 10 N as examined under SEM. The counterface ball for pure Ti presents a transfer layer as seen in Fig.5.25 (a). The worn surface of counterface ball used against TiB50 shown in Fig. 5.25 (b) reveals loosely bound surface, whereas some rough transfer layer and delamination can be seen on counterface ball used against TiB60 as seen from Fig. 5.25 (c). A patchy surface could be observed on the worn surface counterface ball used against TiB70 as seen in Fig. 5.25 (d). Figure 5.25 (e), corresponding to the counterface ball used against TiB80, shows large particle-like debris, compacted continuous transfer layer, and few signs of delamination. A transfer layer could be seen on the worn surface of the ball used against TiB85, which appears to be patchy at a few locations (Fig. 5.25 (f)) under a load of 10 N.

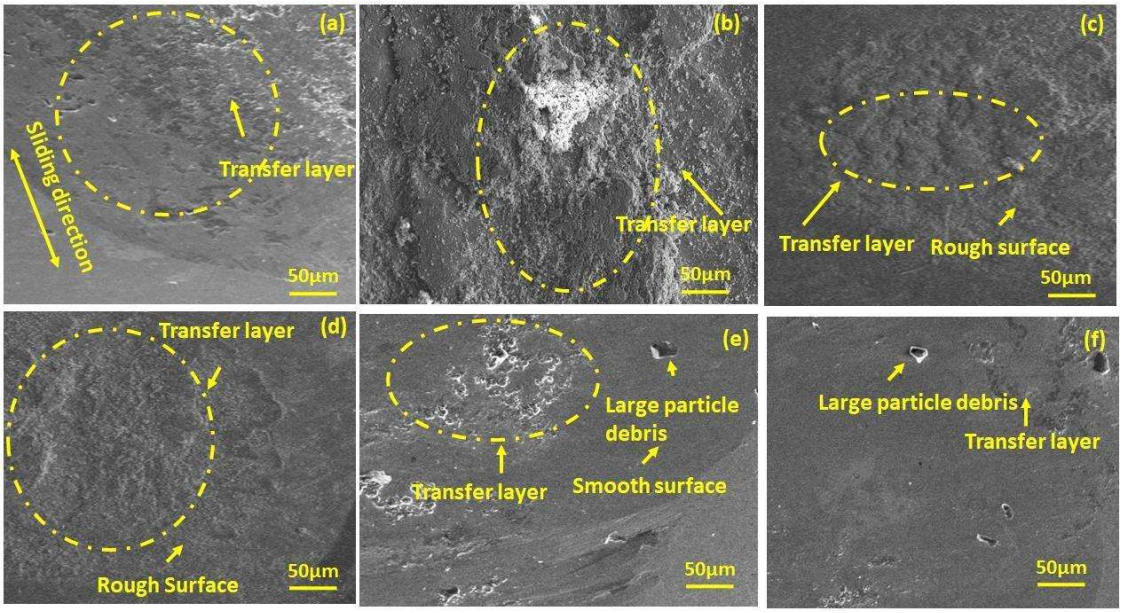

Figure 5. 25 SEM images of worn surface of counterface ball (a)Ti, (b) TiB50 (c) TiB60 (d)TiB70 (e) TiB80, and (f) TiB85 at 7 Hz and 10 N

Figure 5.26 (a through f) depicts the micrographs of the counterface ball slid under a load of 15 N as examined under SEM. The counterface ball for pure Ti presents a transfer layer with few delamination signs as seen in Fig.5.26 (a). The worn surface of counterface ball used against TiB50 shown in Fig. 5.25 (b) reveals debris and transfer layer, whereas some loose transfer layer at various positions of counterface ball is used against TiB60 as seen from Fig. 5.26 (c). A patchy surface could be observed on the worn surface counterface ball used against TiB70 as seen in Fig. 5.26 (d). Figure 5.26 (e), corresponding to the counterface ball used against TiB80, shows large particle-like debris, compacted continuous transfer layer, and few signs of delamination. A transfer layer could be seen on the worn surface of the counterface ball used against TiB85 (Fig. 5.26 (f)).

Figure 5.27 (a through f) depicts the micrographs of the counterface ball slid under a load of 20 N as examined under SEM. The counterface ball for pure Ti shows the presence of transferred material as seen in Fig.5.27 (a) whereas, that corresponding to TiB50 shown in Fig. 5.27 (b) reveals a transfer layer at a few locations. The worn surface of ball used against TiB60 as seen from Fig. 5.27 (c) reveals the presence of transfer layer with signs of cracking at some locations. Figures 5.27 (c), (d) and (f) corresponding to TiB70, TiB80 and TiB85 present a transfer layer with different degree of compaction along with patches of some agglomerated debri particles.

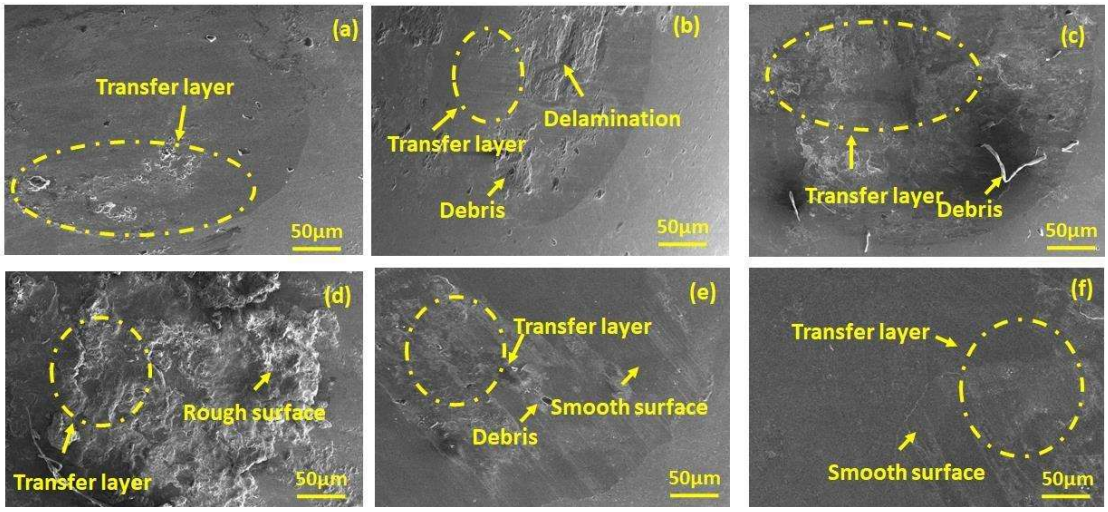

Figure 5. 26 SEM images of worn surface of counterface ball (a)Ti, (b) TiB50 (c) TiB60 (d)TiB70 (e) TiB80, and (f) TiB85 at 7 Hz and 15 N

Figure 5.28 (a through f) depicts the micrographs of the counterface ball slid under a load of 25 N as examined under SEM. The counterface ball slid against pure Ti presents a worn out surface in Fig.5.28 (a), probably due to higher load and this may have resulted in a higher loss of material. The worn surface of counterface ball used against TiB50 shown in Fig. 5.28 (b) reveals loose wear particles and transfer layer which appears to be cracking whereas more cracking of transfer layer appears to have occurred for the ball slid against TiB60 as seen from Fig. 5.28 (c). The presence of loose and agglomerated debris particles could be observed on the worn surface of balls used against TiB70 and TiB80 as seen in Fig. 5.28 (d) and (f), respectively, and the surfaces appear to be rough. However, a transfer layer could be seen on the worn surface of the counterface ball used against TiB85 (Fig. 5.28 (f)) with imminent cracks at a couple of locations.

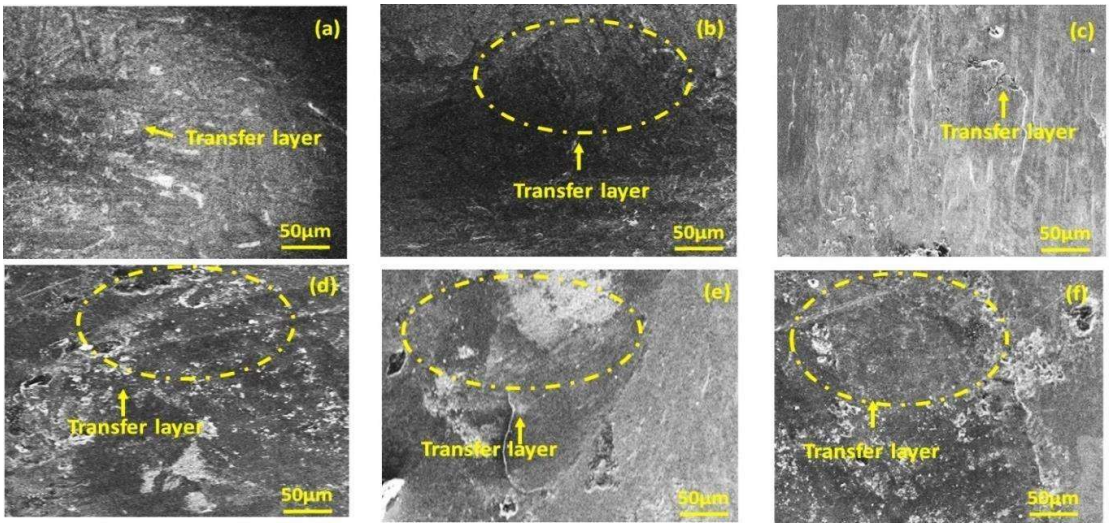

Figure 5. 27 SEM images of worn surface of counterface ball (a)Ti, (b) TiB50 (c) TiB60 (d)TiB70 (e) TiB80, and (f) TiB85 at 7 Hz and 20 N

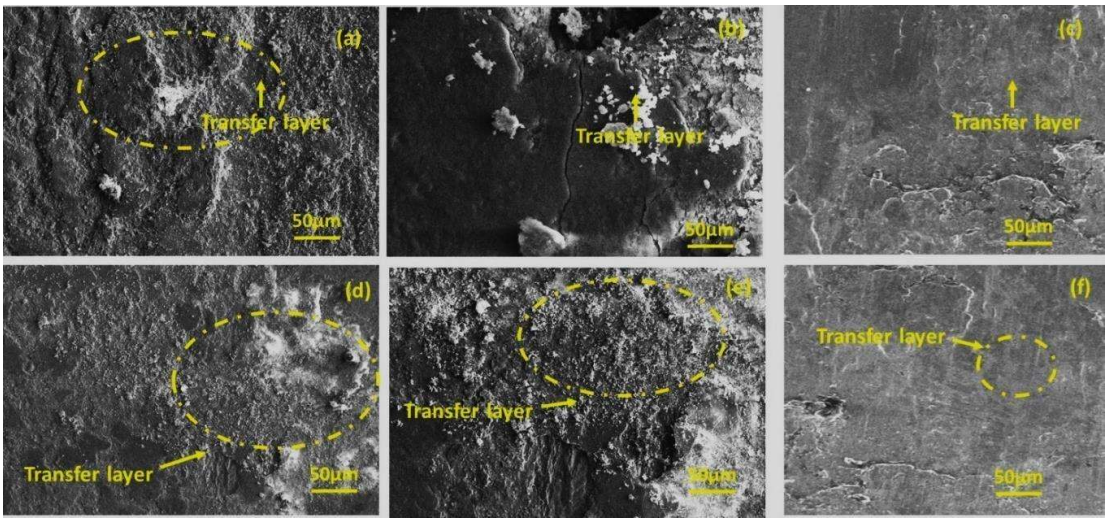

Figure 5. 28 SEM micrograph of worn surface of counterface ball (a)Ti, (b) TiB50 (c) TiB60 (d)TiB70 (e) TiB80, and (f) TiB85 at 7 Hz and 25 N

5.3.4 EXAMINATION OF WEAR DEBRIS

Figure 5.26 (a through f) shows the SEM micrographs and EDS of the wear debris generated during the tribo-test of Ti and TiB composites. The wear debris corresponding to pure Ti shown in Fig. 5.26 (a) has been found to contain some fine as well as larger particles of different shapes along with some agglomerated lumps. The wear debris corresponding to TiB50 and TiB60 appears to have some fine wear particles as well larger

plate like debris which might have come from the detachment of transfer layer as evident from Figs. 5.26 (b) and (c). The debris corresponding to TiB70, TiB80 and TiB85 shown in Figs. 5.26 (d, e, and f) reveals a mixture of relatively fine, regular and irregular shaped particles along with some lumps particularly for TiB85. XRD pattern of pooled debris show the peaks corresponding to TiB, TiO, TiO_2, and B_2O_3. The presence of B_2O_3 might have reduced friction due to its lubricious nature as stated earlier.

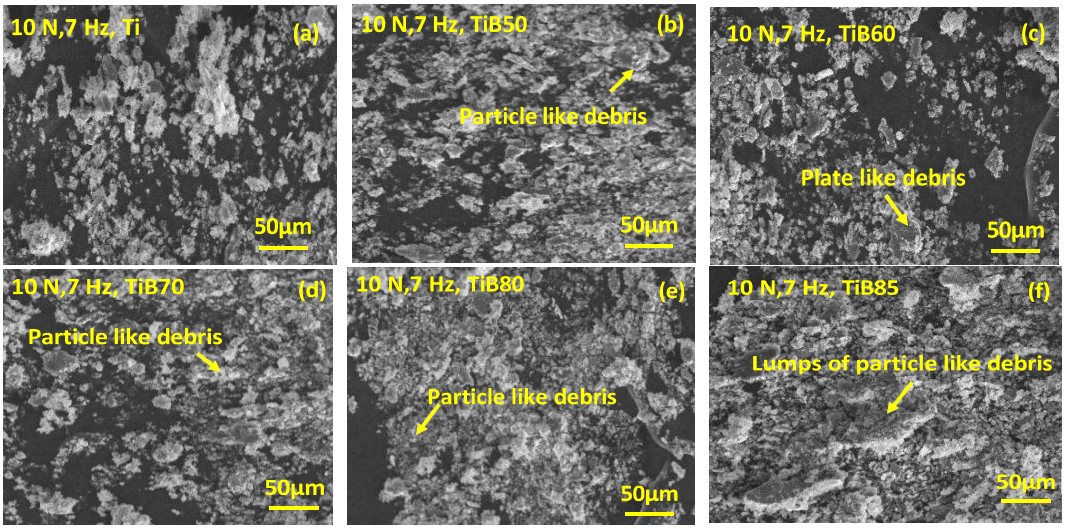

Figure 5.29 SEM micrograph of pooled debris of (a)Ti, (b)TiB50, (c) TiB60, (d)TiB70, (e) TiB80, and (f) TiB85 at 7 Hz

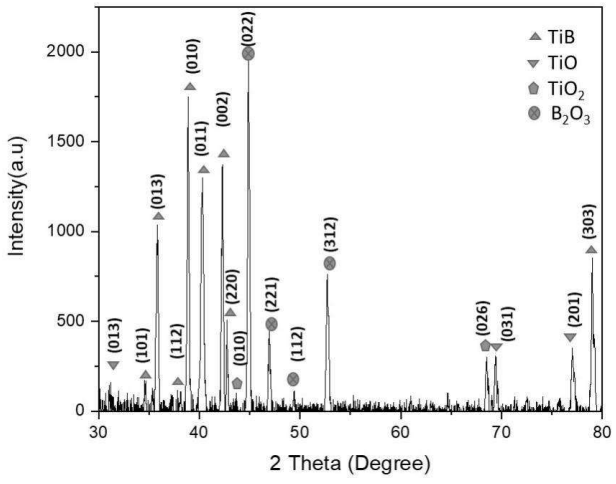

Figure 5.30 **XRD spectra of the debris**

5.4 DISCUSSION

All the composites show a fluctuating trend of coefficient of friction with time at all the loads with amplitude of fluctuations depending on the load and composite. However, the amplitude of fluctuation decreases with increasing load from 10 to 25 N, which may be confirmed by comparing Figs.5.18 (a through f). One may also observe that the amplitude of fluctuation is quite less at relatively higher loads and composites having relatively larger amounts of TiB. The initial surface roughness of mating bodies leads to fluctuations in the coefficient of friction which vanishes with continued sliding and the surfaces get smoother due to wearing out of asperities resulting in reduced fluctuations and stable friction. A relatively larger amplitude of fluctuations in TiB50, TiB60, and TiB70 comparison to TiB80, and TiB85 may be explained on the basis of the SEM micrographs of the worn surfaces of composites and counterface as seen from Figs.5.21 (a, through f) to Fig. 5.24 (a through f) and Figs. 5.25 (a through f) to 5.28 (a through f), respectively. The worn surface of TiB50 composite has relatively deep grooves, signs of delamination, and either the absence of a transfer layer or a relatively lesser area coverage provided by the transfer layer which can be compared from Figs. 5.21 (b) at 10 N, 5.22 (b) at 15 N, 5.23 (b) at 20 N, and 5.24 (b) at 25 N. This might have given rise to direct contact between ball and composite resulting in relatively higher friction in TiB50 in comparison to other composites. A reduction in friction coefficient at 25 N could be attributed to the formation of a smooth transfer layer as shown in Figs. 5.21 (e) at 10 N, 5.22 (e) at 15 N, 5.23 (e) at 20 N, and 5.24 (e) at 25 N for TiB80 composites. The observed variation of average coefficient of friction with load may again be explained on the basis of the generation of wear debris, it's the ability to form a transfer layer over the surface, extent of compaction and area coverage of the transfer layer, presence of oxides and lubricious compounds on the worn surface, transfer of material

from the counterface to composites and composite to counterface ball, all these factor inhibit metal-metal contact and control the friction and wear behaviour as stated earlier in section 4.2. A comparison of Figs. 5.21 to 5.24 corresponding to worn surfaces of Ti and composites and Figs. 5.25 to 5.28 for the counterface ball may explain the observed behaviour in the light of formation - compaction - coverage - detachment - reformation of transfer layer and presence of TiO, TiO_2, and B_2O_3 on the worn surface due to tribo-chemical reactions as revealed by XRD patterns (Figs. 5.30) may explain the reduction in coefficient of friction with load and composition as seen in Figs. 5.19 (a and b). A reduction in both friction and wear due to the formation of the transfer layer has also been reported earlier also by Li et al. (2013) and Zhen et al. (2014, 2016).

A reduced wear rate in composites in comparison to pure Ti may be attributed to their higher hardness due to TiB. The increase in wear rate with load may be due to the increased generation of wear debris leading to a larger loss of material. However, the enhanced frictional heating due to increasing load causes this wear debris to get agglomerated and compacted to form a transfer layer over the sliding surface. This layer compaction and the cover provided by this layer to the underlying substrate with a degree of compaction and extent of cover depending on the load as well as the amount of debris, resulting in the prevention of metal-metal contact between the mating materials and reduction in loss of material and hence, wear rate as seen from Fig. 5.20 (a and b) which indicate a relatively sharp increase from 10 to 15 N but a moderate rate beyond that. The area of coverage and degree of compaction may again be judged on the inspection of the worn surfaces of test materials as well as the counterface. The other contributing factor may be the presence of oxides of Ti (TiO and TiO_2) and B i.e., B_2O_3 which are lubricious in nature. The amount of B_2O_3 is expected to increase with the increasing content of B as one moves from TiB50 to TiB85. Hence, it is not surprising that TiB80 and TiB85 have

shown the lowest wear rate at all loads. The examination of worn surfaces suggests that the mechanism of metal removal in composites is a mixture of ploughing, abrasion, adhesion, and delamination whereas the same for pure Ti are ploughing, abrasion and oxidation. Based on the above observation one may conclude that composite TiB80 has the best performance at all the loads in regard to both the friction and the wear under the range of load and frequency used in the investigation

PART C

5.5 RECIPROCATING WEAR OF COMPOSITES AT 10Hz

In the present section, the results on the effect of load at room temperature (RT) reciprocating wear behavior of vacuum arc melted composites under different loads of 10, 15, 20, and 25 N at a fixed sliding frequency of 10 Hz.

5.5.1 (i) Variation of coefficient of friction with time

The real-time fluctuations of the coefficient of friction (COF) with respect to time for all composites is shown in Fig. 5.31 (a through f), at loads of 10, 15, 20, and 25 N respectively. Composites doesn't show any specific pattern at all loads, a changing pattern is observed for each composite with different amplitudes. The run-in period shows an increase in the coefficient of friction that gets stabilizes and then fluctuates a little about the mean position. Ti shows a stable coefficient of friction from the starting of the test while TiB50, TiB60, TiB70, TiB80, and TiB85 show high fluctuation during the run-in period as shown in Figs. 5.31 (a through f). TiB50 show a stable COF after 200 s for all load while TiB60 show a stable fluctuation after 200 s and further decreases and again stabilize after 400 s for all load. TiB70 show high fluctuation at 10 N compare to other loads and get stabilize after 700 s while at 15 N COF stabilizes near 500 s whereas at 20 and 25 N stabilizes near 250 s. TiB80 shows a stable behavior of COF after 200 s then

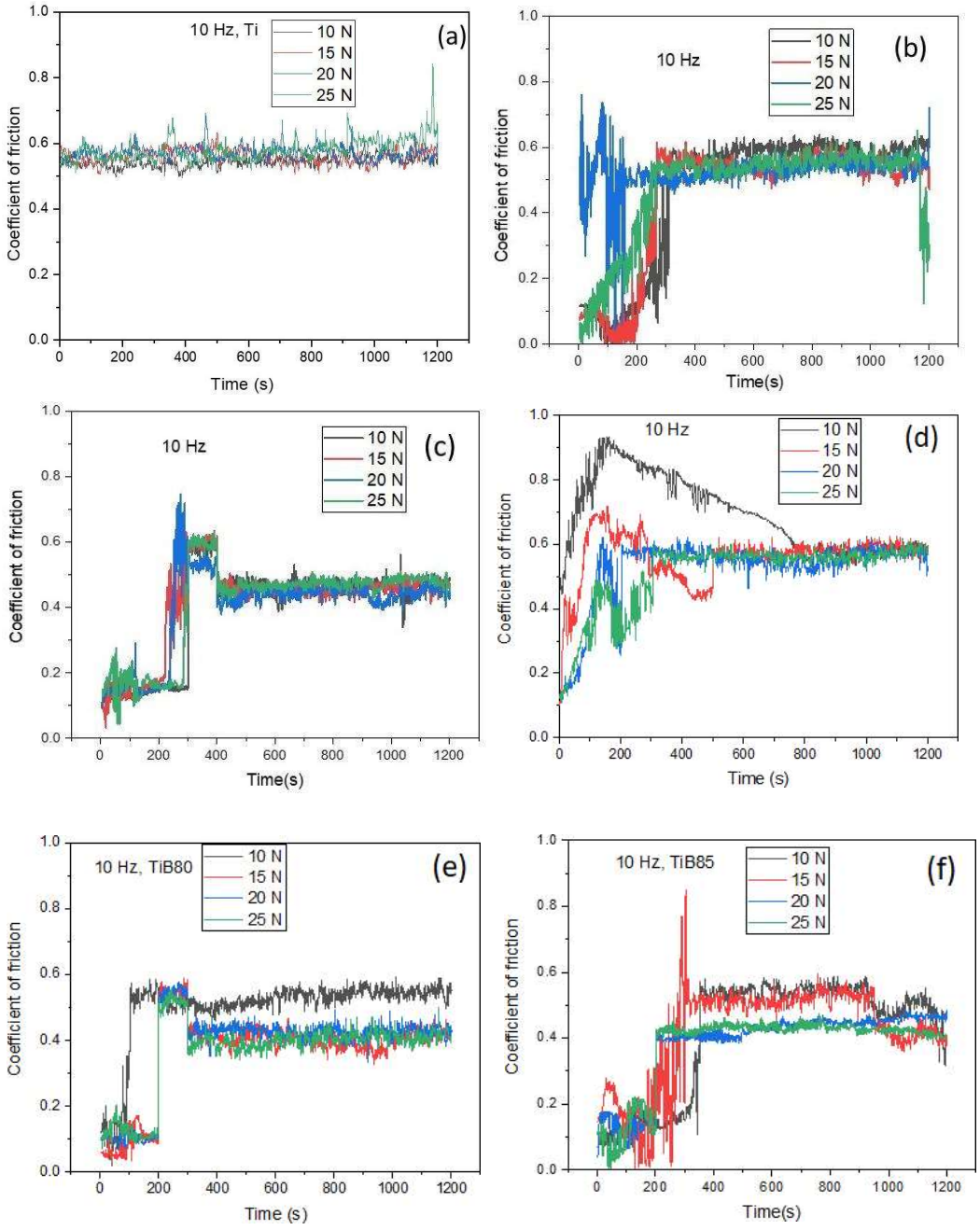

Figure 5.31 Variation of coefficient of friction with time for 10, 15, 20, and 25 N(a) Ti (b) TiB50, (c) TiB60, (d) TiB70, (e) TiB80, and (f) TiB85 composites at different loads

fall a little and again stabilizes around 300 s for 15, 20, and 25 N while 10 N get stabilize around 100s whereas TiB85 shows a stable behavior after 300 s for 20 N and 25 N

whereas for 10 N and 15 N it stabilizes after 200 s.With the increase in load the variations in TiB70 composite are slightly bigger when compared to Ti, TiB50, TiB60, TiB70, TiB80, and TiB85 notably much higher at 25 N.

(i) Variation of average coefficient of friction with normal load and composition

After the friction curve had stabilised, the average coefficient of friction for each three repetitive test was calculated and reported. The variation of COF (average of three tests) with load for all composites is shown in Fig. 5.32(a). The coefficient of friction has a decreasing trend with increasing load from 10 to 25 N, as shown in Fig. 5.32(a) while no such specific trend is observed with increase in vol.% as shown in Fig.5.32 (b). The composite TiB80 show the lowest COF of all the composites tested at all load. The average COF for Ti, TiB50, TiB60, and TiB70 decreases marginally as the load increases from 10 to 25 N. while the decrease for TiB80 is sharp from 10 N to 15 N then decreases sharply from 15 N to 20 N then marginally decreases till 25 N. TiB85 show a marginally decrease from 10 N to 15 N while sharply decrease from 15 N to 20 N then marginally decreases at 25 N. as shown in Fig.5.32(a) Composites with increasing vol.% of TiB, such as TiB80 and, have consistently lower COF than TiB50, TiB60, TiB70, and TiB85 composites at all loads, as shown in Fig.5.32(b). The TiB85 exhibited the lowest COF of any load evaluated in this investigation, with a minimum COF of 0.41 at a load of 25 N. The difference in the coefficients of friction indicated by the composites appears to diminish with increasing load and also has a tendency to decrease with increasing TiB, as seen in Fig. 5.32. However, the average coefficient of friction falls considerably as TiB concentration in TiB60, TiB70, TiB80, and TiB85 increases, as seen in Fig. 5.32 (b). The TiB80 composite also had the lowest coefficient of friction at 20 and 25 N.

(iii) Variation of wear rate with normal load and composition

Figures 5.33 (a) and (b) show the change in wear rate with load and composition, respectively. Wear rate for Ti increases with increased load, although there is no discernible trend. As can be seen in Fig.5.33(a), TiB50 has a growing trend until 20 N and then drops, whereas TiB60, and TiB70 have and decreasing trend until 25 N. However, for composite TiB80 and TiB85 increase is marginal after 20 N, whereas a relatively higher increase in wear rate with load could be seen for Ti, TiB50, and TiB70. As the load is increased from 10 to 25 N, the wear rate trend for Ti, TiB50, and TiB60 is substantially sharper than TiB70, TiB80, and TiB85. However, after 20 N, both composites (TiB80 and TiB85) appear to have the same rate of growth, as seen by the parallel line in Fig. 5.33(a) as the load is increased from 10 to 25 N. Among all composites, TiB85 has demonstrated the least wear. In contrast, Ti has the highest wear rate, whereas TiB50 has the lowest wear rate in composites comprising varying amounts of TiB. The highest wear rate for TiB60 is 10 N and the minimum wear rate is 25 N, whereas the minimum wear rate for TiB80 and TiB85 is 20 N and the maximum is 10 N, as shown in Fig. 5.33. (b). As seen in Fig. 5.32, increasing the TiB content over 41.5 wt.% reduces the wear rate. As illustrated in Fig. 5.33(b), the decline is sharper for relatively greater loads. It shows a pretty rapid drop as the load increases from 10 to 25 N. As shown in Fig. 5.33(b), the wear rate of TiB85 composite with 50.5 wt. percent TiB_2 is much lower and similar to that of TiB80 composite.

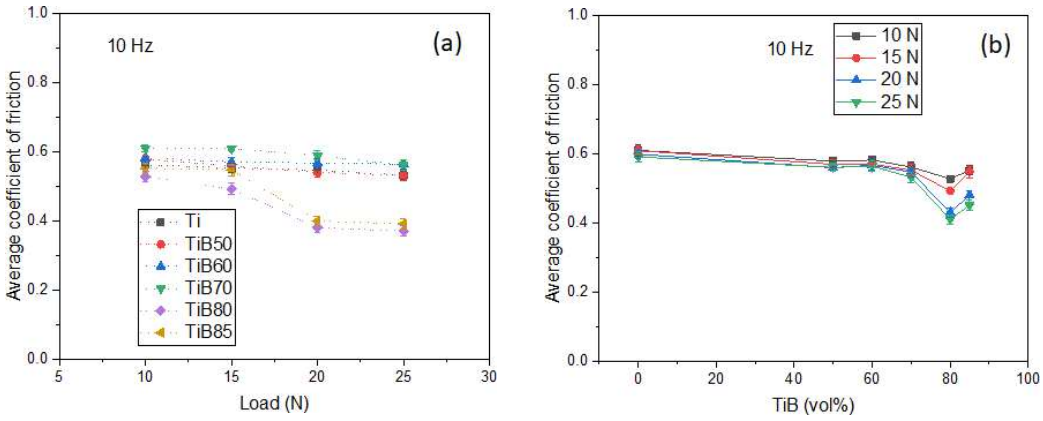

Figure 5.32 Variation of average coefficient of friction with (a) load and, (b) Composition

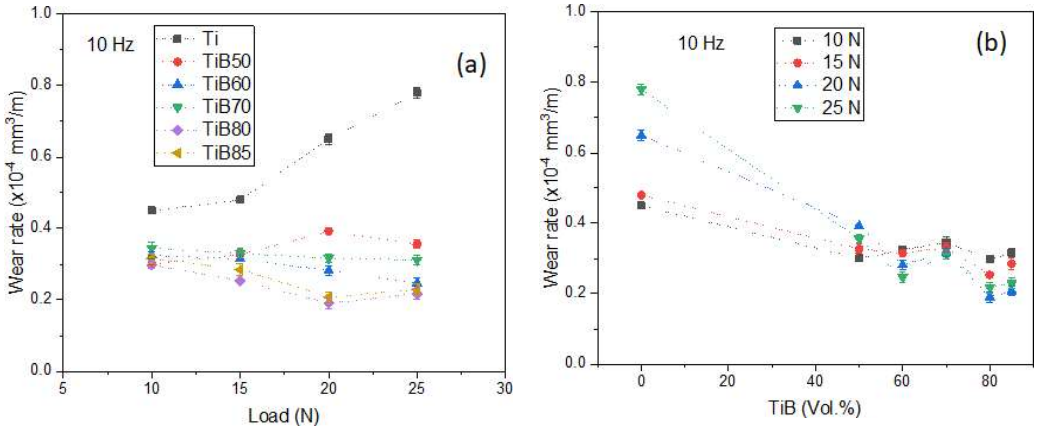

Figure 5.33 Variation of wear rate with (a) load and, (b) Composition

5.5.1 Examination of Worn Surface of Composite

Figure 5.34, 5.35, 5.36, and 5.37 shows the scanning electron micrographs of worn surfaces of Ti-TiB composites slid against counterface ball under a load of 10, 15, 20, and 25 N respectively. The worn track of Ti shown in Fig. 5.34 (a) depict sliding marks, transfer layer and fine debris on the surface on the surface. Fig. 5.34 (b) shows a loose transfer layer, delamination, and particle-like debris on the surface. Fig. 5.34 (c) shows the presence of delamination and a loose transfer layer on the surface of TiB60. Surface compaction, delamination, and debris are visible on the worn surface of TiB70

in Fig. 5.34 (d) surface compaction clearly visible on the right side along with some debris and delamination on the surface of TiB80 in Fig.5.34 (e). The worn surface micrograph of TiB85 composite indicates the presence of delamination and particle like debris all over the surface in Fig. 5.34 (f). the existence of on the TiB60 surface. Delamination, and debris piled up in the delaminated region, and broken surface are visible on the worn surface of TiB70 in Fig. 5.34 (d), while compacted smooth transfer layer, and fine debris are visible on the worn surface of TiB80 in Fig. 5.34 (e). In Fig. 5.34 (f), a worn surface micrograph of TiB85 composite shows delamination, surface compaction, grooves, and particle-like debris all over the surface whereas EDS shows the presence of Ti, B, O and Fe elements

The worn surface in Fig. 5.35 (a) of Ti shows the presence of sliding marks, ploughing and particle-like debris on the surface. The worn surface of TiB50 given in Fig. 5.35 (b) shows the presence of deep grooves, particle like debris in delamination and particle like debris all over the surface in Fig. 5.35 (c) show the presence of delamination and particle like debris all over the surface of TiB60. Surface compaction, delamination, and debris are visible on the worn surface of TiB70 in Fig. 5.35 (d) Surface compaction also some debris (plate and particle like) presence on the surface of TiB80 in Fig. 5.35 (e). The worn surface micrograph of TiB85 composite indicates the presence of delamination and loose transfer layer is visible on surface in Fig. 5.35 (f).

The worn track of Ti shows a deep ploughing marks and plastically deformed surface as seen in Fig. 5.36 (a). Delamination at several places and loose transfer layer is visible on TiB50 worn micrograph as seen in Fig. 5.36 (b) whereas, TiB60 shows surface compaction, delamination, and debris over the worn surface as seen in Fig. 5.36 (c). Loose transfer layer, delamination, and surface compaction clearly visible on right side along with some debris on TiB70 as seen in Fig. 5.36 (d). Some fine particle-like debris in the

inset images from the worn surface of TiB80 as seen in Fig. 5.36 (e). Fine debris in delaminated region and plate like debris on the surface of TiB85 are clearly visible as seen in Fig. 5.36 (f).

Fine particles, ploughing and plastically deformed surface can be seen on worn surface of Ti and very less oxidation on the surface can be seen in EDS as seen in Fig. 5.37 (a). worn surface of TiB50 shows surface compaction, and delamination along with particle-like debris, EDS also reveals the presence of low O content all over the surface as seen in Fig. 5.37 (b). On worn surface of TiB60 presence of transfer layer, sliding marks, and ploughing are visible, EDS shows the O content is more compared to TiB50 as seen in Fig. 5.37 (c). Loose transfer layer at few points of delamination and debris containing O and Fe revealed by EDS all over the surface of TiB70 as seen in Fig. 5.37 (d). A well-compacted transfer layer or oxide layer reveal O and Fe in EDS on the worn surface of TiB80 as seen in Fig. 5.37 (e). In TiB85 worn micrographs shows the presence of delamination and fine debris along the marked region, and EDS shows the O content over the surface as seen in Fig. 5.37 (f).

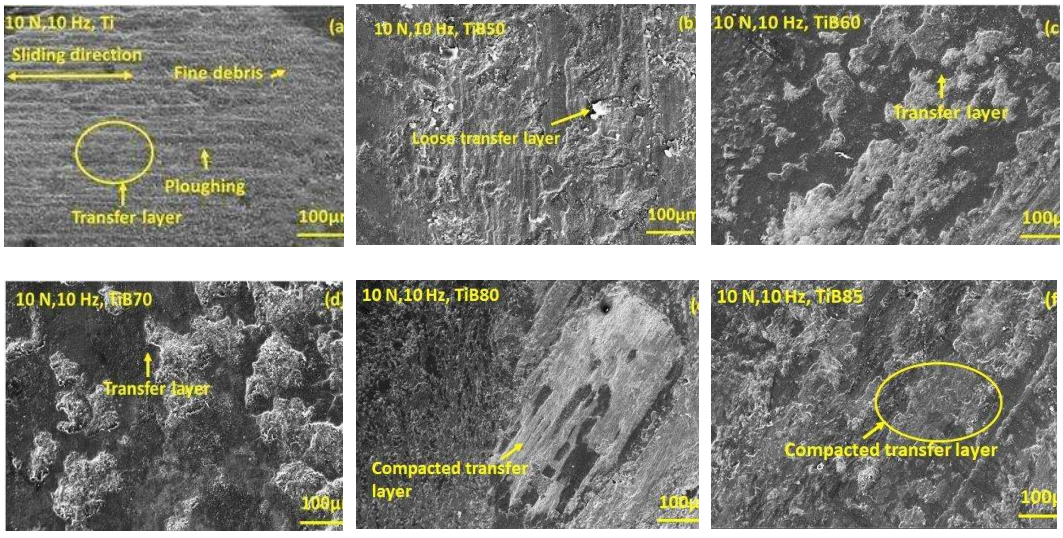

Figure 5.34 SEM images of worn surfaces of composite at a load of 10 N (a)Ti, (b) TiB50, (c) TiB60, (d) TiB70, (e) TiB80 and, (f) TiB85

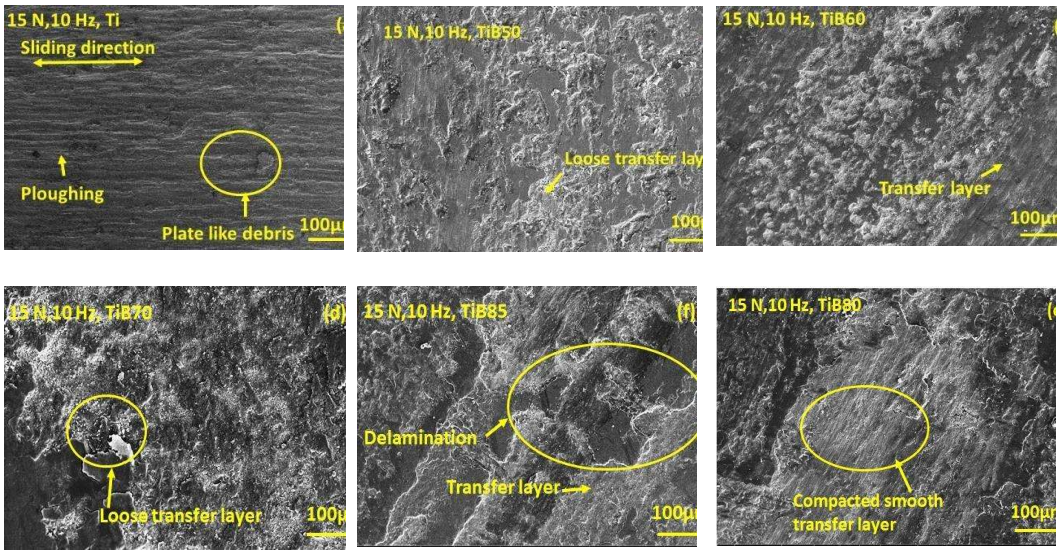

Figure 5.35 SEM images of worn surfaces of composite at a load of 15 N (a)Ti, (b) TiB50, (c) TiB60, (d) TiB70, (e) TiB80 and, (f) TiB85

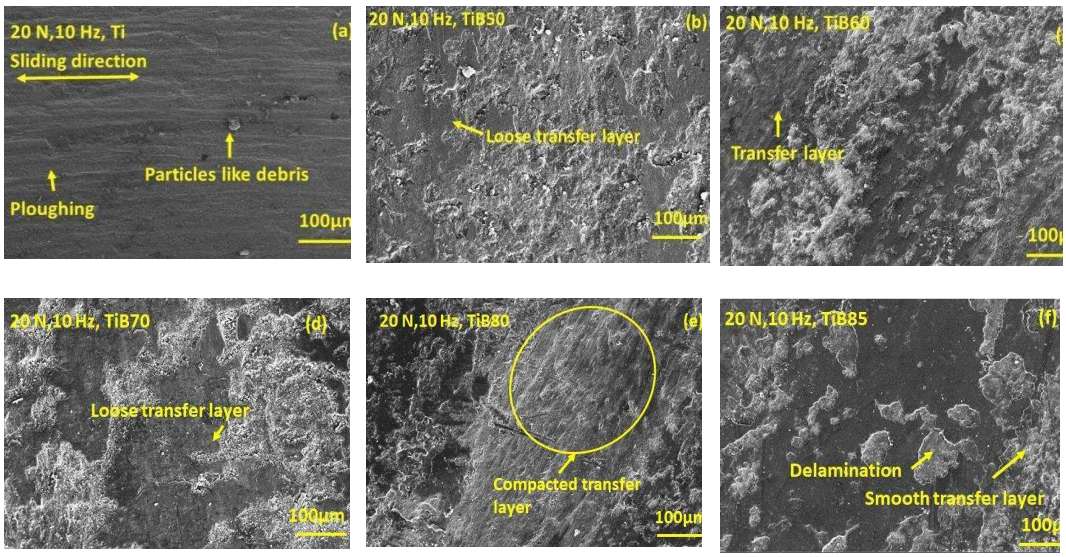

Figure 5.36 SEM images of worn surfaces of composite at a load of 20 N (a)Ti, (b) TiB50, (c) TiB60, (d) TiB70, (e) TiB80 and, (f) TiB85

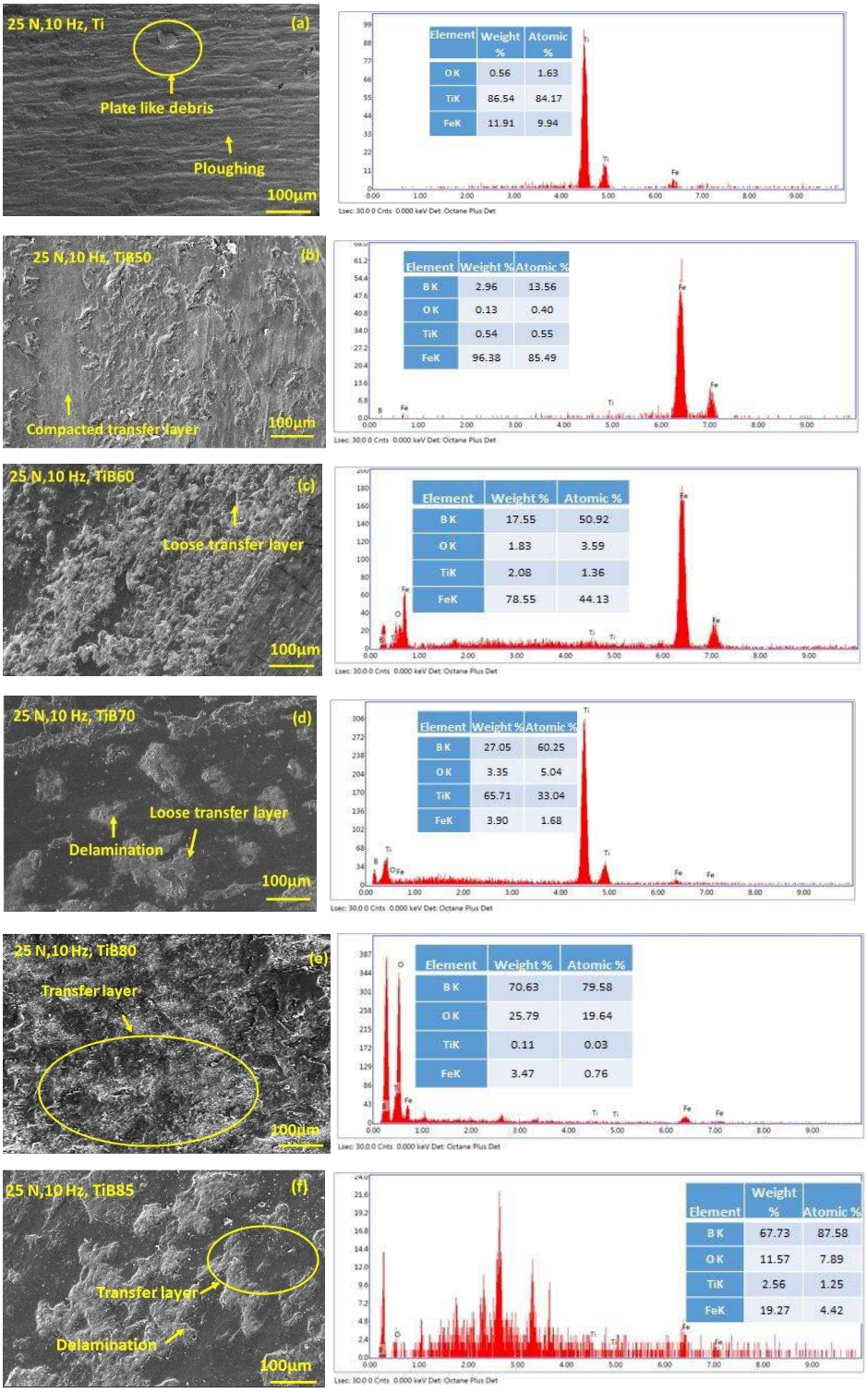

Figure 5.37 SEM images of worn surfaces of composite at a load of 25 N (a)Ti, (b) TiB50, (c) TiB60, (d) TiB70, (e) TiB80 and, (f) TiB85

5.5.3 Examination of Worn Surface of Counterface

The morphology of worn part of counterface balls which slide against the composites (a) Ti, (b) TiB50, (c) TiB60, (d) TiB70, (e) TiB80, and (f) TiB85 respectively, at a load of 10, 15, 20, and 25 N, under HR-SEM was examined to reveal the type of wear might occur during the sliding of the balls with composite. The morphologies of the worn surfaces of steel ball slid against Ti, TiB50, TiB60, TiB70 TiB80, and TiB85 composite at loads of 10, 15, 20, and 25 N are illustrated in Figs. 5.38, 5.39, 5.40, and 5.41 (a through f). These mechanisms are useful in predicting the possibility of wear mechanisms along with the material transfer if any. Figure 5.38 (a through f) depicts the micrographs of the counterface ball slid under a load of 10 N as examined under SEM. The counterface ball for pure Ti shows a losse transfer layer as seen in Fig.5.38 (a). The worn surface of the counterface ball used against TiB50 shown in Fig. 5.38 (b) reveals loosely bound surface and fine debris, whereas some transfer layer at various position and particle like debris on counterface ball used against TiB60 as seen from Fig. 5.38 (c). A patchy surface could be observed on the worn surface counterface ball used against TiB70 as seen in Fig. 5.38 (d). Figure 5.38 (e), corresponding to the counterface ball used against TiB80, shows large particle like debris, compacted transfer layer and delamination. A loose transfer layer could be seen on the worn surface of the counterface ball used against TiB85, which appears to be patchy at a few locations (Fig. 5.38 (f)) under a load of 10 N.

Figure 5.39 (a through f) depicts the micrographs of the counterface ball slid under a load of 15 N as examined under SEM. The counterface ball for pure Ti presents a transfer layer with few delamination signs as seen in Fig.5.39 (a). The worn surface of the counterface ball used against TiB50 shown in Fig. 5.39 (b) reveals debris and a loosely bound surface, whereas some loose transfer layers at various positions of the counterface ball used against TiB60 as seen from Fig. 5.39 (c). A patchy surface could be observed

on the worn surface counterface ball used against TiB70 as seen in Fig. 5.39 (d). Figure 5.39 (e), corresponding to the counterface ball used against TiB80, shows large particle-like debris, compacted continuous transfer layer, and few signs of delamination. A transfer layer could be seen on the worn surface of the counterface ball used against TiB85, which appears to be rough at a few locations (Fig. 5.39 (f)).

Figure. 5.40 (a) shows sliding marks and transfer layer on worn surface micrographs of the ball slid against the Ti. The worn surface of the counterface ball used against TiB50 shown in Fig. 5.40 (b) reveals a rough surface and large debris, whereas Fig. 5.40 (c) shows different intensities of the worn scar with the marks of adhesion. Also, the micrograph given in Fig.5.40 (d) suggests the occurrence of delamination and transfer layer at a few locations. The worn scar corresponding to the TiB80 composite presented in Fig. 5.40 (e) shows a delaminated and compacted transfer layer formation with increase in load. Similar features could be observed for the steel ball slid against TiB85 composite shown in Figs. 5.40 (f).

Figure. 5.41 (a) shows particle-like debris and transfer layer on worn surface micrographs of the ball slid against the Ti. The worn surface of the counterface ball used against TiB50 shown in Fig. 5.41 (b) reveals a loosely bound surface and fine debris, whereas Fig. 5.41 (c) shows different intensities of the worn scar with particle-like debris. Also, the micrograph given in Fig.5.41 (d) suggests the occurrence of delamination and rough surface. The steel ball slid against the TiB80 composite shows a compacted surface with no measurable signatures of lumps or aggregates as evident from Fig. 5.40 (e). The micrograph given in Fig. 5.40 (f) reveals some fine abrasive marks along with the presence of a transfer layer over the counter steel ball surface corresponding to the TiB85.

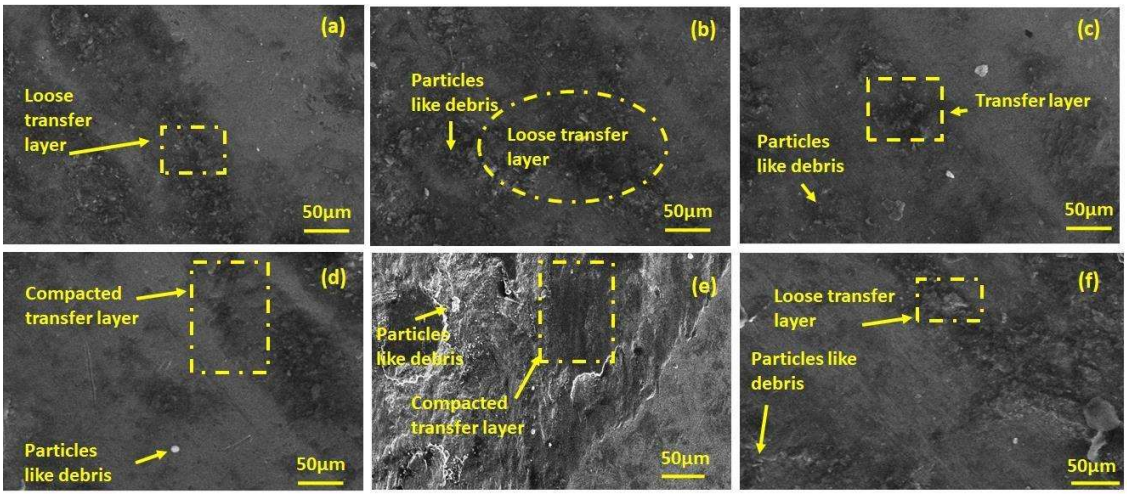

Figure 5.38 SEM images of worn surface of bearing steel ball slid against TiB composite Ti, (b)TiB50, (c) TiB60, (d)TiB70, (e) TiB80, and (f) TiB85 at10 Hz and 10 N

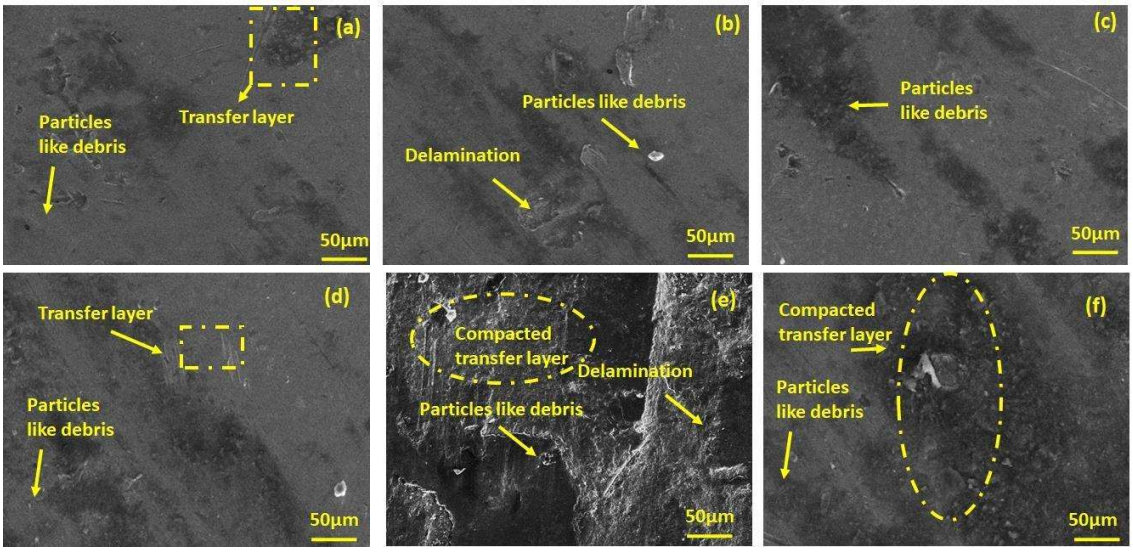

Figure 5.39 SEM images of worn surface of bearing steel ball slid against TiB composite (a) Ti (b)TiB50, (c) TiB60, (d)TiB70, (e) TiB80, and (f) TiB85 at10 Hz and15 N

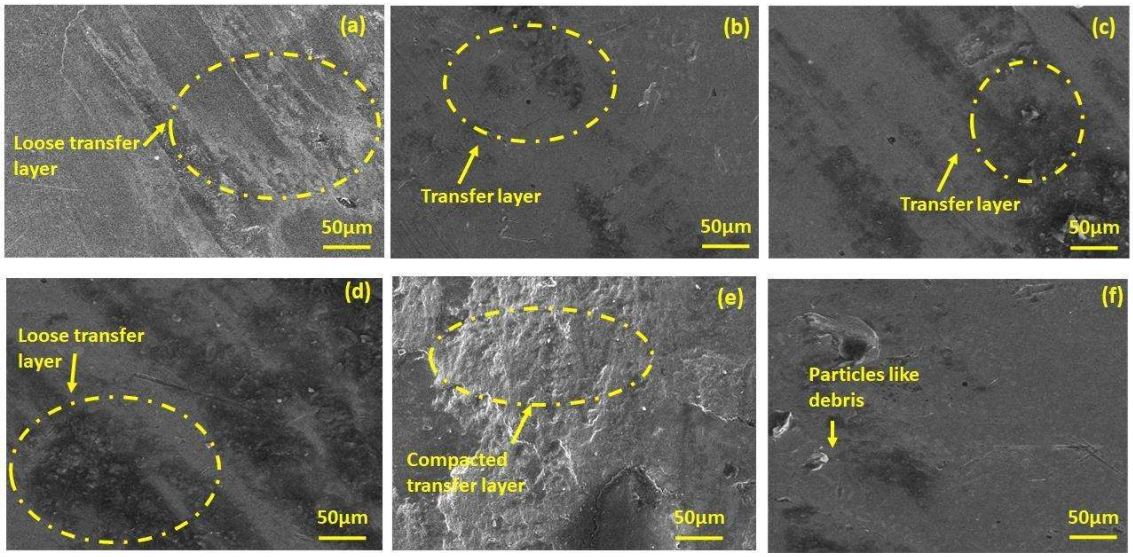

Figure 5.40 SEM images of worn surface of bearing steel ball slid against TiB composite (a) Ti (b)TiB50, (c) TiB60, (d)TiB70, (e) TiB80, and (f) TiB85 at10 Hz and 20 N

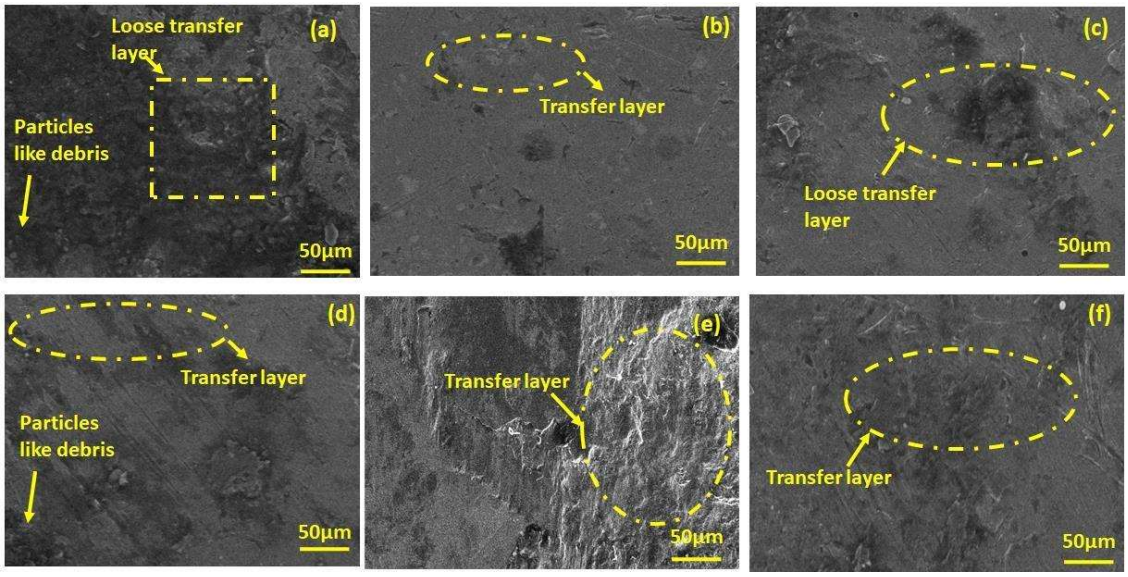

Figure 5. 41 SEM images of worn surface of bearing steel ball slid against TiB composite(a) Ti, (b)TiB50, (c) TiB60, (d)TiB70, (e) TiB80, and (f) TiB85 at10 Hz and 25N

5.5.4 Examination of Debris

The morphology of the wear debris collected after the sliding tests was examined using a SEM to investigate the nature of wear particles of (a) Ti, (b) TiB50, (c) TiB60,

(d) TiB70, (e) TiB80, and (f) TiB85 from Fig. 5.42 (a through f). The wear debris corresponding to the Ti TiB50 composite illustrated in Fig. 5.42 (a) contained both tiny and bigger particles of various sizes. The wear debris corresponding to the TiB60 composite has significantly larger size flakes ranging from hundreds of microns to a few mm as seen in Fig. 5.42 (b and c), whereas that related to TiB70 is a mixture of relatively fine, regular, and irregular-shaped particles of moderate size as shown in Fig. 5.42 (d, e, and f). However, the particles of wear debris corresponding to TiB85 are regular in shape. Figure 5.42 shows the XRD analysis of all debris collected together, revealing the development of diverse oxides of Ti, Fe, and B. X-ray examination revealed the formation of TiO, TiO_2, and B_2O_3 over the worn surface of composites. The presence of B oxides implies the presence of a tribo-layer, which should promote lubricity at the contact during sliding.

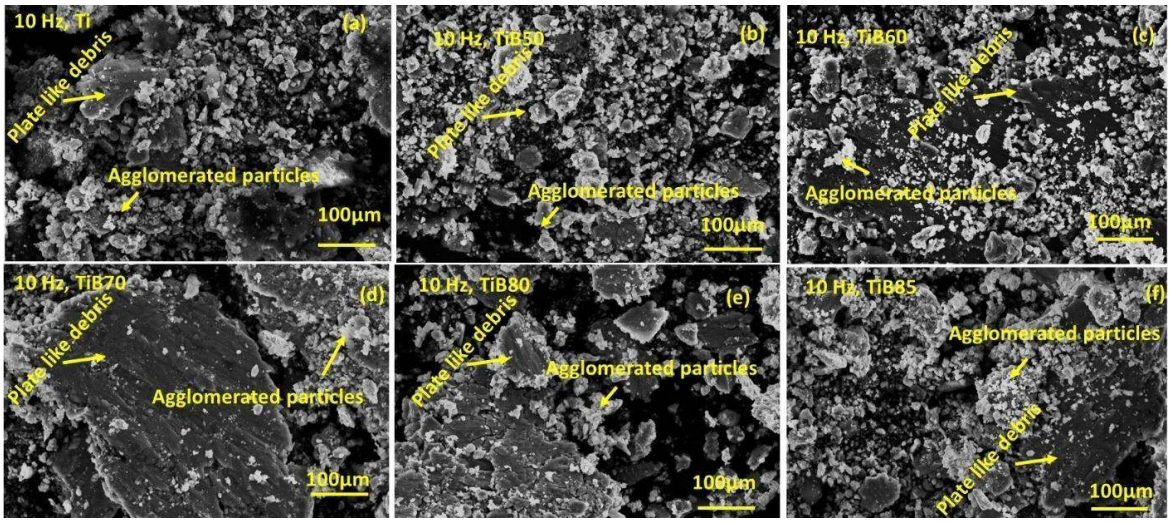

Figure 5. 42 SEM images of pooled debris form bearing steel ball slid against TiB composite (a) Ti, (b) TiB50, (c) TiB60 (d)TiB70, (e) TiB80, and (f) TiB85 at 10 Hz

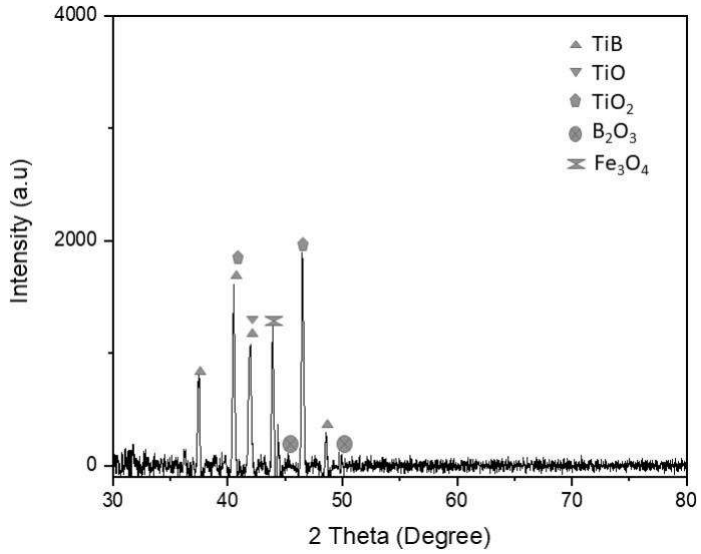

Figure 5. 43 XRD spectra of the debris

5.6 DISCUSSION

The initial roughness of the contacting surfaces may explain the changing trend of fluctuation of the coefficient of friction with time shown in Figs. 5.31 (a to f). It is commonly known that engineering surfaces are rough and have asperities. Contact occurs at these asperities during the relative sliding motion between the two bodies, causing amplitude variability during sliding. However, after a certain period of sliding, the surfaces change to achieve improved conformance, resulting in stabilization based on the parameters of frequency, load, and microstructure. The creation of a smooth and compacted transfer layer of debris, on the other hand, eliminates direct contact between the mating bodies and lowers friction and wear. A comparison of the surfaces worn under loads of 10, 15, and 25 N, as shown in Figs. 5.34 (a through f), 5.35 (a through f), 5.36 (a through f), and 5.37 (a through f), reveals the presence of ploughing, transfer layer and delamination, which appear to have increased with increasing load. As seen in Figs. 5.34 (a), 5.35 (a), 5.36 (a), and 5.37 (a), pure Ti exhibits abrasive wear that rises with increasing load.

Delamination occurs as a result of cyclic stress on the surface, which causes the pulling of TiB colonies from the matrix and the creation of loose particles by brittle fracture, resulting in an increased material removal rate, as seen in many areas with microfracture features on the worn surfaces (Fig. 5.34 (b through f), 5.35 (b through f), 5.36 (b through f), and 5.37 (b through f)). However, microfracture occurrences appear to be less likely on composite surfaces that are either worn under a lower load or contain a larger TiB content. As a result, a decrease in COF and wear rate with increasing load for each composite may be attributed to the creation of loose particles at relatively low loads due to low-stress scratching abrasion and three-body abrasion at comparatively higher loads where the particles trapped between the surface get crushed, resulting in high-localized stress either get compacted or material loss via abrasive action.

The change in COF and wear rate with regard to TiB vol. percent can be described by the interaction of the following factors: (i) the existence of loose wear particles on the worn surface, (ii) the creation of a transfer layer of wear debris on the surface, (iii) the degree of compaction and the extent of cover provided by the transfer layer to the underlying material, and (iv) the presence of oxides in the wear debris/transfer layer. A reduction in wear rate from TiB50 to TiB80 can be explained by the fact that the volume and kind of debris rise with increasing load and TiB content, which forms a protective transfer layer as previously indicated. Because there is more wear debris, there is a greater chance for agglomeration, three-body wear and the creation of a transfer layer covering a larger area proportion of the sliding interface. Because of the increased frictional heat at relatively greater loads, this transfer layer compacts and creates a smooth layer over the surface. The formation-compaction-detachment-reformation of the transfer layer produces wear particles ranging in size from fine to plate-like, as illustrated in Fig. 5.42(a through f) of various composites. The transfer layer was found to contain oxides, as

evidenced by the XRD analysis of the wear debris (Fig. 5.43). Another reason that may be contributing to the decrease in friction and wear rate is the presence of lubricious oxides of Ti in the wear debris, such as TiO, TiO_2, and B_2O_3 as revealed by X-ray diffraction studies. The addition of B_2O_3 has been shown to improve wear resistance while simultaneously lowering COF in Ti-based composites. Based on the results, it can be stated that 80 Vol.% TiB has the optimum performance in terms of coefficient of friction and wear rate under the sliding conditions utilized in the current study.

PART D

5.7. Reciprocating wear of Composites at 15 Hz

The current section presents the results on the effect of load on room temperature (RT) tribological behavior of vacuum arc melted composites at a fixed frequency of 15 Hz.

5.7.1 (i) Variation of coefficient of friction with time

Figure 5.44 (a through f) demonstrates the variation of coefficient of friction (COF) with time at different loads for pure Ti, TiB50, TiB60, TiB70, TiB80, and TiB85, respectively. The variation appears to be stable for Ti with small fluctuations in amplitude at all the loads with almost no running period as seen from Fig. 5.44 (a). However, larger fluctuations could be seen for composites with different running-in periods depending on the load and composition as evident from Figs. 5.44 (b through f) for example the COF appears to get stabilized relatively earlier (200 s) for TiB50 for 20 and 25 N while for 10 and 15 it stabilizes after ~ 400 s as evident from Fig. 5.44 (b). TiB60 shows a stable COF at all the loads soon after the run-in period ~ 200 s is over as shown in Fig. 5.43 (c), whereas TiB70 shows high fluctuation around a mean level at 10,15, 20 and 25 N and stabilizes after 400 s for 10, 15 and 20 N whereas for 10 N it stabilizes around 100 s as

seen from Fig. 5.44 (d). In the case of TiB80, the COF is initially stable at 10, 15 and 25 N(100 s), whereas at 20 N shows a stable COF after 400 s as seen from Fig. 5.44 (e). The COF for composite TiB85 is observed to get stabilized after 400 s for 10, 20 and 25 N whereas for 15 N it stabilizes after ~100 s as seen from Fig. 5.43 (f).

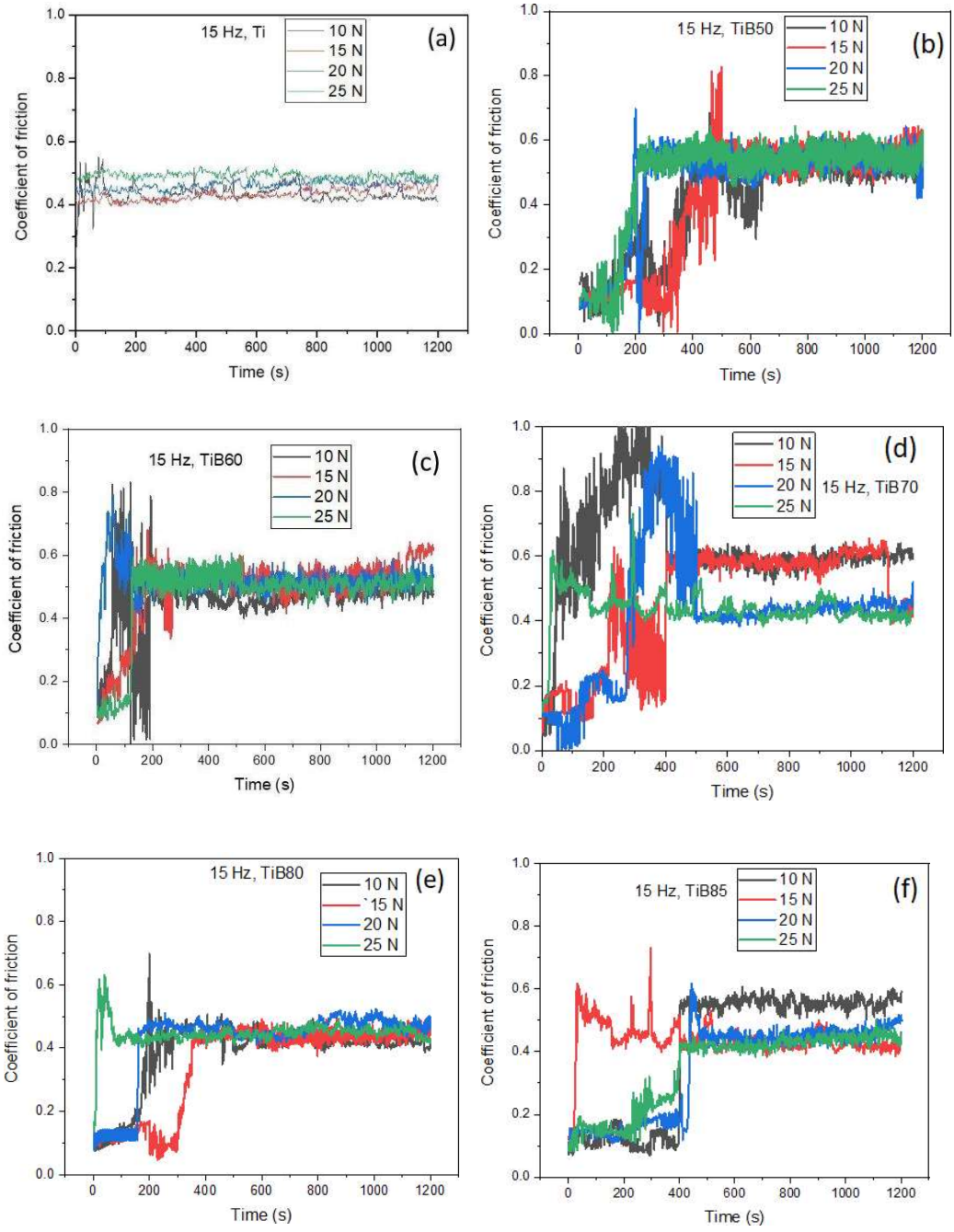

Figure 5. 44 Variation of coefficient of friction with time for 10, 15, 20, and 25 N (a)Ti,

(a) TiB50, (c)TiB60, (d) TiB70, (e)TiB80, and (f) TiB85 composites at
(b) different loads.

(ii) Variation of average coefficient of friction with normal load and composition

Figure 5.45 (a) presents the variation of the average steady-state coefficient of friction with the normal load whereas the variation with respect to composition is illustrated in Fig. 5.45 (b). The average COF is found to increase with increasing load for pure Ti whereas it is observed to either decrease of remain constant for composites with increasing loads as evident from Fig.5.45 (a). TiB80 and TiB85 have shown consistently lower COF among all the composites at all the loads, as evident from Fig. 5.45 (a). As far as the variation w.r.t. composition is concerned, the steady state average COF is observed to increase with increasing TiB content from pure Ti to TiB50 followed by a decrease for TiB60 and increase for 70 vol. % before decreasing again to 80 vol. % followed by a slight increase beyond that at TiB85, at the loads 10 and 15 N, as seen from Fig. 5.45 (b). However, at other loads i.e., 20, and 25 N the steady state average COF decreases as the amount of TiB increases from pure Ti to 50 vol. %, followed by a decrease till 80 vol. % TiB and marginal increase thereafter for 85 vol.% TiB as evident from Fig. 5.45 (b).

(iii) Variation of wear rate with normal load and composition

The variation of wear rate (mm^3/m) with load for all the composites shown in Fig. 5.46 (a) reveals that the wear rate of Pure Ti decreases slightly from 10 to 15 N then increases sharply as the load is raised to 20 N and remains almost same for 25 N. Also, pure Ti has shown the highest wear rate among all the materials at all loads. As far as composites are concerned the wear rate decreases with an increase in load for TiB60, TiB80 and TiB85 whereas for TiB50 and TiB70 it shows a decrease from 10 to 15 N followed by an increase at 20 N before decreasing further at 25 N. The lowest wear rate

is shown by TiB85 whereas TiB70 has shown the highest wear rate among all composites at all the loads as seen from Fig. 5.46 (a).

The variation of wear rate with TiB vol.% depicted in Fig.5.46 (b) indicates a sharp decrease in wear rate from pure Ti to TiB50 at all loads. The wear rate is observed to increase with increasing TiB content from 50 to 70 vol.% at all loads before decreasing slightly till 85 vol.% as seen in Fig. 5.46 (b).

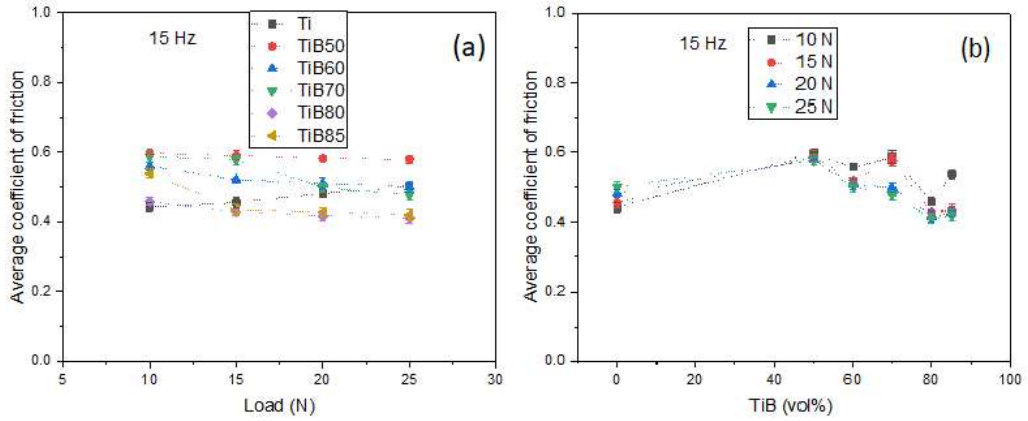

Figure 5.45 Variation of average coefficient of friction with (a) load and (b) Composition

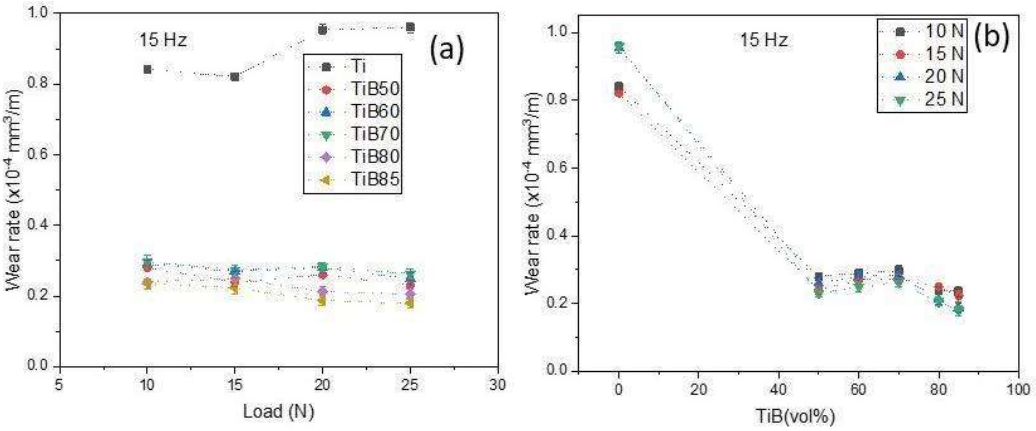

Figure 5. 46 Variation of wear rate of friction with (a) load and, (b) Composition

5.7.2 Examination of Worn Surface of Composite

Figure 5.47, 5.48, 5.49, and 5.50 shows the scanning electron micrographs of worn surfaces of Ti-TiB composites slid against a counterface ball under a load of 10, 15,

20, and 25 N respectively. The worn track of Ti shown in Fig. 5.47 (a) depicts the presence of a transfer layer along with some ploughing on the surface. The worn surface of TiB50 (Fig. 5.47 (b)) shows large particle-like debris with a compacted transfer layer on the surface, whereas Fig. 5.47 (c) shows the presence of ploughing, cracks, and transfer layer on the surface of TiB60. Surface compaction, delamination, and transfer layer are visible on the worn surface of TiB70 as seen in Fig. 5.47 (d) whereas the compacted layer and debris are clearly visible on the surface of TiB80 in Fig.5.47 (e). The worn surface micrograph of the TiB85 given in Fig. 5.47 (f) indicates the presence of delamination and rough surface along with debris all over the surface.

The worn surface in Fig. 5.48 (a) of Ti shows the presence of sliding marks, ploughing and particle-like debris on the surface whereas the worn surface of TiB50 given in Fig. 5.48 (b) shows a scattered transfer layer along with debris particles at a load of 15 N. The worn surfaces of TiB60, TiB70, TiB80 and TiB85 reveal the presence of a continuous and loosely bound transfer layer which appears to have been detached at some locations as seen from Fig. 5.48 (c, d, e and f). However, these differ in the degree of compaction and area coverage.

The worn surface of Ti reveals deep ploughing marks and a plastically deformed surface as seen in Fig. 5.49 (a) whereas a transfer layer and its delamination at several places is visible on TiB50 worn micrograph as seen in Fig. 5.49 (b) at a load of 20 N. whereas, TiB60 shows surface fragmented transfer layer, delamination, and debris over the worn surface as seen in Fig. 5.49 (c). Loose transfer layer, and fine debris all over the surface as seen in Fig. 5.49 (d). Some fine particle-like debris and transfer layer detached at a few places from the worn surface of TiB80 as seen in Fig. 5.49 (e). Fine debris in the delaminated region, compacted transfer layer, and plate-like debris on the surface of TiB85 are clearly seen in Fig. 5.49 (f) corresponding to TiB85.

The presence of fine particles, ploughing marks and plastically deformed region could be observed on the worn surface of Ti along with signs of oxidation as seen from EDS in Fig. 5.50 (a). The worn surface of TiB50 shows surface compaction, along with delamination and EDS also reveals the presence of higher O content over the surface as evident from Fig. 5.50 (b). The worn surface of TiB60 shows the presence of transfer layer, ploughing marks and EDS also indicates the presence of O content on the surface as seen from Fig. 5.50 (c). A loose transfer layer with probable delamination's at a few points and wear debris could be observed on the worn surface of TiB70 as seen in Fig. 5.50 (d) whereas a well-compacted transfer layer and a few delaminated regions along with oxidation are the features shown by the worn surface of TiB80 given in Fig. 5.50 (e). The worn surface micrograph of TiB85 (Fig. 5.50 (f)) shows the presence of a transfer layer which appears to have got detached at a few locations along with some fine debris.

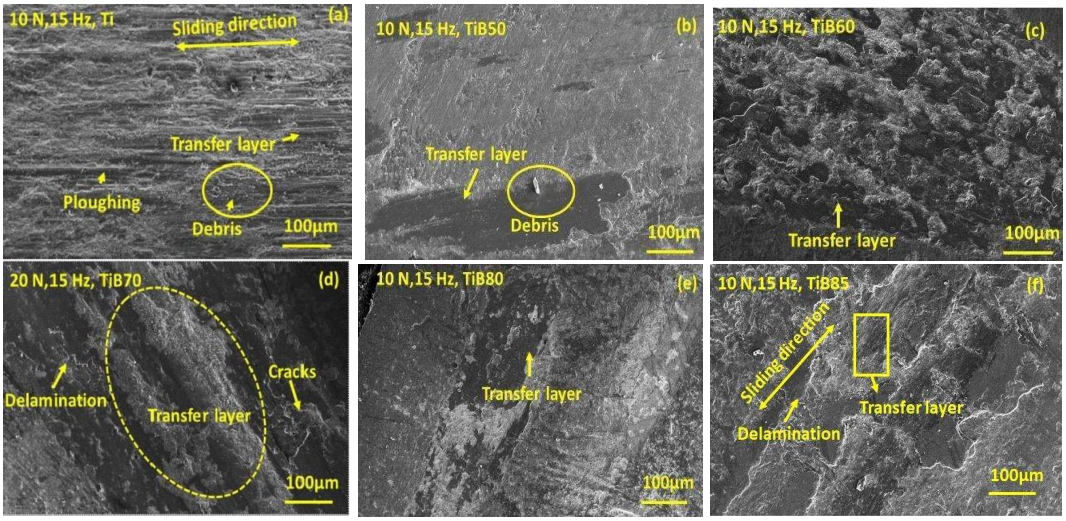

Figure 5.47 SEM images of worn surface TiB composite slid against bearing steel ball (a) Ti, (b) TiB50, (c) TiB60, (d)TiB70, (e) TiB80, and (f) TiB85 at 15 Hz and 10 N

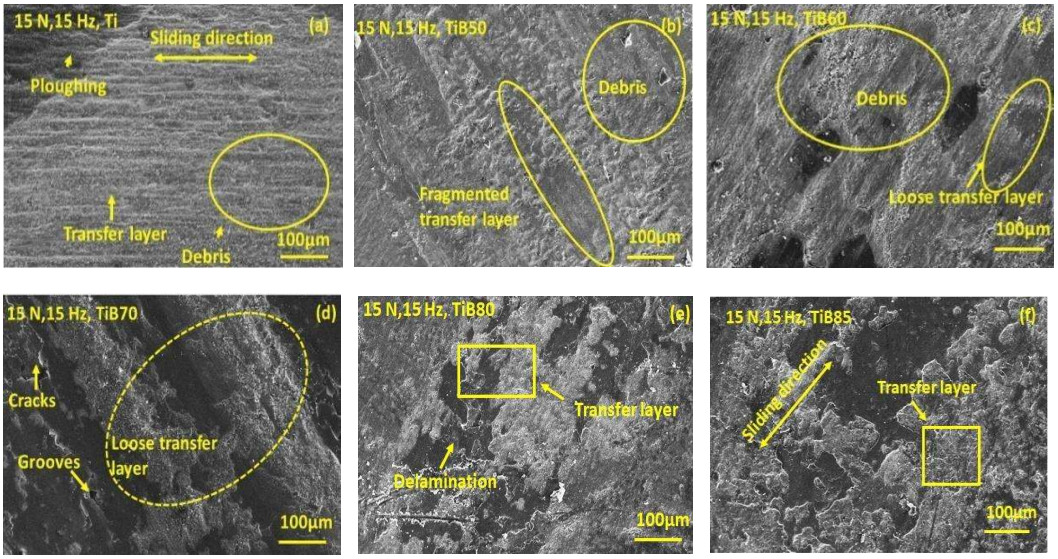

Figure 5.48 SEM images of worn surface TiB composite slid against bearing steel ball (a) Ti, (b) TiB50, (c) TiB60, (d)TiB70, (e) TiB80, and (f) TiB85 at 15 Hz and 15 N

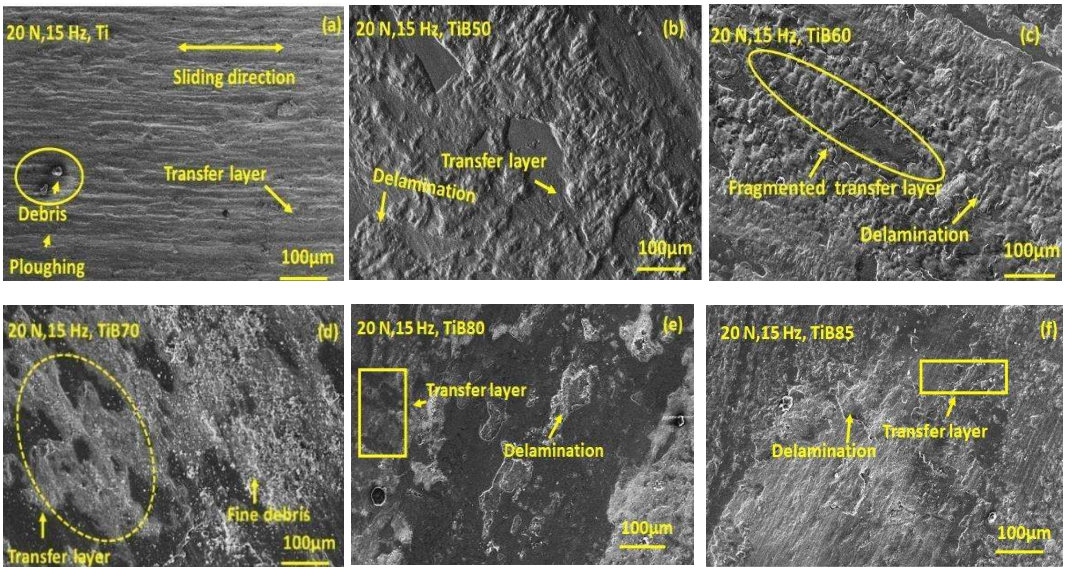

Figure 5.49 SEM images of worn surface TiB composite slid against bearing steel ball (a) Ti, (b) TiB50, (c) TiB60, (d)TiB70, (e) TiB80, and (f) TiB85 at 15 Hz and 20 N

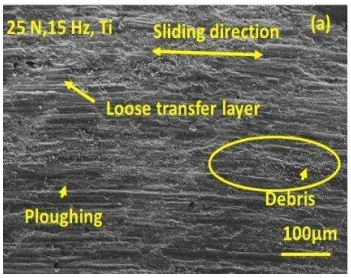
25 N,15 Hz, Ti
Sliding direction
(a)
Loose transfer layer
Debris
Ploughing
100µm

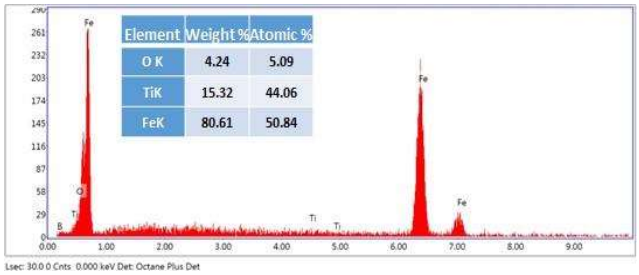
Element Weight % Atomic %
O K 4.24 5.09
TiK 15.32 44.06
FeK 80.61 50.84

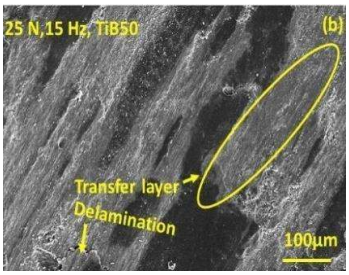
25 N,15 Hz, TiB50
(b)
Transfer layer
Delamination
100µm

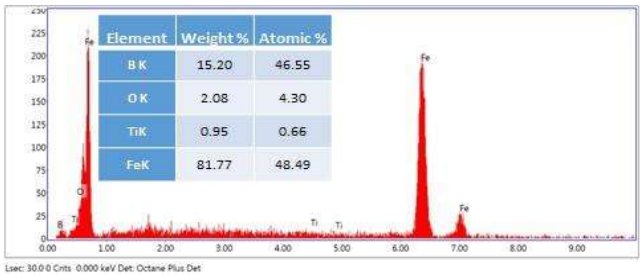
Element Weight % Atomic %
B K 15.20 46.55
O K 2.08 4.30
TiK 0.95 0.66
FeK 81.77 48.49

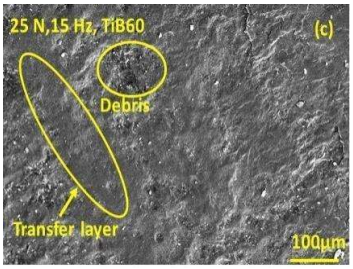
25 N,15 Hz, TiB60
(c)
Debris
Transfer layer
100µm

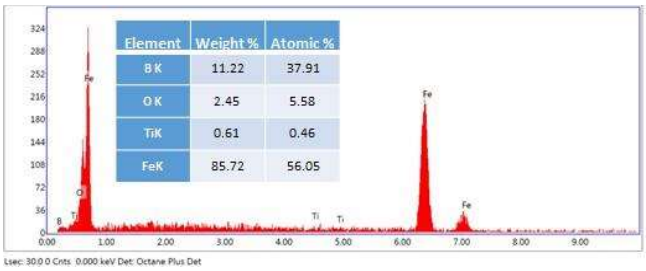
Element Weight % Atomic %
B K 11.22 37.91
O K 2.45 5.58
TiK 0.61 0.46
FeK 85.72 56.05

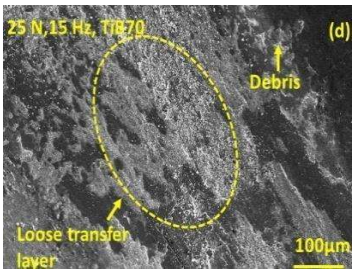
25 N,15 Hz, TiB70
(d)
Debris
Loose transfer layer
100µm

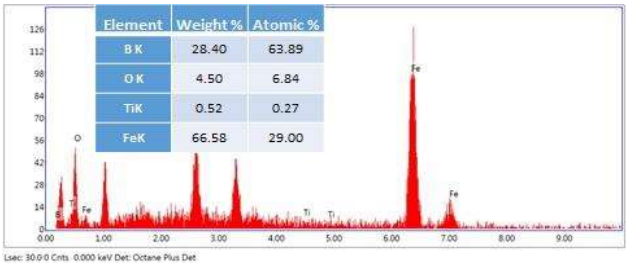
Element Weight % Atomic %
B K 28.40 63.89
O K 4.50 6.84
TiK 0.52 0.27
FeK 66.58 29.00

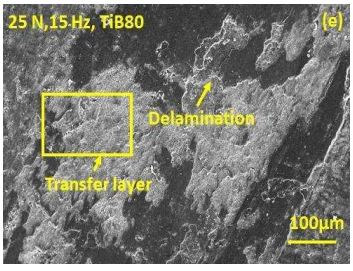
25 N,15 Hz, TiB80
(e)
Delamination
Transfer layer
100µm

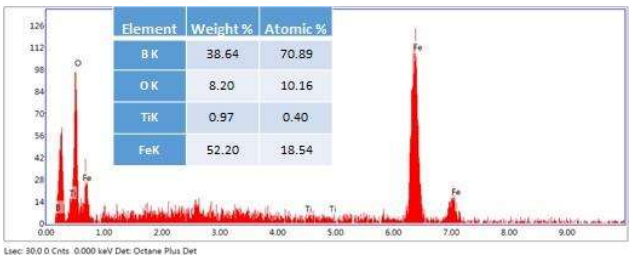
Element Weight % Atomic %
B K 38.64 70.89
O K 8.20 10.16
TiK 0.97 0.40
FeK 52.20 18.54

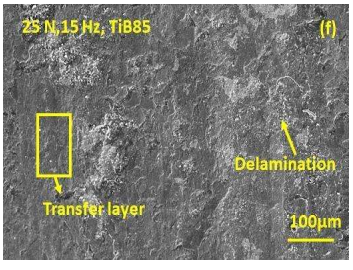
25 N,15 Hz, TiB85
(f)
Delamination
Transfer layer
100µm

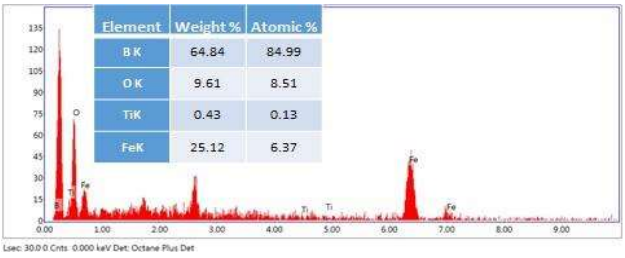
Element Weight % Atomic %
B K 64.84 84.99
O K 9.61 8.51
TiK 0.43 0.13
FeK 25.12 6.37

Figure 5.50 SEM and EDS images of worn surface TiB composite slid against bearing steel ball(a) Ti, (b) TiB50, (c) TiB60, (d)TiB70, (e) TiB80, and (f) TiB85 at15 Hz and 25 N

5.7.3 Examination of Counterface Ball

The morphologies of worn surface of counterface balls slid against Pure Ti and at loads of 10, 15, 20, and 25 N as examined under HR-SEM are illustrated in Figs. 5.51, 5.52, 5.53 and 5.54 (a through f). These images useful in predicting the possibility of wear mechanisms along with the material transfer if any. The worn surface of ball slid against pure Ti, given in Fig.5.51 (a) presents a transfer layer with few signs of debri deposition whereas worn surface of the ball used against TiB50 reveals the presence of debris and transfer layer as seen in Fig. 5.51 (b). The presence of a loose transfer layer of debris at various positions on the worn surface of ball slid against TiB60 could be observed in Fig. 5.51 (c). However, a smooth surface could be seen for the ball used against TiB70 as visible from Fig. 5.51 (d). Figure 5.51 (e), corresponding to the counterface ball used against TiB80, shows the presence of a compacted and continuous transfer layer along with large particle-like debris. A transfer layer could also be seen on the worn surface of the counterface ball used against TiB85, which appears to have got delaminated at a few locations (Fig. 5.51 (f)).

Figure 5.52 (a through f) depicts the micrographs of the counterface ball slid under a load of 15 N as examined under SEM. The counterface ball for pure Ti presents a transfer layer with few delamination signs as seen in Fig.5.52 (a). The worn surface of the ball used against TiB50 shown in Fig. 5.52 (b) reveals debris and a patchy surface, whereas a loose transfer layer at various locations on the worn surface of all used against TiB60 could be seen in Fig. 5.52 (c). A loose and patchy layer could be observed on the worn surface of ball used against TiB70 (Fig. 5.52 (d)) whereas a smooth, compacted and

continuous transfer layer could be seen in Figure 5.52 (e) corresponding to the ball used against TiB80. The worn surface of the counterface ball used against TiB85 also shows the presence of a transfer layer with a rough appearance (Fig. 5.52 (f)).

Figure 5.53 (a through f) depicts the micrographs of the counterface ball slid under a load of 20 N as examined under SEM. The counterface ball for pure Ti presents a smooth transfer with ploughing signs as seen in Fig.5.53 (a). The worn surface of the counterface ball used against TiB50 shown in Fig. 5.53 (b) reveals a smooth surface, whereas some loose debris at various positions of the could be seen on the worn surface of ball used against TiB60 (Fig. 5.53 (c)). A smooth transfer layer could be observed on the worn surface of ball used against TiB70 as seen from Fig. 5.53 (d). Figures 5.53 (e and f), corresponding to the ball used against TiB80 and TiB85, respectively, reveal the presence of a smooth transfer layer with different area coverage.

Figure 5.54 (a through f) depicts the micrographs of the counterface ball slid under a load of 25 N as examined under SEM. The counterface ball for pure Ti presents a cracked transfer layer with few delamination signs as seen in Fig.5.54 (a). The worn surface of the counterface ball used against TiB50 shown in Fig. 5.54 (b) reveals a highly delaminated surface, whereas the presence of a transfer layer could be observed on the worn surface of ball used against TiB60 as seen from Fig. 5.54 (c). A loosely bound transfer layer and debris is seen over the worn surface ball used against TiB70 as evident from Fig. 5.54 (d). Figure 5.54 (e), corresponding to the counterface ball used against TiB80, shows a discontinuous transfer layer along with some loose debris. However, a compacted and patchy transfer layer could be seen on the worn surface of the counterface ball used against TiB85 as seen from Fig. 5.54 (f).

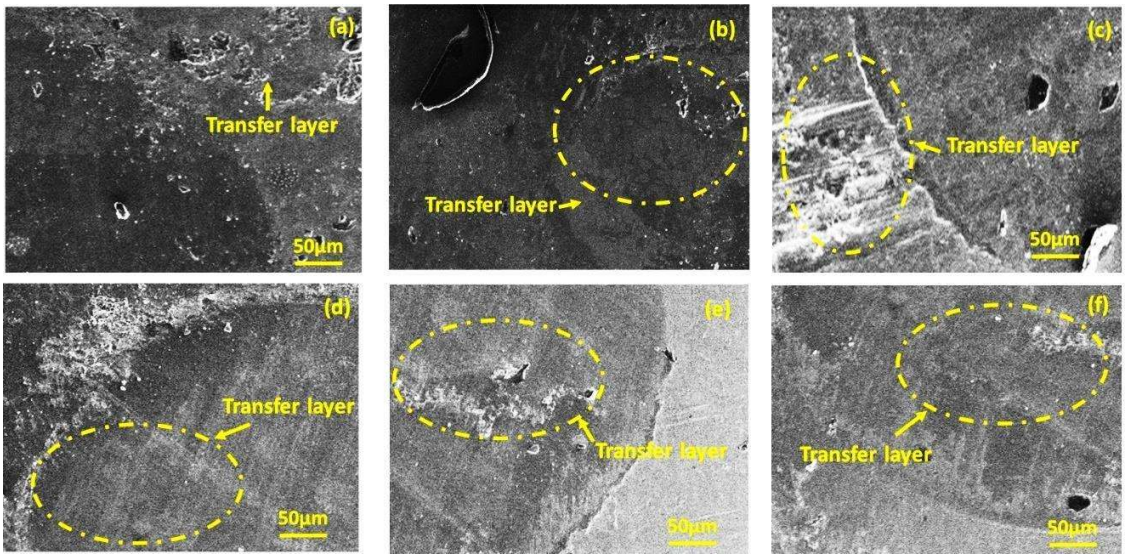

Figure 5.51 SEM images of counterface steel ball(a) Ti, (b) TiB50, (c) TiB60, (d)TiB70, (e) TiB80, and (f) TiB85 at 15 Hz and 10 N

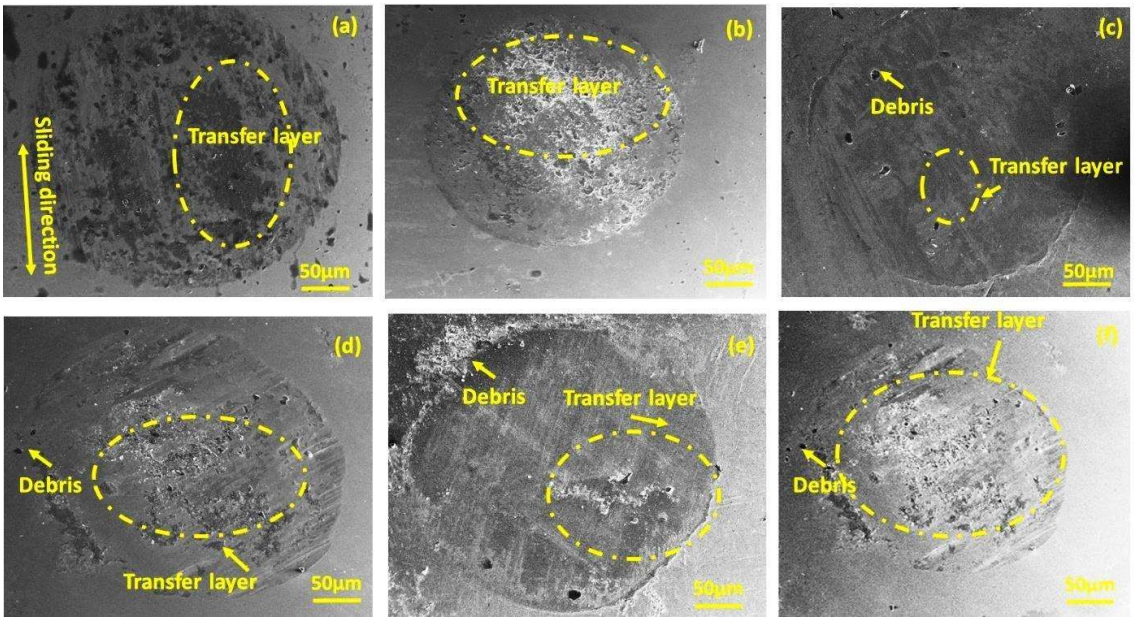

Figure 5. 52 SEM images of counterface steel ball (a) Ti, (b) TiB50, (c) TiB60, (d)TiB70, (e) TiB80, and (f) TiB85 at 15 Hz and 15 N

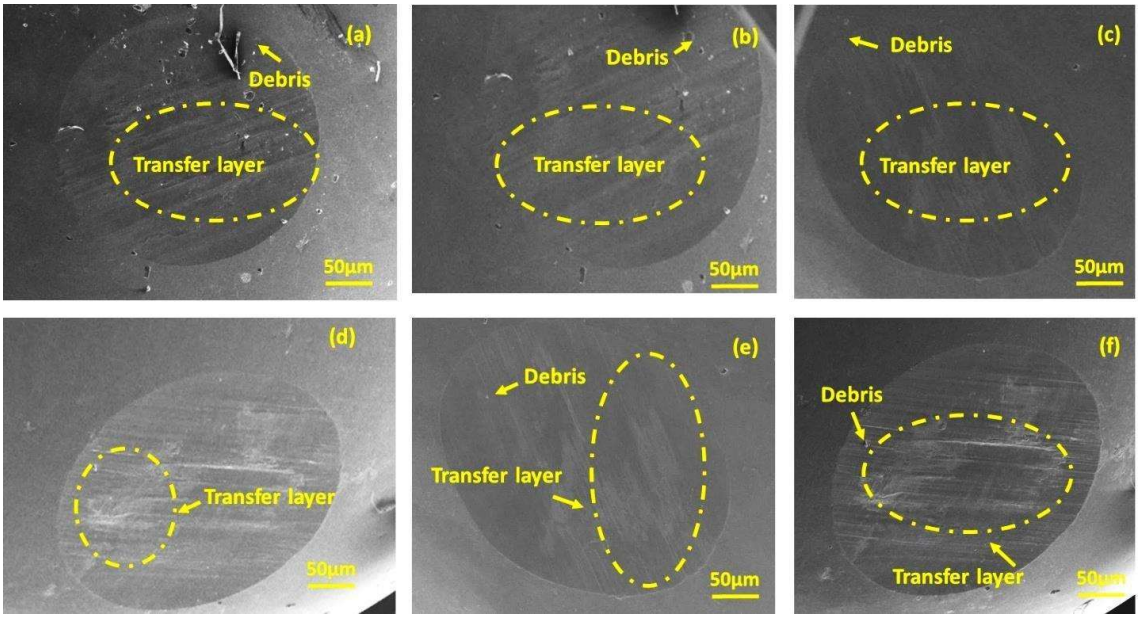

Figure 5.53 SEM images of counterface steel ball(a) Ti, (b) TiB50, (c) TiB60, (d)TiB70, (e) TiB80, and (f) TiB85 at 15 Hz and 20 N

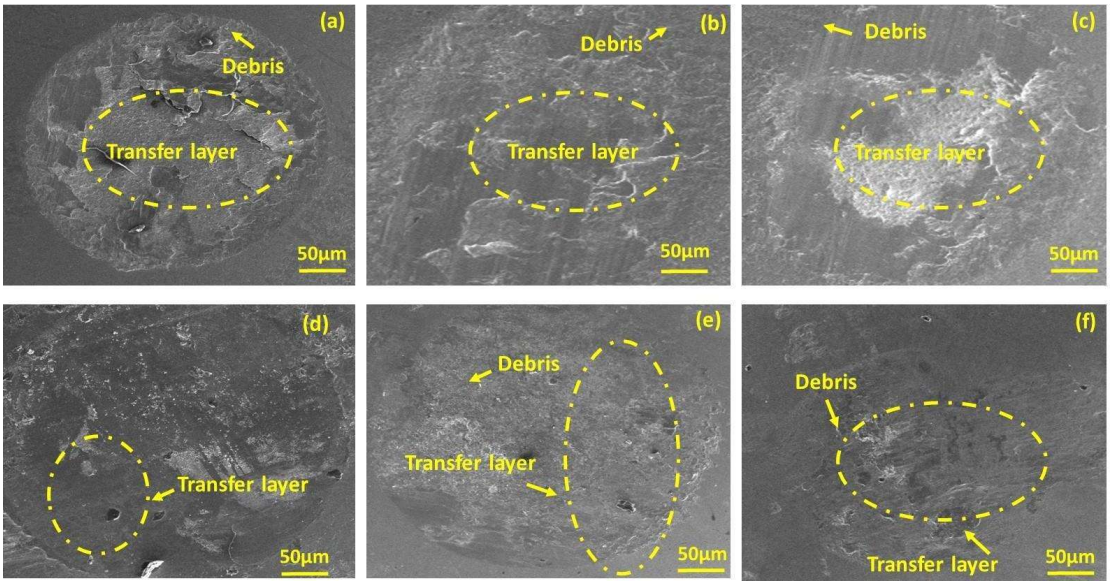

Figure 5.54 SEM images of counterface steel ball(a) Ti, (b) TiB50, (c) TiB60, (d)TiB70, (e) TiB80, and (f) TiB85 at 15 Hz and 25 N

5.7.4 Examination of Debris

The morphology of the wear debris collected after the tests was studied using SEM and XRD to investigate the nature of wear particles. The wear debris corresponding to Ti and TiB50 shown in Fig. 5.55 (a and b) is found to contain some fine as well as

larger particles of different shapes whereas a relatively large plate-like debris could be seen for TiB60 and TiB70 as shown on Figs. 5.55 (c and d). The debris for TiB80 and TiB85 shown in Fig. 5.55 (e and f), is a mixture of relatively regular and irregular-shaped particles/plate of moderate size as compared to the particle size of Ti, TiB50, TiB60, and TiB70. Figure 5.56 shows the x-ray spectrum of pooled debris which reveals the peaks corresponding to TiB, TiO, and TiO_2, Fe_2O_3, B_2O_3, TiB, and FeTi.

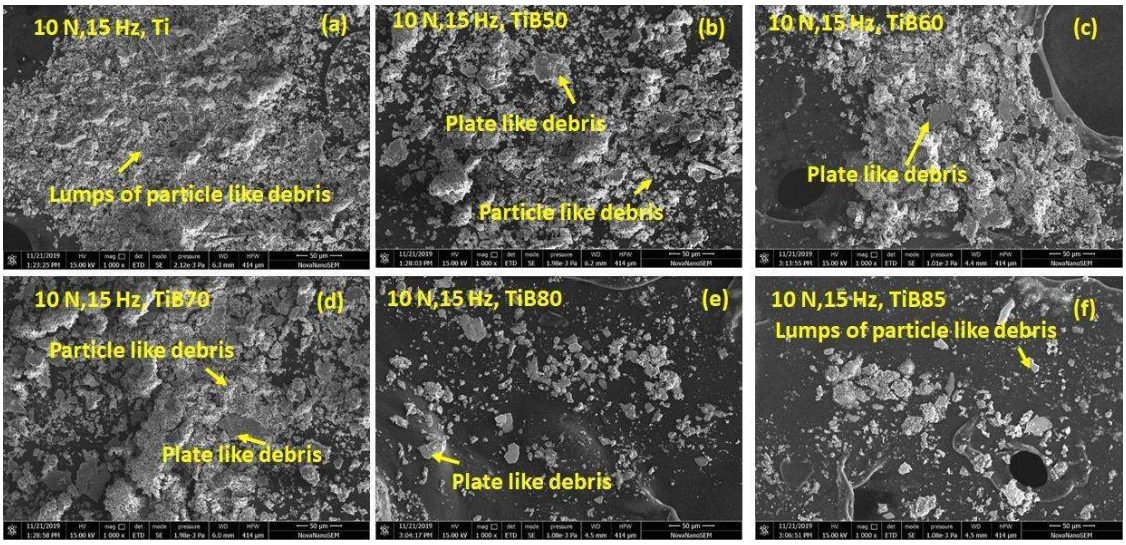

Figure 5.55 SEM images of counterface steel ball(a) Ti, (b) TiB50, (c) TiB60, (d)TiB70, (e) TiB80, and (f) TiB85 at 15 Hz and 10 N

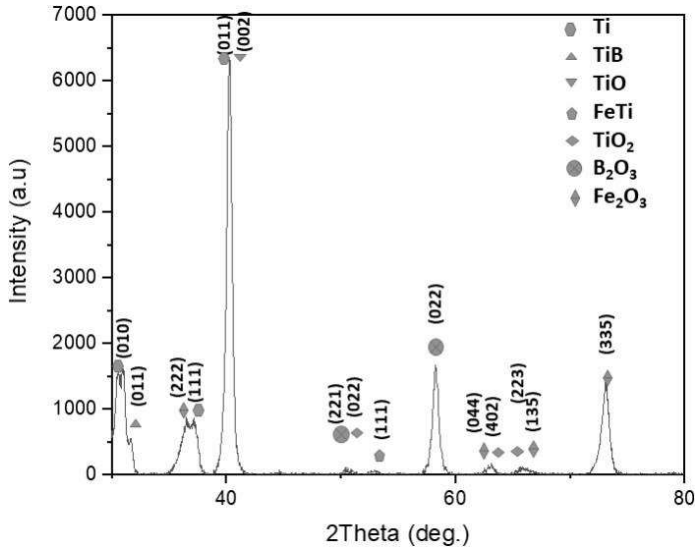

Figure 5.56 XRD patterns of wear debris at 15 Hz

5.8 DISCUSSION

A fluctuating trend of coefficient of friction with time is shown by composites at all the loads where the amplitude of fluctuation varies with the load and composite. However, the amplitude of fluctuation decreases with increasing load from 10 to 25 N, which may be confirmed by comparing Figs.5.44 (a through f). The initial roughness of the contacting surfaces may account for the changing trend of coefficient of friction change with time as explained earlier in other sections. An increase in load causes an increase in the generation of wear debris, which either becomes stuck between the mating surfaces or emerges from the sliding interface as wear particles, causing mass loss and hence, an increase in the wear rate. The entrapped worn debris may either stay loose, causing greater material loss due to abrasive action, or (ii) be churned into smaller particles and produce a transfer layer of debris, which may be loosely bound or well-compacted depending on the test conditions. A weakly bonded transfer layer is prone to abrasion and can be readily removed from the surface. As seen in Figures 5.47 (a), 5.48 (a), 5.49 (a), and 5.50 (a), pure Ti exhibits abrasive nature of wear that rises with increasing load and it causes a higher friction whereas TiB85 shows a reduced coefficient of friction and wear at 25 N could be attributed to the formation of a smooth transfer layer as shown in Figs. 5.21 (e) at 10 N, 5.22 (e) at 15 N, 5.23 (e) at 20 N, and 5.24 (e) at 25 N.The presence of a transfer layer over the surface, its compaction level and area coverage, presence oxides and lubricious compounds on the worn surface, transfer of material from the counterface to composites and composite to counterface ball may again be invoked to explain the observed friction and wear behaviour of Ti and composites, as these factors inhibit metal-metal contact and control the friction and wear performance as stated earlier in section 4.2. A comparison of worn surfaces of pure Ti, composites and steel ball against these shown in Figs. 5.47 to 5.50 (a through f) and Figs. 5.51 to 5.54(a

through f), respectively, can help in explaining the observed behaviour (Fig. 5.45 (a and b)) apart from the formation - compaction - coverage - detachment - reformation of transfer layer and presence of TiO, TiO_2, and B_2O_3 on the worn surfaces (Figs. 5.56) as highlighted in previous sections. A decrease in friction and wear due to the formation of the transfer layer has also been reported earlier also by Li et al. (2013) and Zhen et al. (2014, 2016) which is in consonance with the results of present study.

Higher hardness in composites due to TiB results in a reduced wear rate in comparison to pure Ti. As the load increases the wear debris formation increases which in turn increases the mass loss of materials. However, the increased load result in frictional heating which causes agglomeration or compaction of the wear debris to form a transfer layer over the sliding surface. This compacted transfer layer provides a cover to the underlying substrate depending upon the area of coverage and its degree of compaction i.e. compact or loosely bound, resulting in the prevention of metal-metal contact between the mating materials with consequent reduction in loss of material, therefore, wear rate as seen from Fig. 5.46 (a and b). The SEM images of the worn surfaces of composites and counterface reveal the degree of compaction and area covered by the transfer layer by which prevents further wear of materials. The formation and presence of lubricious oxides of Ti (TiO and TiO_2) and B i.e., B_2O_3 as revealed by X ray diffraction (Fig. 5.56) on the worn surfaces is another factor contributing to reduction in wear rate. The content of B_2O_3 formation was expected to increase with increase in TiB content in the composites as one moves from TiB50 to TiB85. Therefore, lowest wear rate at all the loads shown by TiB80 and TiB85 is not surprising. The examination of the worn surfaces suggests the metal removal mechanism of composites is a mixture of delamination, ploughing, abrasion, and adhesion, whereas the same for pure Ti are ploughing, plastic deformation, abrasion and oxidation. Based on the above observation

one may conclude that composites TiB80 and TiB85 have the optimum performance at all the loads in regard to both the friction and the wear under the range of load and frequency used in the investigation.

Summary

Effect of frequency on Friction and wear behaviour

(i) Average coefficient of friction of Ti and Composites at different frequencies and loads

Figures 5.57 (a to d) present a comparison of the average steady-state coefficient of friction at different frequencies at loads 10, 15, 20 and 25N for Pure Ti and the composites. One may observe that pure Ti has a higher coefficient of friction at 4 and 10 Hz in comparison to composites except for TiB50 at all the loads whereas at 7 and 15 Hz its COF is lower than TiB50 as seen from Fig. 5.57. The reasons for the same have already been discussed in the preceding text. Among the composites TiB80 has shown the lowest coefficient of friction under all the frequencies and loads used in the present study.

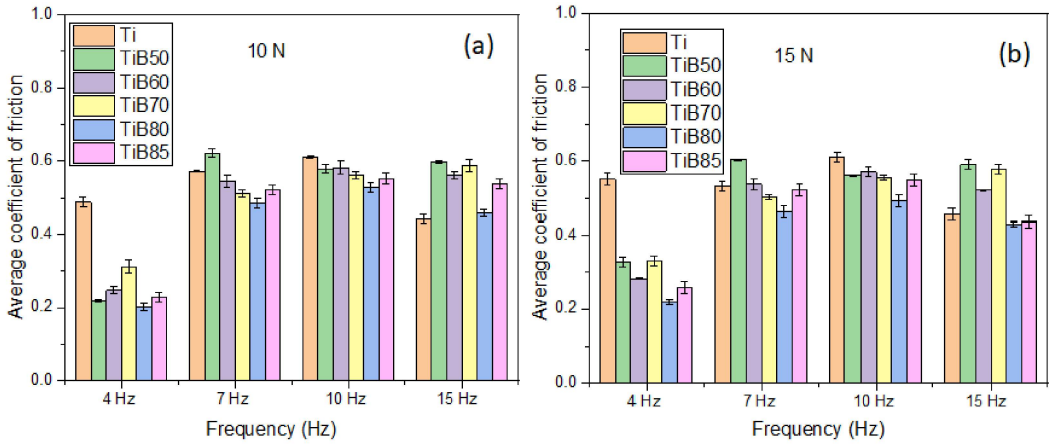

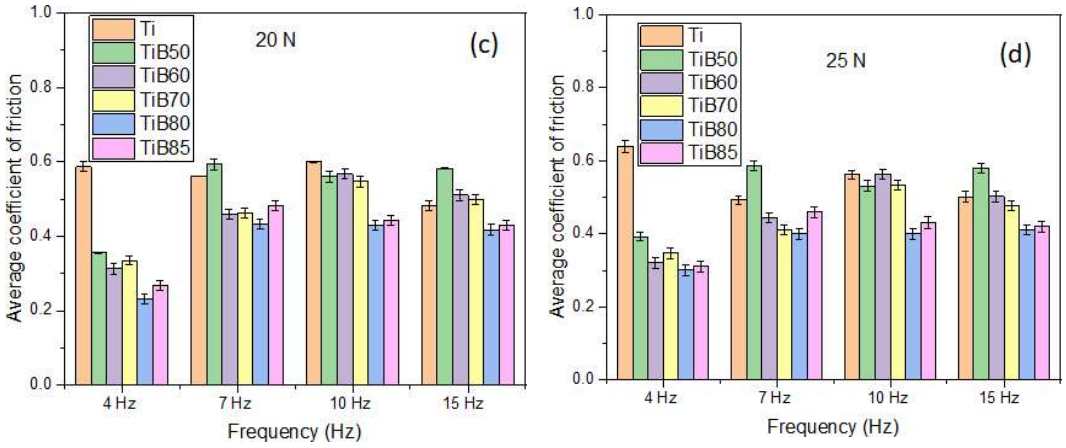

Figure 5. 57 Average coefficient of friction of Ti and Ti-TiB composites at different frequencies and loads

(ii) Wear rate of Ti and Composites at different frequencies and loads

Figures 5.58 (a to d) depict the wear rate of Pure Ti as well as Ti-TiB composites at different frequencies at loads of 10, 15, 20, and 25 N. One may observe that pure Ti has the highest wear rate with an increasing trend with increase in frequency at loads of 10 and 25 N (Fig. 5.58 a and d) whereas the wear rate is found to increase first as the frequency is raised from 4 to 7 Hz and decreases further at 10 Hz before increasing again at 15 Hz at the loads of 15 and 20 N (Fig. 5.58 (b and c). A comparison of wear rates at different frequencies shown in Fig. 5.58 (a to d) reflects that the wear rate of Ti has the highest wear rate at all the frequencies. All the composites show a similar trend of variation of wear rate with frequency. However, among the composites the wear rate shown by TiB80 and TiB85 are lowest and almost same with a marginal difference based on the particular frequency and load.

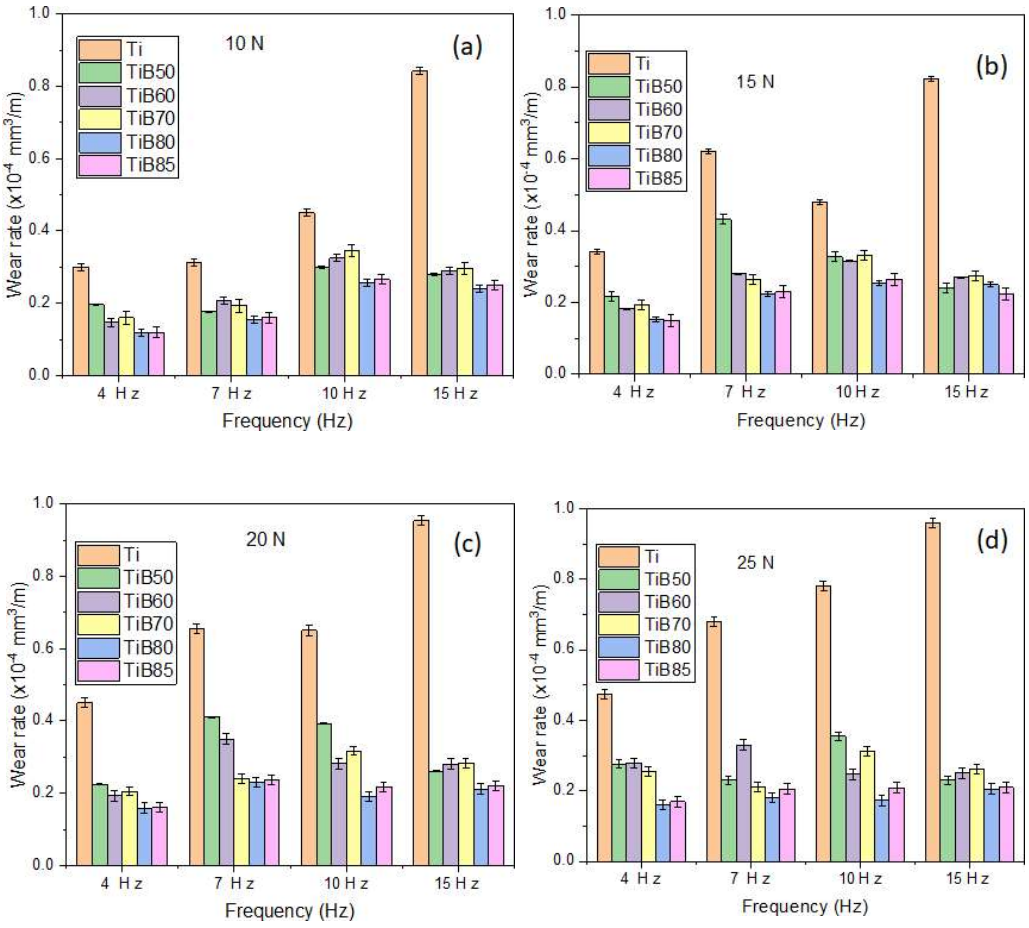

Figure 5. 58 Wear rate of Ti and Ti-TiB composites at different frequencies and loads

Based on the results of friction and wear as well as the hardness of composites, it can be concluded that a composite containing 80 vol.% TiB i.e., TiB80 has shown the optimum tribological performance in terms of coefficient of friction and wear rate under the dry sliding condition in the range of load and frequency used in the current study. Despite having a similar wear rate, the composite having 85 vol. % TiB has shown a slightly higher coefficient of friction as compared to TiB80 due to the presence of a loose transfer layer, which results in abrasion by hard debris particles and consequent increase in the coefficient of friction.